

ผลของบรรยากาศในการเคลือบต่อความบกพร่องที่ชั้นผิวของเซอริโคเนียขนาดนาโน
และการประยุกต์ใช้เป็นตัวเร่งปฏิกิริยาสำหรับการสังเคราะห์ไบโอดีเซล



นางสาวณิชภัทร เชนโต

สถาบันวิทยบริการ

วิทยานิพนธ์นี้เป็นส่วนหนึ่งของการศึกษาตามหลักสูตรปริญญาวิศวกรรมศาสตรมหาบัณฑิต

สาขาวิชาวิศวกรรมเคมี ภาควิชาวิศวกรรมเคมี

คณะวิศวกรรมศาสตร์ จุฬาลงกรณ์มหาวิทยาลัย

ปีการศึกษา 2550

ลิขสิทธิ์ของจุฬาลงกรณ์มหาวิทยาลัย

EFFECT OF CALCINATION ATMOSPHERE ON SURFACE DEFECT OF NANO ZrO_2 AND ITS

APPLICATION AS CATALYSTS FOR BIODIESEL SYNTHESIS



Miss Nichapat Senso

สถาบันวิทยบริการ

A Thesis Submitted in Partial Fulfillment of the Requirements
for the Degree of Master of Engineering Program in Chemical Engineering

Department of Chemical Engineering

Faculty of Engineering

Chulalongkorn University

Academic year 2007

Copyright of Chulalongkorn University

501007


Thesis Title EFFECT OF CALCINATION ATMOSPHERE ON SURFACE
DEFECT OF NANO ZrO₂ AND ITS APPLICATION AS
CATALYSTS FOR BIODIESEL SYNTESIS

By Miss Nichapat Senso

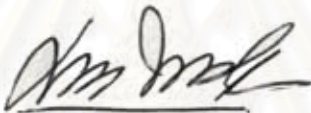
Field of Study Chemical Engineering

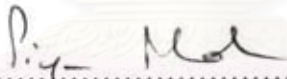
Thesis Advisor Professor Piyasan Prasertthdam, Dr.Ing.

Accepted by the Faculty of Engineering, Chulalongkorn University in Partial
Fulfillment of the Requirements for the Master's Degree.



..... Dean of the Faculty of Engineering
(Associate Professor Boonsom Lerthirungwong, Dr.Ing)

THESIS COMMITTEE


..... Chairman
(Associate Professor ML. Supakanok Thongyai, Ph.D.)


..... Thesis Advisor
(Professor Piyasan Prasertthdam, Dr.Ing.)


..... Member
(Assistant Professor Bunjerd Jongsomjit, Ph.D.)


..... Member
(Assistant Professor Okorn Mekasuwandumrong, Ph.D.)

ฉันทภัทร เข้มโส : ผลของบรรยากาศในการแคลไซน์ต่อความบกพร่องที่ชั้นผิวของเซอร์โคเนียขนาดนาโน และการประยุกต์ใช้เป็นตัวเร่งปฏิกิริยาสำหรับการสังเคราะห์ไบโอดีเซล. (EFFECT OF CALCINATION ATMOSPHERE ON SURFACE DEFECT OF NANO ZrO_2 AND ITS APPLICATION AS CATALYSTS FOR BIODIESEL SYNTHESIS) อ. ที่ปรึกษา : ศ.ดร. ปิยะสาร ประเสริฐธรรม , 97 หน้า

งานวิจัยนี้ได้ศึกษาผลการผลึกเซอร์โคเนียขนาดนาโนที่ใช้เป็นตัวรองรับตัวเร่งปฏิกิริยา ซึ่งทำการผลิตโดยวิธีเซอร์โวลเทอร์มอล โดยวัตถุประสงค์ของงานวิจัยนี้เพื่อทำการศึกษาผลของบรรยากาศ (อากาศ ไฮโดรเจน ไนโตรเจน และออกซิเจน) ในการเผาเซอร์โคเนียที่อุณหภูมิ 500 องศาเซลเซียส หลังจากนั้นนำไปทำการเคลือบฝังลงบนทั้งสแตนเลสโรดและนำไปเผาภายใต้บรรยากาศอากาศอีกครั้ง ผลของการเผาเซอร์โคเนียภายใต้บรรยากาศต่างๆส่งผลถึงคุณสมบัติของตัวเร่งปฏิกิริยาทั้งสแตนเลส/เซอร์โคเนีย และทำการศึกษาดัชนีของตัวรองรับเซอร์โคเนียโดยใช้ XRD, BET, Raman spectroscopy, ESR, titration และ TEM เทคนิค พื้นที่ผิว BET ขนาดอนุภาคและองค์ประกอบโมโนคลีนิกของการทรีสต์ตัวรองรับเซอร์โคเนีย อยู่ในช่วงระหว่าง 76 ถึง 95 ตารางเมตรต่อกรัม 3.5 ถึง 6.9 นาโนเมตร และ 21 ถึง 29 เปอร์เซ็นต์โดยน้ำหนักตามลำดับ ESR แสดงผลของความบกพร่อง F-center บนตัวรองรับเซอร์โคเนีย จะเพิ่มขึ้นเมื่อทำการเผาที่เผาที่บรรยากาศรีดิวซ์มากขึ้น ประสิทธิภาพของตัวเร่งปฏิกิริยาของ ตัวเร่งปฏิกิริยาทั้งสแตนเลส บนตัวรองรับเซอร์โคเนียที่ทำการทรีสต์ที่บรรยากาศต่างๆ ทำการศึกษาในปฏิกิริยาทรานเอสเทอร์ริฟิเคชันของไตรอะซิติกและเมทานอล ค่าการกระตุ้นของตัวเร่งปฏิกิริยาที่พัฒนาเรียงตามลำดับดังนี้ $WZ \text{ cal. } H_2 (53\%) > WZ \text{ cal. } N_2 (40\%) > WZ \text{ cal. } O_2 (17\%) = WZ \text{ cal. } Air (16\%)$ ผลที่ได้สอดคล้องกับค่าความเป็นกรดซึ่งทำนายโดยการไตเตรท ความเป็นกรดจะเพิ่มขึ้น ทำนายโดยวิธีไตเตรชัน และ Zr^{3+} ทำนายโดย ESR การเพิ่มขึ้นของความเป็นกรดเกิดจากการเพิ่มขึ้นของการกระจายตัวของ WO_x บนตัวรองรับเซอร์โคเนีย

ภาควิชา.....วิศวกรรมเคมี.....
สาขาวิชา... วิศวกรรมเคมี.....
ปีการศึกษา.....2550.....

ลายมือชื่อนิสิต.....ฉันทภัทร เข้มโส.....
ลายมือชื่ออาจารย์ที่ปรึกษา.....ปิยะสาร.....

4970314521 : MAJOR CHEMICAL ENGINEERING:

KEY WORDS: NANO ZrO_2 / Zr^{3+} / F-CENTER / SURFACE DEFECT /
CALCINATION ATMOSPHERE / BIODIESEL / TUNGSTATED ZIRCONIA / WZ
/ TRANSESTERIFICATION

NICHAPAT SENSO: EFFECT OF CALCINATION ATMOSPHERE ON
SURFACE DEFECT OF NANO ZrO_2 AND ITS APPLICATION AS
CATALYSTS FOR BIODIESEL SYNTHESIS. THESIS ADVISOR: PROF.
PIYASAN PRASERTHDAM, Dr. Ing, 97 pp.

In this present research, the nanocrystalline ZrO_2 supports were prepared using the solvothermal method. The obtained ZrO_2 powders were treated at $500^\circ C$ in various atmospheres (Air, H_2 , N_2 and O_2). Then, the ZrO_2 supports were impregnated with tungsten (VI) chloride which were calcined further to form the oxide phase. Effect of calcination atmospheres on the physiochemical properties of W/ZrO_2 catalysts and ZrO_2 supports were investigated using XRD, BET, Raman spectroscopy, ESR, titration and TEM techniques. BET surface area, crystallite sizes and monoclinic contents of all treated- ZrO_2 supports were slightly different and ranged between 76 to $95\ m^2/g$, 3.5-6.9 nm and 21-29 wt.%, respectively. The ESR results revealed that the F-center defects on ZrO_2 supports increased as the calcination atmospheres became more reducible. Catalytic performances of the W catalysts supported on these treated-catalysts were studied in the liquid phase transesterification reaction of triacetin and methanol. The catalytic activities were improved in the order: WZ cal. H_2 (53%) > WZ cal. N_2 (40%) > WZ cal. O_2 (17%) = WZ cal. Air (16%). This result was in good agreement with the increased order of acidity determined by titration and Zr^{3+} determined by ESR. Increasing of acidity was probably due to the increase of dispersion of WO_x species on ZrO_2 supports.

Department.....Chemical Engineering..... Student's signature.....*นิชภัปต์ เสนอ*.....

Field of study...Chemical Engineering.....Advisor's signature.....*ปิยสาร ประเสริฐดาม*.....

Academic year2007.....

ACKNOWLEDGEMENTS

First and foremost, I would like to express my most sincere thanks to my advisor, Professor Piyasan Prasertthdam, for his great guidance and support. I am most deeply indebted to Assistant Professor Bunjerd Jongsomjit for his continuous support and encouragement over the years. I would also like to thank Associate Professor ML. Supakanok Thongyai for chairman. Special thanks belong to Assistant Professor Okorn Mekasuwandumrong for kindly serving as my committee members.

I am grateful to all former and current students for making the laboratory such an agreeable workplace. I would like to acknowledge my friends for the good spirit shared especially Mr. Sataporn Kamhom. Their friendship encouraged me to overcome many difficulties. I wish to thank Khun Teerayuth Chormanee (gikky)

Finally, I would like to dedicate this dissertation to my family for their edification, support and endless love. Without them, I would not have been the person I am and certainly this work would never have reached completion.



สถาบันวิทยบริการ
จุฬาลงกรณ์มหาวิทยาลัย

CONTENTS

	page
ABSTRACT (IN THAI).....	iv
ABSTRACT (IN ENGLISH).....	v
ACKNOWLEDGEMENTS.....	vi
CONTENTS.....	vii
LIST OF TABLES.....	x
LIST OF FIGURES.....	xi
CHAPTERS	
I INTRODUCTION.....	1
II LITERATURE REVIEWS.....	4
2.1 Solid acid catalysts based on supported tungsten oxides...	4
2.2 Tungsten support on zirconia catalysts in transesterification reaction.....	11
2.3 General of defect in zirconia and technique to detect it.....	15
III THEORY.....	23
3.1 General feature of zirconia.....	23
3.1.1 The formation of zirconia in glycol solvent.....	24
3.2 Defects structure of crystal material.....	25
3.2.1 Vacancies: Schottky defects.....	25
3.2.2 Interstitial defects: Frenkel defects.....	26
3.2.3 Coupled charge substitutions and vacancies.....	26
3.2.4 Color centers.....	27
3.3 Surface defects.....	27
3.3.1 Definition of F-center defect.....	30
3.4 Biodiesel.....	32
3.4.1 Transesterification reaction.....	33
3.4.2 The Reaction of biodiesel when the catalyst is potassium hydroxide	35

CHAPTERS	page
IV EXPERIMENTAL.....	39
4.1 Sample preparations.....	39
4.1.1 Chemicals.....	39
4.2 Preparation of nanocrystalline ZrO ₂	40
4.3 Preparation of tungstated zirconia catalyst.....	40
4.4 Reaction studies.....	40
4.5 Equipment.....	41
4.5.1 Autoclave Reactor.....	41
4.5.2 Gas Chromatography(GC).....	43
4.6 Characterization.....	44
4.6.1 Powder X-ray diffraction(XRD).....	44
4.6.2 Transmission electron microscopy and selected area electron diffraction (TEM) and (SAED).....	44
4.6.3 Brunauer-Emmett-Teller surface area (BET).....	44
4.6.4 Titration technique involved an ion-exchange....	45
4.6.5 Electron spin resonance spectroscopy(ESR).....	45
4.6.6 IR Raman spectroscopy.....	45
4.6.7 XPS.....	45
V RESULTS AND DISCUSSION.....	47
5.1 Characteristics of zirconia calcined at different atmospheres	47
5.2 Characteristics of tungstated zirconia (WZ) catalysts.....	52
5.3 Relative catalyst activity.....	63
VI CONCLUSION AND RECOMMENDATION	
6.1 Conclusion.....	64
6.2 Recommendation and future work.....	64

	page
REFERENCES.....	65
APPENDICES.....	69
Appendix A. CALCULATION FOR CATALYST PREPARATION..	70
Appendix B. CALCULATION FOR PERCENT OF TETRAGONAL AND MONOCLINIC PHASE.....	72
Appendix C. CALCULATION OF CRYSTALLITE SIZE.....	74
Appendix D. CALCULATION OF TRIACETIN CONVERSION....	76
Appendix E. CONDITION OF GAS CHROMATOGRAPHY	78
Appendix F. TRANSMISSION ELECTRON MICROSCOPY AND SELECTED AREA ELECTRON DIFFRACTION (TEM) AND (SAED).....	80
Appendix G. ESR SPECTRA OF ALL CATALYSTS SAMPLES AT DIFFERENT CALCINATION ATMOSPHERES...	88
Appendix H. RAMAN SPRCTRA OF ALL CATALYSTS SAMPLES AT DIFFERENT CALCINATION ATMOSPHERES.....	91
Appendix I. LIST OF PUBLICATIONS.....	94
VITA.....	97

สถาบันวิทยบริการ
จุฬาลงกรณ์มหาวิทยาลัย

LIST OF TABLES

	page
Table 3.1 Chemical structure of common fatty acids and their methyl esters	37
Table 3.2 Characteristics of common fatty acids and their methyl esters.....	37
Table 4.1 Chemicals used for sample prepararions	39
Table 4.2 Operating conditions for gas chromatography.....	42
Table 5.1 Surface area, XRD phases for ZrO ₂ samples calcinations at difference atmosphere.....	54
Table 5.2 Surface acidity for WZ sample calcinations at difference atmosphere	54
Table B.1 Calculation of the fraction of crystal phase of zirconia.....	73
Table B.2 Calculation of the fraction of crystal phase of tungsten support on zirconia catalysts.....	73
Table E1 Operating conditions for gas chromatography	78
Table G1 Show the power, amplitude of ESR spectra for WZ sample when calcinations 400 °C at difference atmosphere.....	90



 สถาบันวิทยบริการ
 จุฬาลงกรณ์มหาวิทยาลัย

LIST OF FIGURES

	page
Figure 3.1 The unit cells of the crystal systems.....	24
Figure 3.2 Crystal structure of cubic, tetragonal and monoclinic zirconia.....	24
Figure 3.3 Mechanism of glycothermal-derived ZrO ₂	25
Figure 3.4 Cation and anion charge-balanced Shottky defects in NaCl.	25
Figure 3.5 Pair of charge-balanced Frenkel defects in AgI.	26
Figure 3.6 Substitution of a Ca ²⁺ cation for a Na ⁺ cation in NaCl, accompanied by the formation of a vacant cation site in order to maintain charge neutrality.....	27
Figure 3.7 Transesterification reaction.....	33
Figure 3.8 Shows the reactions for the transesterification of triacetin with methanol.....	35
Figure 3.9 The reaction when the catalyst is potassium hydroxide(KOH).....	36
Figure 3.10 Hydrolysis of a triglyceride to form free fatty acids.....	36
Figure 4.1 Autoclave reactor.....	42
Figure 4.2 Diagram of the reaction equipment for the synthesis of zirconia.....	42
Figure 5.1 X-ray diffraction pattern of nano Zirconia prepared by solvothermal method and calcinations at different atmosphere.....	48
Figure 5.2 ESR spectra of sample nano ZrO ₂ calcinations at different atmosphere : O ₂ , H ₂ , N ₂ , Air and As-syn	49
Figure 5.3 XRD patterns of WZ prepared by impregnation tungsten on zirconia (calcinations at different atmosphere) and WZ calcinations at air atmosphere	51
Figure 5.4 ESR spectra of tungstated zirconia prepared by impregnation tungsten on zirconia(calcinations at different atmosphere) and tungstated zirconia calcinations at air atmosphere.....	53
Figure 5.5 Raman spectra of nano Zirconia prepared by solvothermal method and calcinations at different atmosphere.....	56

	page
Figure 5.6 Raman spectra of tungstated zirconia prepared by impregnation tungsten on zirconia(calcinations at difference atmosphere) and tungstated zirconia calcinations at air atmosphere.....	57
Figure 5.7 TEM micrographs of W impregnation on ZrO ₂ calcinate with O ₂	59
Figure 5.8 TEM micrographs of W impregnation on ZrO ₂ calcinate with H ₂	60
Figure 5.9 TEM micrographs of W impregnation on ZrO ₂ calcinate with N ₂	61
Figure 5.10 TEM micrographs of W impregnation on ZrO ₂ calcinate with Air.....	62
Figure 5.11 Relative activities of acid catalysts for transesterification of triacetin with methanol using a 6:1(methanol:triacetin)and 60°C (solid acids = 2 wt%).....	63
Figure D1 Gas chromatopac report of relative activities of acid catalysts for transesterification of triacetin with methanol using a 6:1 (methanol:triacetin) and 60°C (solid acids = 2 wt%) when the steady-state rate was reached after 7 h.....	77
Figure E1 Operating condition of GC for this research.....	79
Figure F.1 TEM micrographs of W/ZrO ₂ calcinate with air.....	80
Figure F.2 TEM micrographs of W/ZrO ₂ calcinate with H ₂	82
Figure F.3 TEM micrographs of W/ZrO ₂ calcinate with N ₂	84
Figure F.4 TEM micrographs of W/ZrO ₂ calcinate with O ₂	86
Figure G1 ESR spectra of sample nano ZrO ₂ calcinations at different atmosphere : CO ₂ , O ₂ , NH ₃ , He, Ar, Air, N ₂ , H ₂	88
Figure G2 ESR spectra of tungstated zirconia prepared by impregnation tungsten on zirconia(calcinations at difference atmosphere) and tungstated zirconia calcinations at air atmosphere: Air, O ₂ , N ₂	89
Figure H1 Raman spectra of WZ commercial prepared by sol-gel method and calcinations at atmosphere(Air) and no calcinated (no cal.).....	91
Figure H2 Raman spectra of ZrO ₂ prepared by solvothermal method and impregnation with H ₂ O and calcinations at atmosphere.....	92
Figure H3 Raman spectra of ZrO ₂ prepared by solvothermal method and calcination at H ₂ atmosphere and impregnation with H ₂ O and calcinations at atmosphere.....	93

CHAPTER I

INTRODUCTION

We have known that energy from natural sources such as petroleum gas & oil, for this time being, their prices are increasing everyday because of the demand of energy for serving in industries for many countries. Biodiesel is one of those renewable energy sources which is attracted by many researchers because it can be made of natural material, for example vegetable oil and fat from animal origin. Moreover, they can be easier convert to biodiesel comparing with petroleum oil and natural gas. Biodiesel will provide many advantages since it is effective fuel and it can reduce production cost. But the major problem is that used vegetable oil and used animal oil contain free fatty acids (FFA) at high level, so it is needed to pre-treatment for disposal free fatty acids at the preliminary process of biodiesel production. The main reactions which play important role on produce biodiesel are “esterification” that strong liquid acid catalysts such as sulfuric acid [1-6] and “transesterification”.

However, using strong liquid acid catalysts usually has side effects which are high corrosive, hard to separate and expensive cost because those catalysts can not be reused. Hence, there are new investigation for solid acid and base catalyst such as sulfated zirconia (SZ) and tungstated zirconia (WZ) [7]. Because these catalysts provide esterification and transesterification reaction at the same time and the strong acidity of zirconia-supported sulfated catalysts has attracted much attention because of its ability to catalyze a wide range of reactions such as cracking, alkylation, and isomerization, all needing solid acids as catalysts [8,9,10,20]. Since sulfated zirconia catalysts promoted with noble metals are subject, among others, to sulfate reduction and subsequent poisoning of the metallic function under reducing atmospheres[11-17,21,22], the W-based oxoanions originally proposed by Hino and Arata and other researchers [18,19,23,24], seem to be good candidates for the skeletal isomerization of alkanes higher than C₄ requiring strong acid sites. It is known that anionic dopants create additional electron-deficient regions that increase the Bronsted acid strength of a metal oxide surface by improving the ability of neighboring hydroxyl groups to act as proton donors [25,26]. As an alternative to sulfated zirconia, WO₃/ZrO₂ was also reported to be active for the isomerization of C₄-C₈ alkanes

[18,27,28]. Although WO_3/ZrO_2 was less active than sulfated zirconia, but it has several advantages over sulfated zirconia. For example, the WO_3 are much more stable than the sulfate ones at high temperatures[21] and tungstated zirconia catalysts go exhibit significantly less deactivation during catalytic reaction[7].

Lopez et al. [7] reported that the usage of tungstated zirconia catalyst has activities site equivalent to sulfuric acid for catalyzing biodiesel-forming transesterification reaction. Other advantages of tungstated zirconia such as its deactivation appear to be not rapid for transesterification reaction of triglycerides with methanol [7-9]. Ramu et al. [10] reported that the various of percentage in loading tungstated on zirconia and various calcination temperatures have affected the phase changed of ZrO_2 and also affect catalyst activity on esterification reaction for biodiesel production process. In addition, some papers reveal that surface structure and phase of supported ZrO_2 has effect on the catalyst activity also [1,11-13].

Since surface structure and defected structure of supported ZrO_2 affects the properties of crystalline material (such as nano scale level, Zr^{3+}). However to study the detail of defected structure is very difficult because of its various structure types. From defective theory of Frenkel and Schottky, they investigated defection, but it did not cover all types of materials. There are many researchers who study about how to create the defection on ZrO_2 surface using various methods. Lui et al. [12] created defection on ZrO_2 surface by calcinations at different temperatures. Others method are to calcine the samples in different atmospheres [11]. Different types of surface ZrO_2 which discovered by Zhao et al.[11] were reported after they studied the ZrO_2 forming and found that defection of ZrO_2 surface provided Zr^{3+} center and F-center when treated by H_2 atmosphere. The reducibility of H_2 is the main factor to form F-center. It is very difficult to reduce ZrO_2 with H_2 due to the high interaction between Zr-O bonds. However F-center can be formed by the reaction of hydroxyl on ZrO_2 surface.

There are many works reporting that the surface defect can control the properties of ZrO_2 . The objective of this work is to study the surface defect on ZrO_2 nanocrystallite and its application as catalysts (tungstated zirconia) when they are calcined at different ambient

atmospheres(H_2 , O_2 , N_2 , Air). Their properties of the catalysts for the transesterification for biodiesel synthesis were also investigated.

And using the electron spin resonance(ESR)[11,13] for investigates the defection on surface ZrO_2 , and they are many methods for analyzing such as the aqueous exchange titration method used for estimation of acid site density [8] and BET [12].

This dissertation was divided to six chapters. Chapter I involved an overview of the importance of biodiesel, transesterification in biodiesel and surface defect and also its application. In chapter II, knowledge and open literature dealing with surface defect was presented. The literature review as accentuated the technique of surface defect creation and the report concerning the effect of surface defect on crystal ZrO_2 . In Chapter III, we know theory about biodiesel synthesis, defective theory of Frenkel and Schotty, general feature of zirconia.

And The experimental procedure as well as the instrument and technique used for characterizing the resulting ZrO_2 were also described in the Chapter VI. The main mechanisms explaining the formation of surface defect were also mentioned together with the comparison between the surface defect controlling technique studied in this work and the other techniques. In Chapter V, the role of calcination atmosphere on surface defect of nano ZrO_2 and its application as W/ZrO_2 catalysts for biodiesel synthesis was investigated. The mechanism as a self promotion of surface defect was proposed based on the literatures and our results. Finally, conclusions of this work and some recommendations for future research work were provided in Chapter VI.

CHAPTER II

LITERATURE REVIEWS

2.1 Solid acid catalysts based on supported tungsten oxides

Solid acid catalysts play an important role in hydrocarbon conversion reactions in the chemical and petroleum industries [37,38]. In such cases, zirconia is frequently used as catalyst or support. It is well known that zirconia has three stable crystalline phases: tetragonal, monoclinic, and cubic zirconia, and their concentration and transformation between each other depend on zirconia doping and/or thermal treatment. The zirconia doped by a variety of compounds such as sulfate [39], phosphate, and heteropolyacids [4] creates additional electron-deficient regions that may generate new acid sites and increase the strength of Brønsted acidity responsible for an enhanced catalytic activity in alkanes isomerization reactions [23,37-40]. In addition, modifying by these anions mentioned above, tetragonal zirconia phases can be stabilized at high temperature [41-47], which is reported to be favorable in catalytic reactions such as alkanes isomerization. The acidic nature and crystalline structure of zirconia can be also modified by other oxides such as tungsten oxide [44-48]. Hino and Arata and other researcher reported that WO_3/ZrO_2 mixing oxide is an alternative material in the acid-catalyzing reactions requiring strong acidity [23,50]. Although the crystalline structure of zirconia has been extensively studied, less attention has been paid on the defective characteristics and distorted crystalline structure of the WO_x species doped zirconia nanophases, which are usually acted as catalytic active sites involving in many catalysis reactions [51,52].

ZrO_2 has been studied extensively in the field of surface science due to the wide range of its applications and the expectation that insight into surface properties on the fundamental level will help to improve its properties. The surface defect is one of the important topics in this field because the properties of the nanocrystal ZrO_2 are often dependent on a nature and density of the surface defect sites. As known that, ZrO_2 is a

useful material for many applications. Therefore, several studies have addressed its applications such as transesterification reaction. The common techniques used for creating surface defect were also reported by many researchers. Moreover, several methods for probing surface defect of ZrO_2 were discussed as well.

Odendi et al.[58] believed that the nucleation of the tetragonal zirconia was associated with lattice defects and anionic vacancies, which are produced upon crystallization. The pH of the medium used in the hydrothermal reaction was found to be the factor controlling the crystallization and a model of m- ZrO_2 and t- ZrO_2 crystallization was proposed. According to this model, there are three control regimes for the crystallization of ZrO_2 : At low pH the solubility is high, so that the hydrothermal crystallization occurred via dissolution/precipitation mechanism producing m- ZrO_2 . In a neutral or mild acidic medium, the solubility is very low, so that the crystallization occurred in situ by structural (topotactic) rearrangement of zirconium hydroxide, and the product in this region will be predominantly t- ZrO_2 . At high pH the solubility of zirconium hydroxide is very high; yet, the obtained product is predominantly metastable t- ZrO_2 . The topotactic crystallization prevails at high pH, because of a higher energy state of the obtained zirconium hydroxide gel (Denkewicz et al., 1990). It was reported later that the strong base OH^- favored the formation of Zr-O-Zr bridges between the non-bridging structural hydroxyl groups present in the gel so favouring its arrangement, its nucleation and its consequent crystallization.

Corte's-Ja'come et al.[59] report that WO_3-ZrO_2 catalysts were synthesized by precipitating the aqueous solutions of zirconium oxynitrate and ammonium metatungstate with ammonium hydroxide. The white slurry precipitate was treated under three different conditions. In the as-made materials, the amorphous phase was formed in the aged and refluxed samples, while well-crystallized tetragonal and monoclinic phases were obtained in the hydrothermally treated sample. The real amount of tungsten loaded in the samples was similar for the three samples, independently of the treatments; however, the tungsten surface atomic density in the annealed WO_3-ZrO_2 samples varied between 6 and 9 W atoms/nm². Two different contrast types of aggregates were determined by scanning

electron microscopy, the white particles which are rich in W, and the gray ones which are rich in zirconium; both of them were formed in the calcined solids prepared under aging or reflux condition. A very high dispersion of tungsten species on the zirconia surface was achieved in the hydrothermally treated sample. The degree of the interaction between WO_x and ZrO_2 surface strongly modified the Zr-O bond lengths and bond angles in the structure of tetragonal zirconia as proved by X-ray diffraction analysis and the rietveld refinement. The catalyst obtained under hydrothermal condition exhibited the highest dispersion of tungsten species in the zirconia, which in turn causes strong structural deformation of the tetragonal ZrO_2 phase responsible of the strongest surface acidity and, consequently, the optimum catalytic activity for *n*-hexane isomerization.

Kim et al.[60] report that a series of model-supported WO_3 catalysts were synthesized on preformed Al_2O_3 , Nb_2O_5 , TiO_2 , and ZrO_2 supports by impregnation of aqueous ammonium metatungstate, $(NH_4)_{10}W_{12}O_{41} \cdot 5H_2O$. The molecular and electronic structures of the supported tungsten oxide phases were determined with in situ Raman and UV-vis spectroscopy, respectively. The supported tungsten oxide structures are the same on all oxide supports as a function of tungsten oxide surface density (W/nm^2). Below monolayer coverage ($<5 W/nm^2$), both monotungstate and polytungstate surface WO_x species are present under dehydrated conditions and the polytungstate/monotungstate ratio increases with increasing surface coverage. Above monolayer coverage ($>5 W/nm^2$), crystalline WO_3 nanoparticles are present on top of the surface WO_x monolayer. Above $\sim 10 W/nm^2$, bulk-like WO_3 crystallites become dominant. The number of catalytic active sites and surface chemistry of the supported tungsten oxide phases were chemically probed with CH_3OH dehydration to CH_3OCH_3 . The specific oxide support was found to significantly affect the relative catalytic acidity of the surface WO_x species ($Al_2O_3 \sim TiO_2 > Nb_2O_5 > ZrO_2$) to that of the supported WO_3 nanoparticles. Consequently, no general relationship exists between the molecular/electronic structures or domain size and the specific catalytic acidity of the supported tungsten oxide phases present in the model-supported WO_3 catalysts.

Liu et al.[61] to study the effect of WO_3 (5–50 wt%) and ZnO (0.7–22 wt%) on the catalytic properties of $\text{Pt}/\text{WO}_3/(\text{ZnO})-\text{ZrO}_2$ for *n*-heptane (*n*- C_7) hydroisomerization was investigated. The optimized WO_3 and ZnO contents are 20 wt% and 3.4 wt%, respectively. The catalytic performance is achieved at 81% *n*- C_7 conversion and 89% C_7 isomer selectivity at 250 °C, which is reproducible and can be kept constant over 82 h under reaction conditions. Both WO_3 and ZnO can stabilize the tetragonal phase of ZrO_2 . The Brønsted acid-to-Lewis acid ratio should be optimized to achieve high catalytic performance. The activity for $\text{Pt}/\text{WO}_3/\text{ZrO}_2$ using $\text{Zr}(\text{OH})_4$ as the catalyst support (*n*- C_7 conversion, 88% at 250 °C) is much higher than that for $\text{Pt}/\text{WO}_3/\text{ZrO}_2$ with ZrO_2 as the support (*n*- C_7 conversion, 9% at 250 °C) with the same Pt and WO_3 loadings. BET, SEM-EDX, and pyridine-FTIR analyses show that acid treatment can successfully enhance the surface area (from 73 to 91 m^2/g), increase the number of Brønsted acid sites, and lower the surface Zn:Zr ratio (from 0.43 to 0.15) for $\text{ZnO}-\text{ZrO}_2$ with 22 wt% ZnO . The yield of C_7 isomers is increased from nil to 47% at 300 °C on $\text{Pt}/\text{WO}_3/\text{ZnO}-\text{ZrO}_2$ catalyst after acid treatment. It is suggested that *n*-heptane hydroisomerization activity is related to acidity, surface area, and crystalline phase of ZrO_2 .

Colonna et al.[62] to study a combined atomic force microscopy (AFM) and X-ray photoelectron spectroscopy (XPS) study of tungsten oxide model catalysts is presented. The model catalysts were prepared by applying the real preparation method to a $\text{ZrO}_2(100)$ single crystal support. AFM imaged several granular structures of scattered dimensions on the surface of $\text{ZrO}_2(100)$ in the as prepared samples. After heating, at low loading the tungsten species rearranged into small WO_x particles strongly interacting with the substrate. At high tungsten content large WO_3 aggregates also formed. XPS analysis confirmed these changes. The estimated surface density of the interacting W-containing species closely matched that of real catalysts.

Parida et al.[63] to study the effect of W concentration and activation temperature of the catalysts a series of WO_x/ZrO_2 samples with varying concentration of W (10–25 wt.%) were prepared and activated at 650/750 °C. XRD of sample shows 15 wt.% W stabilizes the tetragonal phase of zirconia up to 750 °C. Above and less than 15 wt.%

shows peaks corresponding to monoclinic WO_3 and monoclinic ZrO_2 , respectively. Further, the tungsten modification stabilizes the specific surface area of ZrO_2 . There is an increase in the surface area observed up to 15 wt.% W, which declines of further increase in the concentration. The NH_3 TPD confirms the presence of acid sites with varying strength from the broad desorption profile. The 15 wt.% W and activated at 750°C shows maximum acidity. The results of the nitration reaction of chlorobezene imply the 15 wt.% W and activation at 750°C shows maximum activity. Not only yield, a better *para*-selectivity is also achieved with WO_3/ZrO_2 samples. Effect of activation temperature, W concentration and reaction parameters such as reaction temperature, reaction time, the presence of solvent and solvent free medium on activity and selectivity are studied in details.

Haiyan et al.[64] investigated the synthesis of nanostructure porous tungsten-promoted zirconia (WO_3/ZrO_2) has been performed by hydrolyzing zirconium *iso*-propoxide in the presence of cationic surfactant: etyltri methyl ammonium bromide (CTAB). The structure of the sample was characterized by X-ray diffraction (XRD), N_2 adsorption–desorption and transmission electron microscopy (TEM). Thermal chemical behavior and acidity were studied by thermal gravimetric and differential thermal analysis (TG-DTA) and NH_3 -temperature-programmed desorption (NH_3 -TPD), respectively. The *iso*-butane/butene alkylation on WO_3/ZrO_2 was carried out in a fixed bed reactor. The results revealed that WO_3/ZrO_2 sample prepared through a surfactant-assisted route had good structure characteristics (such as high percent of t- ZrO_2 , high surface area and large pore diameter) and moderate acidity for the alkylation of butene with *iso*-butane. The catalytic performance of WO_3/ZrO_2 sample was also much better than that prepared by inipient wetness impregnation and sol–gel method. A parallel relationship could be drawn between the catalytic activity and the acid amounts as well as the acidic strength of the catalysts.

A. Marica et al.[65] to study $\text{WO}_3\text{--ZrO}_2$ samples were obtained by precipitating zirconium oxynitrate in presence of WO_4 Q species in solution from ammonium metatungstate at $\text{pH} \sim 10.0$. Samples were characterized by atomic absorption

spectroscopy, thermal analysis, X-ray diffraction, Raman spectroscopy, X-ray photoelectron spectroscopy, high-resolution transmission electron microscopy and energy filtered-TEM. The ammonia retained in the dried sample produced a reductive atmosphere to generate W^{5+} ions coexisting with W^{6+} ions to produce a solid solution of tungsten in the zirconia lattice to stabilize the zirconia tetragonal phase when the sample was annealed at 560 °C. When the sample was annealed at 800 °C, the W atoms near crystallite surface were oxidized to W^{6+} , producing patches of WO_3 on the zirconia crystallite. The HR-TEM analysis confirmed the existence of the solid solution when the sample was annealed at 560 °C, and two types of crystalline regions were identified: One with nearly spherical morphology, an average diameter of 8 nm and the atomic distribution of tetragonal zirconia. The second one had a non-spherical morphology with well-faceted faces and dimensions larger than 30 nm, and the atom distribution of tetragonal zirconia. When samples were annealed at 800 °C two different zirconia crystallites were formed: Those where only part of the dissolved tungsten atoms segregated to crystallite surface producing patches of nanocrystalline WO_3 on the crystallite surface of tetragonal zirconia stabilized with tungsten. The second type corresponded to monoclinic zirconia crystallites with patches of nanocrystalline WO_3 on their surface. The tungsten segregation gave rise to the WO_3 - ZrO_2 catalysts.

Ankur et al.[66] report that the liquid-phase acylation of veratrole with acetic anhydride and alkylation of toluene with 1-dodecene were carried out over WO_x/ZrO_2 solid acid catalysts. The catalysts were prepared by wet impregnation method using zirconium oxyhydroxide and ammonium metatungstate. Catalysts with different WO_3 loading (5–30 wt.%) were prepared and calcined at 800 °C and catalyst with 15% WO_3 was calcined from 650 to 850 °C. All the catalysts were characterized by nitrogen adsorption, XRD and NH_3 -TPD. The catalyst with 15% WO_3 calcined at 800 °C (15 WZ-800) was found to be the most active in acylation and alkylation reactions. The effect of temperature, molar ratio and catalyst weight on the conversions of acetic anhydride and dodecene were studied in detail. The catalyst 15 WZ-800 gave 67% acetic anhydride conversion in veratrole acylation under the reaction conditions of 70 °C, veratrole/acetic

anhydride molar ratio 2, time 4 h and 99% dodecene conversion with >99% monododecyl toluene selectivity at 100 °C, toluene/1-dodecene molar ratio 10 and time 1 h.

Colonna et al.[67] investigated a combined atomic force microscopy (AFM) and X-ray photoelectron spectroscopy (XPS) study of tungsten oxide model catalysts is presented. The model catalysts were prepared by applying the real preparation method to a ZrO₂(100) single crystal support. AFM imaged several granular structures of scattered dimensions on the surface of ZrO₂(100) in the as prepared samples. After heating, at low loading the tungsten species rearranged into small WO_x particles strongly interacting with the substrate. At high tungsten content large WO₃ aggregates also formed. XPS analysis confirmed these changes. The estimated surface density of the interacting W-containing species closely matched that of real catalysts

Rossi et al.[76] report that the activity of WO_x/ZrO₂ (ZW) catalysts for *n*-butane isomerization was investigated in the temperature range 423–673 K. Reference samples of crystalline WO₃ and ZrO₂ displayed low catalytic activity. When ZW catalysts were calcined at 873 or 1073 K, samples prepared from amorphous hydrous zirconia showed activity levels—both on area rate and turnover frequency per total tungsten bases—that were 1 order of magnitude higher than those of the samples prepared from crystalline zirconia. The higher the calcination temperature in the range 873–1073K the higher was the activity. The deactivation due to coking was fast, but treatment with flowing oxygen at 773 K completely restored the catalytic activity for several cycles. The activity decrease with time on stream was satisfactorily described up to 623K by the empirical equation $r = at - n$. Active isomerization sites in the catalysts produced coke (average composition H/C = 1.5). The presence of hydrogen in the reactant stream substantially decreased the deactivation rate, most probably by hindering the dehydrogenation reactions which ultimately lead to coke formation. Treating catalysts in hydrogen at 673 or at 443 K before the reaction shortened the induction period, suggesting that hydrogen adsorption had a role in generating hydroxyls active for the isomerization (Brønsted acid

sites). The activity trend with surface density of tungsten indicated a polynuclear isomerization site.

2.2 Tungsten support on zirconia catalysts and other catalysts for transesterification reaction.

Lo'pez et al.[7] to study the fundamental insight into the transesterification of triglycerides on solid catalysts. In an effort to identify catalyst characteristics that would be ideal for biodiesel synthesis, this study compared the catalytic activity of a number of solid and liquid catalysts in the transesterification of triacetin with methanol at 60 °C. And report that (1) homogeneous catalysts were more active than heterogeneous ones on a weight basis, (2) the solid acids studied underwent less deactivation than ETS-10 (Na, K) under these experimental conditions, (3) internal mass transfer limitation may have severely limited the performance of microporous heterogeneous acid catalysts, such as ETS-10 (H) and zeolite Hb, (4) Amberlyst-15, SZ, Nafion NR50 and WZ showed reasonably good activities at this moderate temperature(60°C), indicating that there are suitable alternatives to the homogeneous catalysts without the drawbacks of corrosion, difficulty in handling, and once through use provided more mass of catalysts is used, and finally (5) on a site basis SZ exhibited the same activity as sulfuric acid, suggesting that, since their acid strengths are similar, probably follow similar reaction mechanisms.

Sankar et al.[56] to study dimethyl carbonate synthesis with 80 mol% yield is achieved through transesterification of ethylene carbonate with methanol at ambient conditions (RT and atmospheric pressure) using alkali and alkaline-earth tungstates as solid catalysts. The catalysts are efficient even at the subambient temperatures. Reactions under CO₂ pressure indicate that CO₂ atmosphere retards the transesterification reaction completely below 100 °C. Experimental conditions of 150 °C and 3.4 MPa CO₂ pressure are required to obtain maximum DMC yield of 71 mol%. Synthesis of DMC by one-pot synthesis using epoxide, CO₂ and methanol is not as effective as that by two-step method with the present catalyst system. Raman and IR spectra of methanol-interacting tungstates

indicate the formation of a methoxide ion species adsorbed at the catalyst surface as one possible reaction intermediates.

Lo'pez et al.[1] report that the liquid-phase transesterification of triacetin with methanol at 60 °C and esterification of acetic acid with methanol at 60°C (liquid phase) and 120°C (gas phase) were investigated to characterize the effect of calcination temperature on tungstated zirconia catalytic activity. The results showed a strong influence of calcination temperature on the activity for both of these reactions. The most active form of WZ occurred at a surface WO_x density of 6.6 W-atoms nm^{-2} , higher than that required for saturation coverage (5–6 W-atoms nm^{-2}). The increase in esterification and transesterification catalytic activity coincided with the formation of polymeric tungsten species in the presence of the tetragonal phase of the ZrO_2 support. The activity drop at high WO_x surface densities (>6.6 W atoms nm^{-2}) is attributed to the loss of active sites. Selective poisoning experiments showed that Brønsted acid sites apparently contribute most of the activity. The optimum calcinations temperature for WZ was identical for all transesterification and esterification conditions studied. The aqueous exchangetitration method used for estimation of acid site density was better able to predict the catalytic activity than the NH_3 -TPD method.

Ayhan Demirbas.[68] report that sunflower seed oil was subjected to the transesterification reaction with calcium oxide (CaO) in supercritical methanol for obtaining biodiesel. Methanol is used most frequently as the alcohol in the transesterification process. Calcium oxide (CaO) can considerably improve the transesterification reaction of sunflower seed oil in supercritical methanol. The variables affecting the methyl ester yield during the transesterification reaction, such as the catalyst content, reaction temperature and the molar ratio of soybean oil to alcohol, were investigated and compared with those of non-catalyst runs. The catalytic transesterification ability of CaO is quite weak under ambient temperature. At a temperature of 335 K, the yield of methyl ester is only about 5% in 3 h. When CaO was added from 1.0% to 3.0%, the transesterification speed increased evidently, while when the catalyst content was further enhanced to 5%, the yield of methyl ester slowly reached

to a plateau. It was observed that increasing the reaction temperature had a favorable influence on the methyl ester yield. In addition, for molar ratios ranging from 1 to 41, as the higher molar ratios of methanol to oil were charged, the greater transesterification speed was obtained. When the temperature was increased to 525 K, the transesterification reaction was essentially completed within 6 min with 3 wt% CaO and 41:1 methanol/oil molar ratio.

Davi A.C. Ferreira et al.[69] In this work, they present the results obtained from the methanolysis of soybean oil using tin(IV)-based commercial compounds as catalysts. In order to characterize the behavior of such catalytic systems in the reaction medium, different reaction times, temperatures and catalyst amounts were used. The efficiency of the catalytic system in terms of yield (% of fatty acid methyl esters formed) varies in the following order: dibutyltin dilaurate > di-n-butyl-oxo-stannane > modified di-n-butyl-oxo-stannane > butylstannic acid. Parameters as degree of solubility of the catalyst and rate stirring were also investigated.

Dora E. López et al.[70] report that although homogeneous alkali catalysts (e.g., NaOH) are commonly used to produce biodiesel by transesterification of triglycerides (vegetable oils and animal fats) and methanol, solid acid catalysts, such as acidic resins, are attractive alternatives because they are easy to separate and recover from the product mixture and also show significant activity in the presence of fatty acid impurities, which are common in low-cost feedstocks. To better understand solid acid catalyst performance, a fundamental transesterification kinetic study was carried out using triacetin and methanol on Nafion® (perfluorinated-based ion-exchange resin) catalysts. In particular, Nafion® SAC-13 (silica-supported Nafion) and Nafion® NR50 (unsupported Nafion) were investigated, because both show great promise for biodiesel-forming reactions. The reaction kinetics for a common homogeneous acid catalyst (H₂SO₄) were also determined for comparison. Liquid-phase reaction was performed at 60 °C using a stirred batch reactor. The swelling properties of the resin in solvents of diverse polarity that reflect solutions typically present in a biodiesel synthesis mixture were examined. The initial reaction rate was greatly affected by the extent of swelling of the resin, where, as

expected, a greater effect was observed for Nafion® NR50 than for the highly dispersed Nafion® SAC-13. The reaction orders for triacetin and methanol on Nafion® SAC-13 were 0.90 and 0.88, respectively, similar to the reaction orders determined for H₂SO₄ (1.02 and 1.00, respectively). The apparent activation energy for the conversion of triacetin to diacetin was 48.5 kJ/mol for Nafion® SAC-13, comparable to that for H₂SO₄ (46.1 kJ/mol). Selective poisoning of the Brønsted acid sites on Nafion® SAC-13 using pyridine before transesterification revealed that only one site was involved in the rate-limiting step. These results suggest that reaction catalyzed by the ion-exchange resin can be considered to follow a mechanism similar to that of the homogeneous catalyzed one, where protonated triglyceride (on the catalyst surface) reaction with methanol is the rate-limiting step.

Vicente et al.[71] to study consists of the development and optimisation of the potassium hydroxide-catalysed synthesis of fatty acid methyl esters (biodiesel) from sunflower oil. A factorial design of experiments and a central composite design have been used. The variables chosen were temperature, initial catalyst concentration by weight of sunflower oil and the methanol:vegetable oil molar ratio, while the responses were biodiesel purity and yield. The initial catalyst concentration is the most important factor, having a positive influence on biodiesel purity, but a negative one on biodiesel yield. Temperature has a significant positive effect on biodiesel purity and a significant negative influence on biodiesel yield. The methanol:vegetable oil molar ratio is only significant for the biodiesel purity, having a positive influence. Second-order models were obtained to predict biodiesel purity and yield as a function of these variables. The best conditions are 25°C, a 1.3% wt for the catalyst concentration and a 6:1 methanol:sunflower oil molar ratio.

Stavarache et al.[72] to study the batch transesterification of vegetable oil with methanol, in the presence of potassium hydroxide as catalyst, by means of low frequency ultrasound (40 kHz) was studied with the aim of gaining more knowledge on intimate reaction mechanism. The concentration of fatty acid methyl esters, of mono-, di- and triglycerides of the actual reaction mixture were determined at short reaction time by

HPLC. The effect of ultrasounds on the lipids transesterification correlated with triglyceride structures is discussed. It was found that under ultrasonic activation the rate-determining reaction switches from $DG \rightarrow MG$ (classical mechanic agitation) to $MG + ROH \rightarrow Gly + ME$ (ultrasonically driven transesterification).

Ferreira et al.[73] In this work, they present the results obtained from the methanolysis of soybean oil using tin(IV)-based commercial compounds as catalysts. In order to characterize the behavior of such catalytic systems in the reaction medium, different reaction times, temperatures and catalyst amounts were used. The efficiency of the catalytic system in terms of yield (% of fatty acid methyl esters formed) varies in the following order: dibutyltin dilaurate > di-n-butyl-oxo-stannane > modified di-n-butyl-oxo-stannane > butylstannoic acid.

2.3 General of defect in zirconia and technique to detect it.

Huiwen Liu et al.[12]. Report that nano-ZrO₂ has two kinds of ESR signals. They can be assigned to bulk Zr³⁺ and surface F-center paramagnetic centers, respectively. Zr³⁺ ESR signal is a bulk-related signal, while the F-center signal is surface related. Therefore, the F-center signal intensity increases with a S_{BET} increase while the Zr³⁺ signal intensity changes in reverse. The critical value of nano particle size above which the F-center signal is negligible is about 50 nm. Study of tetragonal nano-ZrO₂ samples indicates that their F-center ESR signal is closely related to their S_{BET} value or particle size rather than their crystallite size.

Zhao et al.[11] report that the surface properties of ZrO₂ in He, H₂, O₂, air and wet air at temperatures ranging from 25 to 600°C have been investigated by means of ESR method. The Zr³⁺ centers characterized by ESR can be described as the oxygen coordinatively unsaturated Zr sites, mainly located at the corner sites of ZrO₂ microcrystallites, on the surface of ZrO₂. More Zr³⁺ centers were formed on the surface of ZrO₂ by treating the sample in He at temperatures above 400 °C. And the formation of

the Zr^{3+} centers may be associated with the removal of surface hydroxyl. Although Zr^{4+} in ZrO_2 cannot be reduced at temperatures of up to 600 °C in H_2 , some surface hydroxyl can be reduced to form F-centers at temperatures higher than 250 °C. And O^{2-} can be produced from the Zr^{3+} centers and F-centers at temperatures above 400 °C, and it may be associated with both H_2 and the trace amount of O_2 in H_2 .

Morterra et al.[75] report that CO adsorption at room temperature, followed by means of in situ FTIR spectroscopy, and EPR spectroscopy have been used to demonstrate the formation, by vacuum thermal activation, of coordinatively unsaturated (cus) Zr^{3+} centers at the surface of monoclinic ZrO_2 . The same techniques have also been adopted for a preliminary characterization of the reactivity of (cus) Zr^{3+} centers: they turn out to be highly resistant to oxidation by molecular oxygen, whereas they interact with water and with carbon dioxide, yielding more easily coordinatively saturated configurations, still reduced, rather than undergoing oxidation to the $4+$ state.

Gregorio and V. Keller.[36] report that the structure of the ZrO_2 support (monoclinic or tetragonal) and thus the preparation procedure has no influence, neither on the nature and surface structure of deposited tungstate species nor on their reducibility. This is essential in the explanation of the catalytic properties in the skeletal isomerization observed with monoclinic ZrO_2 support, as will be presented and discussed in the forthcoming Part II. Whatever the structure of the ZrO_2 support, catalysts with near-saturation monolayer coverages are mainly constituted of amorphous tungstate species in which the tungsten atoms are tetrahedrally coordinated, in direct interaction with the support and thus very difficult to reduce. The increase in tungsten loading leads progressively to the formation of tungstate species in which the tungsten is in octahedral coordination, that is more easy to reduce. The reduction of these species yields W(IV) surface species. A further increase of the tungsten content leads to the formation of WO_3 crystallites behaving as bulk-like tungsten oxide and resulting first in β -W (WO_3) metallic phase for reduction at 723K and finally in pure α -W metallic phase for more intense reduction treatments.

Ilieva et al.[37] report that the reduction behavior of gold supported catalysts on mesoporous titania and zirconia was studied. The TPR, ESR, HRTEM and XPS methods were applied for the characterization of the state and structure of the catalysts. It was established that the nature of support plays a decisive role in the reactivity of the catalysts, in particular in their redox properties. The mesoporous nanostructured materials used in this study as supports for gold nanoparticles show very different behavior under hydrogen treatment. The ability of nanostructured zirconia to create F-centers leads to different charging of the supports surface, i.g. the supported gold nanoparticles which is the main reason for the observed differences between the both studied gold supported catalysts on mesoporous titania and zirconia.

Martínez et al.[39] report that two series of tungstated zirconia (WZ) solid acids covering a wide range of tungsten surface densities (δ , Wat/nm²) were prepared by nonconventional impregnation and coprecipitation routes, leading to samples with enhanced surface area (.70–120 m²/g) on annealing at 973–1073 K. The materials were thoroughly characterized by N₂ physisorption, XRD, Raman, XPS, H₂-TPR, and DR UV-vis spectroscopy. The catalytic behavior of the Pt-promoted WZ catalysts (1 wt% Pt) was evaluated for the hydroconversion of *n*-hexadecane used as model feed representative of Fischer–Tropsch waxes. Both series of catalysts displayed a pronounced maximum in the reaction rate and a minimum in the selectivity to branched feed isomers (*iso*-C16) at an intermediate tungsten density (δ_{\max}). Interestingly, we found that δ_{\max} shifted toward higher values for coprecipitated catalysts ($\delta_{\max, \text{COP}} = 6.8$ Wat/nm²) compared with the impregnated ones ($\delta_{\max, \text{IMP}} = 5.2$ Wat/nm²). This has been ascribed to a better inherent capacity of the coprecipitation route for dispersing tungsten species on the ZrO₂ surface, as inferred from modeled XPS data. This determines that both the formation of highly interconnected amorphous WO_x domains required for the generation of catalytically active Brønsted acid sites and the onset of growth of inactive three-dimensional WO₃ crystallites (ascertained by XRD and Raman) occur at higher tungsten surface densities in WZ solids generated by coprecipitation than in those obtained by impregnation. Despite the observed shift in δ_{\max} , the two most active samples within each series displayed

nearly the same intrinsic activity per total W atoms, suggesting that a similar nature and size for the supported active WO_x domains should be attained by both impregnation and coprecipitation routes at $\delta = \delta_{\text{max}}$. Moreover, the method of preparation was found to affect the optical and electronic properties of the supported WO_x species. Thus, coprecipitation provides WZ solids displaying a lower valence–conduction energy gap, as well as enhanced reducibility for the polytungstate domains due to an improved electronical linkage with the zirconia support, in opposition to a more isolated character of the WO_x clusters generated by impregnation.

Onfroy et al.[51] report that relationship between the acidity, catalytic activity, and surface structure for tungsten oxide supported on zirconia was investigated for a series of solids prepared by equilibrium adsorption on monoclinic zirconia. The catalysts were active for propanol dehydration only above a threshold in W loading. The acidity was studied by infrared spectroscopy of adsorbed probe molecules (2,6-dimethylpyridine and CO), and the onset of activity was correlated with that of the formation of relatively strong Brønsted acid sites. The variation in the abundance of these sites correlated with the catalytic activity. Lewis sites were present but could not be directly associated with the activity. Raman, IR, and UV spectroscopy results indicated that the active sites were related to polymeric W surface species.

Elsevier B.V. et al.[41] Report that in the present work, they provide evidence of an increase in the Zr^{3+} paramagnetic center concentration under colloidal transformation in ZrO_2 prepared by the totally inorganic sol–gel method. The samples of thermally treated (100–950 °C in air) ZrO_2 precipitates and dried sol–gel products—xerogels—were examined by TEM, XRD, DTA, EPR and IR-spectroscopy. Under the same heat treatment condition, the concentration of Zr^{3+} (axially symmetric signal at $g = 1.977$ – 1.979 and $g = 1.958$ – 1.963) became higher in the xerogel samples rather than in precipitate samples and reached the maximum (0.1018 g in xerogel) after calcinations at 500°C in air.

Matsunashi et al.[57] report that reversible formation of F^+ -centers was observed over platinum promoted sulfated zirconia in the presence and absence of hydrogen. The intensity of ESR signal of F^+ centers was increased by treatment in He stream and it was decreased rapidly by supply of hydrogen in gas phase. This behavior seems to be related to proton spillover.

Foster et al.[58] they performed plane wave density functional theory (DFT) calculations of formation energies, relaxed structures, and electrical levels of oxygen vacancies and interstitial oxygen atoms in monoclinic zirconia. The atomic structures of positively and negatively charged vacancies and interstitial oxygen atoms are also investigated. The ionization energies and electron affinities of interstitial oxygen atoms and oxygen vacancies in different charge states are calculated with respect to the bottom of the zirconia conduction band. Using the experimental band offset values at the interface of ZrO_2 films grown on silicon, we have found the positions of defect levels with respect to the bottom of silicon conduction band. The results demonstrate that interstitial oxygen atoms and positively charged oxygen vacancies can trap electrons from the bottom of the zirconia conduction band and from silicon. Neutral oxygen vacancy serves as a shallow hole trap for electrons injected from the silicon valence band. The calculations predict negative U for the O_2 center and stability of V1 centers with respect to disproportionation into V21 and V0 in monoclinic zirconia.

Onfroy et al.[74] report that the relationship between the acidity, catalytic activity, and surface structure for tungsten oxide supported on zirconia was investigated for a series of solids prepared by equilibrium adsorption on monoclinic zirconia. The catalysts were active for propanol dehydration only above a threshold in W loading. The acidity was studied by infrared spectroscopy of adsorbed probe molecules (2,6-dimethylpyridine and CO), and the onset of activity was correlated with that of the formation of relatively strong Brønsted acid sites. The variation in the abundance of these sites correlated with the catalytic activity. Lewis sites were present but could not be directly associated with the activity. Raman, IR, and UV spectroscopy results indicated that the active sites were related to polymeric W surface species.

Bobricheva et al.[78] report that ESR spectroscopy was used to investigate paramagnetic sites in sulfated zirconia. Catalysts derived from zirconium oxide and zirconium hydroxide were studied. It was demonstrated that paramagnetic sites assigned to near-surface F-centers were formed during activation at temperatures above 573 K. The catalyst derived from zirconium hydroxide shows after activation at 873 K two types of paramagnetic sites: F-centers and Zr^{3+} sites. Both F-centers and Zr^{3+} sites in this catalyst form complexes with reagents upon *n*-butane or hydrogen adsorption at range of 423–523 K in contrast to paramagnetic sites of the oxide-derived catalyst.

Loridant et al.[79] report that W/ZrO₂ catalysts were prepared using anionic exchange of peroxotungstate species with hydroxyl groups of zirconium hydroxide at low pH. The solids were dried and calcined under air at 700 °C. Each step of this novel method of preparation was investigated by Raman spectroscopy. A reference sample was also prepared by incipient wetness impregnation of ZrO₂·*n*(H₂O) with an ammonium tungstate solution and characterized throughout its preparation process. Complementary data were collected from X-ray diffraction, chemical analysis, surface area measurements, and thermal analysis. The Raman spectra of the H₂WO₄-H₂O₂ precursor solutions evidenced the presence of (W₂O₃(O₂)₄(H₂O)₂)₂⁻ dimers. These low nuclearity species were exchanged with zirconium hydroxide at low pH. The Raman spectra of the dried solids did not reveal peroxotungstate species but were typical of tetrahedral (WO₄)₂⁻ species. A slight agglomeration of W species was observed with an increase in the W content. However, for an equivalent W loading, a higher W dispersion was obtained by anionic exchange, compared to the impregnation method. Furthermore, a remarkable homogeneity of the exchanged samples was evidenced by the micro-Raman spectra. The in situ Raman spectra recorded during calcination characterized both crystalline phases and supported tungsten species. Significant modifications were observed during the calcination process. The exchanged and the impregnated samples, with the same W loading, evidenced a similar type of tungsten species with one WdO bond. However, their behavior during calcination up to 700°C was different. This was attributed to different strengths of interaction with the support. Moreover, the spectra recorded after calcination

on various points of the exchanged sample with a high W content revealed a better spatial homogeneity than the impregnated one.

Khaodee et al.[80] this paper studied the effect of temperature ramping rate during calcination on characteristics of nanoscale zirconia and its catalytic performance for isosynthesis. The physical properties, i.e. BET surface area, cumulative pore volume, cumulative pore diameter and the phase composition in zirconia, acid-base properties and surface properties such as Zr^{3+} quantity, were characterized. Increase in the temperature ramping rate of calcinations resulted in a higher composition of the tetragonal phase, but it showed insignificant influence on the other physical properties. Considering the catalytic activity, the acid sites did not affect the activity, but the basic sites depended on the fraction of the tetragonal phase in zirconia which was related to the selectivity to isobutene. The intensity of Zr^{3+} on the surface varied with the change in the heating rate of calcination. Both the tetragonal phase composition in zirconia and the quantity of Zr^{3+} were the key factors affecting the selectivity to isobutene in hydrocarbons. Moreover, the maximum value of the product selectivity to isobutene on the ZrO_2 (5.0) catalyst was attained at the highest concentration of Zr^{3+} .

Ivanovskaya et al.[81] to study the nature of paramagnetic defects in nanosized ZrO_2 samples prepared by the sol-gel method was studied by ESR. Conditions of formation of different centers (Zr^{3+} , F centers, $O^{\cdot-}$, $O_2^{\cdot-}$) in ZrO_2 were elucidated. The Zr^{3+} and $O^{\cdot-}$ centers arise in the course of thermal dehydration of $Zr(OH)_4$ under the conditions when the formation of a Zr, O, Zr bridging bond is hindered. The F centers are formed in ZrO_2 on heating in a reducing atmosphere or as a result of structural rearrangements accompanied by a decrease in the amount of lattice oxygen in the coordination surrounding of Zr(IV).

Sandra et al.[13] report that Electron paramagnetic resonance (EPR) measurements have been made on a variety of commercially available samples of the monoclinic form of the high-dielectric constant (high k) materials ZrO_2 and HfO_2 with the aim of characterizing the defects they contain. All EPR measurements were at about

9.5GHz and at room temperature. An axially symmetric spectrum with $g = 1:961(2)$, $g = 1:976(2)$ is observed in most of the ZrO_2 samples and a similar one with $g = 1:940(3)$, $g = 1:970(2)$ is seen for most of the HfO_2 samples; they are attributed to centres involving Zr^{3+} and Hf^{3+} , respectively.

Their average concentration lies in the approximate range $1015\text{--}1017\text{ cm}^{-3}$, depending on the product specification, and, with one exception is unaffected by g-irradiation. Grinding granules to powder and/or g-irradiation yields further EPR spectra of defects, some of which are likely to involve oxygen, those are probably in the near surface region.

Ashutosh et al.[16] to study reactions of $Zr(OiPr)_4(PriOH)$ with di- and trichloroacetic acid in 1:1 molar ratio in toluene gave the products $Zr_2(l-OiPr)_2(lOOCCHCl_2)(OiPr)_4(OOCCHCl_2)(HOiPr)$ (1) and $r_2(lOiPr)_2(lOOCCL_3)(OiPr)_4(OOCCL_3)(HOiPr)$ (2), respectively, in quantitative yields. The molecular geometry of both (1) and (2) is constituted by a slightly distorted edge-shared bioctahedron and both have almost similar bond dimensions. Addition of dichloroacetic acid in 1:2 molar ratio to $Zr(OiPr)_4(HOiPr)$ in toluene although yielded the bisubstituted crude product $Zr(OiPr)_2(OOCCHCl_2)_2(HOiPr)$ (3) but its solution in toluene left for crystallization formed a tri-nuclear oxo product $Zr_3(l_3-O)(l-OiPr)_2(l-OOCCHCl_2)_3(g-OOCCHCl_2)_2(OiPr)_3$ (3a). The three zirconium atoms in the structure of (3) are forming an isosceles triangle with a triply bridged oxo moiety at its center.

สถาบันวิทยบริการ
จุฬาลงกรณ์มหาวิทยาลัย

CHAPTER III

THEORY

3.1 General feature of zirconia

Zirconia exhibits three polymorphs, the monoclinic, tetragonal, and cubic phases. As shown in Figure 3.1, crystal structures of cubic, tetragonal and monoclinic zirconia are shown in Figure 3.1.1. The monoclinic form is stable up to $\sim 1170^{\circ}\text{C}$, at which temperature it transforms into the tetragonal phase, which is stable up to 2370°C [50]. The stabilization of the tetragonal phase below 1100°C is important in the use of zirconia as a catalyst. Above 2370°C , the cubic phase is stable and it exists up to the melting point of 2680°C . Due to the martensitic nature of the transformations, neither the high temperature tetragonal nor cubic phase can be quenched in rapid cooling to room temperature. However, at low temperature, a metastable tetragonal zirconia phase is usually observed when zirconia is prepared by certain methods, for example by precipitation from aqueous salt solution or by thermal decomposition of zirconium salts. This is not the expected behaviors according to the phase diagram of zirconia (i.e., monoclinic phase is the stable phase at low temperatures). The presence of the tetragonal phase at low temperatures can be attributed to several factors such as chemical effects, (the presence of anionic impurities) [31,32] structural similarities between the tetragonal phase and the precursor amorphous phase [32,33-34] as well as particle size effects based on the lower surface energy in the tetragonal phase compared to the monoclinic phase [32-33]. The transformation of the metastable tetragonal form into the monoclinic form is generally complete by $650\text{-}700^{\circ}\text{C}$.

Crystal system	Unit cell shape
Monoclinic	$a \neq b \neq c, \alpha = \gamma = 90^{\circ}, \beta \neq 90^{\circ}$
Tetragonal	$a = b \neq c, \alpha = \beta = \gamma = 90^{\circ}$
Cubic	$a = b = c, \alpha = \beta = \gamma = 90^{\circ}$

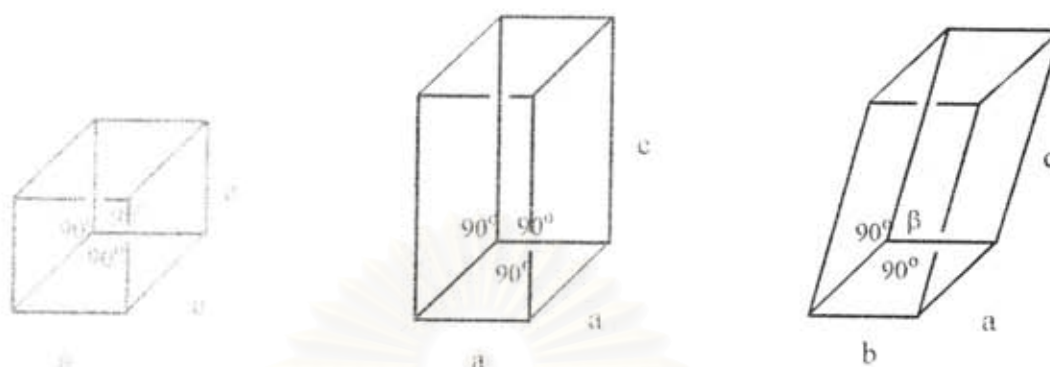


Figure 3.1 : The unit cells of the crystal systems.[35]

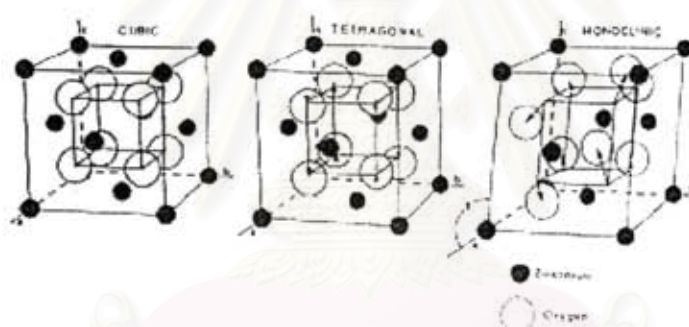


Figure 3.2 : Crystal structure of cubic, tetragonal and monoclinic zirconia.
(Heuer, 1987)

3.1.1 The formation of zirconia in glycol solvent

When 1,4-butanediol (1,4-BG) was used, pure tetragonal zirconia was obtained at 300°C for 2 h. For the reaction in 1,4-butanediol, the cleavage of the C-O bond was also accelerated by the participation of the intramolecular group forming tetrahydrofuran, which was actually detected by a gas chromatographic analysis of the supernatant after the reaction in 1,4-BG (Inoue, M.; Kominami, H.; and Inui, T., 1993)

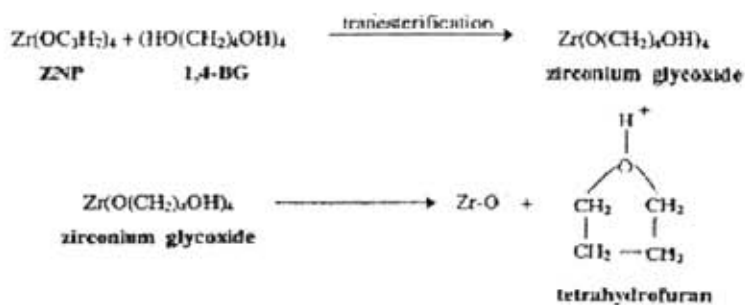


Figure 3.3 : Mechanism of glycothermal-derived ZrO_2

3.2 Defects structure of crystal material.

3.2.1 Vacancies: Schottky defects

Consider the simplest crystal defect, namely that of an atomic site becoming vacant, with the missing atom migrating to the crystal surface. This process will be energetically unfavorable, costing the system a change in energy.

The simple case of a vacant site is called a Schottky defect. In order to maintain a neutral charge distribution across a local length scale, it is common for both positive and negative vacant sites to be produced in thermal equilibrium and to be evenly distributed throughout the sample. This is represented in Figure 3.2.1

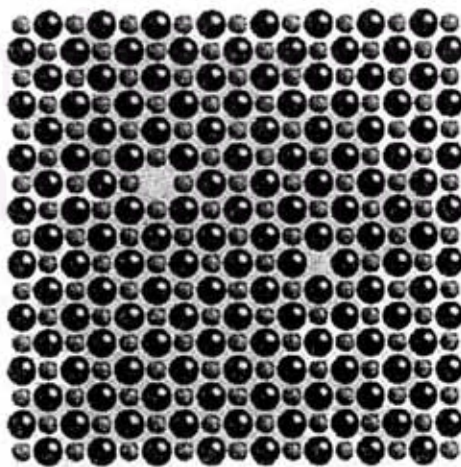


Figure 3.4 : Cation and anion charge-balanced Schottky defects in NaCl.

3.2.2 Interstitial defects: Frenkel defects

In crystals that do not pack with high efficiency, it is possible for atoms to occupy sites that are normally vacant, called interstitial sites. A Frenkel defect occurs when an atom leaves its normal site to create a vacancy, and is then displaced into one of the interstitial sites. This process is illustrated in Figure 3.2.2.

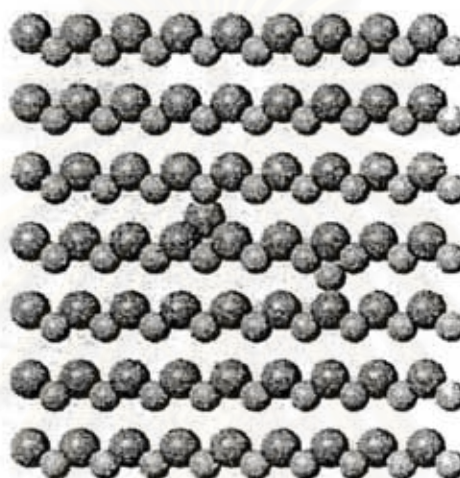


Figure 3.5 : Pair of charge-balanced Frenkel defects in AgI.

3.2.3 Coupled charge substitutions and vacancies

The vacancies that mentioned above occur as equilibrium processes. Other point defects can be produced as non-equilibrium structures through the process of crystal growth. A common defect is the substitution of a different type of atom, usually one of similar charge. For example, NaCl can contain K^+ defects substituting for the cation sites, or F^- substituting on the anion sites. A substitution of a different charged cation will require production of a compensating charge defect. For example, substituting a Ca^{2+} cation in NaCl will require the formation of a charge-compensating cation vacancy. This structure is illustrated in Figure 3.2.3.

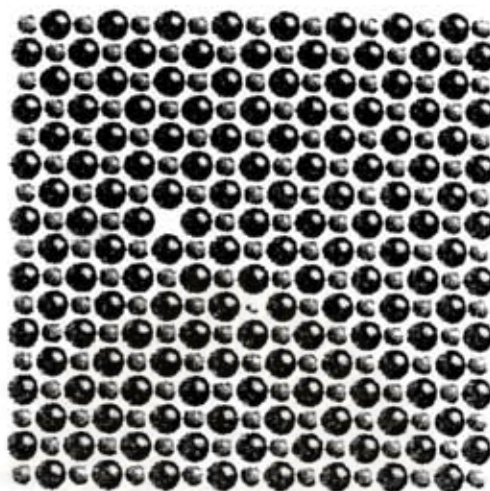


Figure 3.6 : Substitution of a Ca^{2+} cation for a Na^{+} cation in NaCl , accompanied by the formation of a vacant cation site in order to maintain charge neutrality.

3.2.4 Color centers

The charge substitutions that have been considered have been restricted to ions. It is also possible for electrons to occupy vacant anion sites in order to maintain charge neutrality. The electron forms its own energy bands. The color center is able to absorb electromagnetic radiation in the visible spectrum, and this gives color to what would otherwise be a transparent crystal. As a result, the presence of the color center can be detected in an optical absorption experiment.

3.3 Surface defects

There is a sense in which the surface itself with its coordinatively atoms is the most numerous type of defect. The bulk of the experimental results, spectroscopic or otherwise, necessarily relate to adsorption on the more numerous and expected sites on oxide surface, such as coordinatively unsaturated cations or anions, hydroxyls, acid-base pair, etc. However the most active sites will be connected with defects in the normal surface, which have unusual geometrical and/or local chemical compositional features. These may be present in concentrations that are one or two orders of magnitude less than

those of the regular sites and experimental detection can be correspondingly different.

In general, the majority of the experimental phenomena discussed above were connected with adsorption on the more numerous and expected sites on the oxide surface (coordinatively unsaturated cations, anions, hydroxyls, and their pair). However, the appearance of the most active surface centers suggests a connection with defects in the solid. The other factors influencing the properties of the real oxide surfaces are: (i) the presence of different lattice defects in the surface layer, and (ii) their chemical composition, which in many cases, may differ from that in the bulk.

In spite of the fact that the concentration of the defect centers on the surface is one or even two orders of magnitude less than the concentration of regular active sites, their reactivities are very often higher. This is why such defect centers can participate in the reaction.

The presence of the so-called dangling bonds (unsaturated valencies) at the surface creates electron energy states, usually named intrinsic states, which are present even in the case of pure and strictly stoichiometric surface. Additional structural defects on the surface which may be or may be not associated with adsorbed impurities, said to create extrinsic surface states.

The role of intrinsic defects in the activation of adsorbed molecules has not yet been elucidated. The physics of such defects is also still in development. In contrast, the influence of extrinsic defects on chemisorption and catalysis has been the object of many investigations.

Crystal with periodical arrangements of all of their structural elements cannot exist and real crystals show the presence of various imperfections described as defects. Those atoms into other sites or interstitial positions may due to (i) the displacement of atoms from the lattice sites normally occupy them, (ii) the presence of some vacant sites, or (iii) the displacement of part of a crystal with respect to another part along a crystal plane, etc. These defects are usually classified according to their dimensions into point

defects (vacancies interstitial or foreign atoms), linear defects (dislocations) and spatial defects such as pores or foreign inclusion. For example, besides being a strong base, the highly dehydroxylated MgO surface is a good reducing agent. The reducing sites are apparently defects, possibly surface cation vacancies: the dissociative chemisorption of Bronsted acids blocks the reactivity of the reducing sites.

Investigation of small-surface-area bulk alkali earth-metal oxides, including MgO, e.g. as single crystal, show that their photoluminescence is caused by defects in the crystalline lattice, namely by the F^+ and F^\bullet centers, i.e. the oxygen vacancies have captured one or two electrons, respectively. Such centers can be easily detected directly by EPR and/or by UV-vis spectroscopic studies of the adsorption of molecules that easily form cation or anion radicals. Detailed analysis of such spectra obtained by using molecules which different but known values of ionization potential (IP) or electron affinity, allows us to obtain information about such an adsorption center, for example, on the basis of data on the transition to the radical state, and so to make a conclusion about its redox properties.

The main method used to investigate such centers is electron paramagnetic resonance (EPR) spectroscopy. It should be remembered that the formation of radicals could proceed on the surface of practically all oxide systems, when easily ionizable adsorbates which are able to cause the formation of both main and side-reaction products, are used.

A connection with the problem of defect sites, studies of mechanically activated oxide systems seem to be very interesting and useful. It is well known that mechanical activation (by grinding) affects an increase in the number of defects formed upon mechanical activation.

Mechanical treatment is an effective method for creating defects in solids. Various mechanical activation effects are related to the formation of such defects and their subsequent chemical transformations. Some of these defects are free radicals, for example in the case of SiO_2 ($=\text{Si-O-})_3\text{Si}^\bullet$ and $(=\text{Si-O-})_3\text{SiO}^\bullet$. A new type of natural defect,

namely silanone (Si=O) groups was identified on the surface of mechanically activated SiO₂. A study was carried out by using their thermal stabilities, optical properties (a characteristic absorption band was found with a maximum at 5.3 eV) and Calcination, relative to simple molecules, such as CO₂ and N₂O, and radicals, such as H, D and CH₃. Studies of the IR and Raman spectra of the oxides MgO, Cr₂O₃, MoO₃, Co₃O₄ and CuO in the regions of the cutoff vibrations allowed identification of sample amorphization during mechanical activation and also the decrease in the coordination number of both cations and anions as compared with nonactivated oxides. The latter bring to increases in the reactivities. According to IR spectra of adsorbed CO in the case of CuO and Co₃O₄, the reduction of Cu²⁺ to Cu⁺ and Co³⁺ to Co²⁺ cations was observed during mechanical activation.

In the diffuse reflectance electron spectroscopy (DRES) spectra of MoO₃, the valence-to-conduction band transition exhibited a considerable blue shift with decreasing particle size. Excitonic absorptions observed in these spectra are also affected by the smaller particle size and by the altered crystallite surface. An increasing intensity of the bands was observed, and a linear dependence between the position of the band attributed to polaron conductance and the logarithm of the carrier concentration per Mo atom was obtained, both of these facts reveal that a sub-stoichiometric MoO_{3-x} species was formed upon mechanical treatment. According to the ESR data, both milled and non-milled MoO₃ samples contained Mo⁵⁺ centers interacting with OH groups in close vicinity, but their concentration was much smaller in the case of non-milled MoO₃. The main portion of these Mo⁵⁺ ions had C_{2v} or C_{4v} symmetry. These latter ions appear to result from the mechanical activation process and are suggested to be the precursors of a crystallographic shear structure. Exposure to O₂ reveals that all of these Mo⁵⁺ sites are located in the bulk and not necessarily on the surface, whereas free electrons are present at the surface. The high surface sensitivity of the IR technique when using adsorbed probe molecules revealed the formation of coordinatively unsaturated Mo⁴⁺ surface states in MoO₃ which was mechanically activated.

3.3.1 Definition of F-center defect

An F-center is a type of crystallographic defect*¹ in which an anionic*² vacancy in a crystal filled one or more electrons. Depending on the charge of the missing ion in the crystal. Electrons in such a vacancy tend to light in the visible spectrum, such that a material that usually transparent*³ becomes colored. Thus the origin of the name, F-center, which originates from the German Farbzentrum. The translation of this term also provides the synonym color center, which can also refer to such defects. F-centers are often paramagnetic and can then be studied by electron paramagnetic resonance techniques. The greater the number of F-centers, the more intense is the color of the compound. F-centers can be created say by passing sodium vapours over NaCl, when Cl-ions combine with the metal ions producing non-stoichiometric defects within the lattice. The metal ions producing non-stoichiometric defects within the lattice. The electrons released in this process diffuse to occupy the vacant places. Also ionizing radiation can produce F-centers.

*¹ is crystalline solids have a very regular atomic structure: that is, the local positions of atoms with respect to each other are repeated at the atomic scale. These arrangements are called crystal structures, and their study is called crystallography. However, most crystalline materials are not perfect: the regular pattern of atomic arrangement is interrupted by crystal defects. The various types of defects are enumerated here.

*² This article is about the electrically charged particle. For other uses, see Ion (disambiguation).

An ion is an atom or molecule which has lost or gained one or more electrons, making it positively or negatively charged.

A negatively charged ion, which has more electrons in its electron shells than it has protons in its nuclei, is known as an anion (pronounced /'æna,ɒn/; *an-eye-on*). Conversely, a positively-charged ion, which has fewer electrons than protons, is known as a cation (pronounced /'kæta,ɒn/; *cat-eye-on*). An ion consisting of a single atom is

called a monatomic ion, but if it consists of two or more atoms, it is a polyatomic ion. Polyatomic ions containing oxygen, such as carbonate and sulfate, are called oxyanions. Ions are denoted in the same way as electrically neutral atoms and molecules except for the presence of a superscript indicating the sign of the net electric charge and the number of electrons lost or gained, if more than one. For example: H^+ and SO_4^{2-} .

*³ In optics, transparency is the material property of allowing light to pass through. In mineralogy, another term for this property is diaphaneity. The opposite property is opacity. Transparent materials are clear: they can be seen through. Translucent materials allow light to pass through them only diffusely: they cannot be seen through.

3.4 Biodiesel

Biodiesel is an alternative fuel for diesel engines of the most renewable fuels currently available and it is also non-toxic and biodegradable that comprised of mono-alkyl esters of long chain fatty acids derived. Biodiesel can be used as B100 (neat) or in a blend with petroleum diesel. A blend of 5 %biodiesel with 95% petrodiesel, by volume, is termed "B5". (Used in Thailand). The well-known advantages of biodiesel compared with petro-diesel are: (1) lower dependence on foreign crude oil, (2) renewable resource, (3) limitation on greenhouse gas emissions because of the closed CO_2 cycle, (4) lower combustion emission profile (especially SO_x), (5) potential improvement of rural economics, (6) biodegradability, (7) use without engine modifications, (8) good engine performance, (9) improved combustion because of its oxygen content, (10) low toxicity, and finally (11) ability to be blended in any proportion with regular petroleum-based diesel fuel.

Biodiesel is produced by chemically reacting a fat or oil with an alcohol, in the presence of a catalyst. The product of the reaction is a mixture of methyl esters and this process is called transesterification. Transesterification is extremely important for biodiesel. Biodiesel as it is defined today is obtained by transesterifying the triglycerides with methanol. Methanol is the preferred alcohol for obtaining biodiesel because it is the

cheapest (and most available) alcohol. However, for the reaction to occur in a reasonable time, a substance called a catalyst (catalysts are substances that, often present in small amounts, accelerate the speed of a reaction; in many cases virtually no reaction would occur without a catalyst), must be added to the mixture of the vegetable oil and methanol.

3.4.1 Transesterification reaction

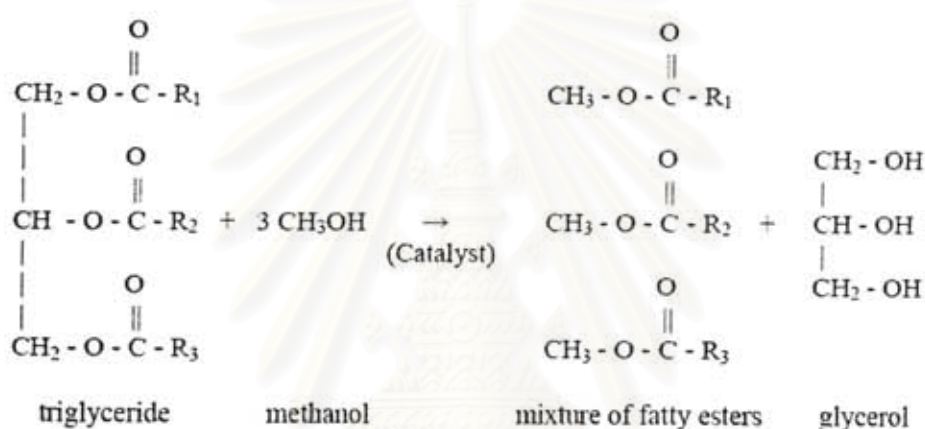


Figure 3.7 : Transesterification Reaction

where R_1 , R_2 , and R_3 are long chains of carbons and hydrogen atoms, sometimes called fatty acid chains. There are five types of chains that are common in palm oil. (others are present in small amounts):

Palmitic : $R = -(\text{CH}_2)_{14} - \text{CH}_3$ 16 carbons,

(including the one that R is attached to.) (16:0)

Stearic : $R = -(\text{CH}_2)_{16} - \text{CH}_3$ 18 carbons, 0 double bonds (18:0)

Oleic : $R = -(\text{CH}_2)_7 \text{CH}=\text{CH}(\text{CH}_2)_7\text{CH}_3$ 18 carbons, 1 double bond (18:1)

Linoleic : $R = -(\text{CH}_2)_7 \text{CH}=\text{CH}-\text{CH}_2-\text{CH}=\text{CH}(\text{CH}_2)_4\text{CH}_3$

18 carbons, 2 double bonds (18:2)

For the reaction add 100% excess methanol to ensure that the reaction goes to completion. In general, reactions can be encouraged to progress by adding an excess of one of the reactants or by removing one of the products. The reaction of triolein with 100% excess.

For the transesterification to occur, usually 6 moles of alcohol are used for every mole of triglyceride, which is more than the equation indicates. The reason is that the reaction is desired to proceed in the direction of the arrow, i.e., to the right. In other terms, the equilibrium of the reaction needs to be shifted toward the right side of the equation. As the term equilibrium indicates, not all reactions easily proceed to completion and after some time the starting materials and reaction products are present in constant amounts (the equilibrium has been attained). In many cases, the fact that a reaction can proceed in the reverse fashion (from right to left in the equation) also plays a role in formation of the equilibrium. To force the equilibrium in the direction of the products (as is almost always desired), one or more parameter(s) of the reaction may need to be changed. Such parameters include the molar ratio as well as others such as temperature, pressure and use of a catalyst.

Besides triglycerides, mono- and diglycerides can also exist. They are formed as intermediates during the transesterification reaction. This is one of the problems when conducting chemical reactions in general, not only the transesterification reaction. It is almost always the goal of chemical reactions to obtain products that are as pure as possible. However, hardly any chemical reaction proceeds to full completion (see the discussion of equilibrium above). Therefore, often intermediates (in the case of transesterification the intermediates are partially reacted triglycerides, i.e., the mono- and diglycerides) can contaminate the final product. Other materials that can contaminate biodiesel are residual methanol (or other alcohol), glycerol, and catalyst.

For in this work used triacetin is a material, so transesterification of triacetin with alcohols proceeds via three consecutive and reversible reactions where the FFA ligands combine with the alcohol to produce a fatty acid alkyl ester, diand monoglyceride intermediates, and finally a glycerol byproduct. The stoichiometric reaction requires 1

mole of TG and 3 mole of methanol to produce 3 mole of linear ester and 1 mole of glycerol[7]. Show in Figure 3.8

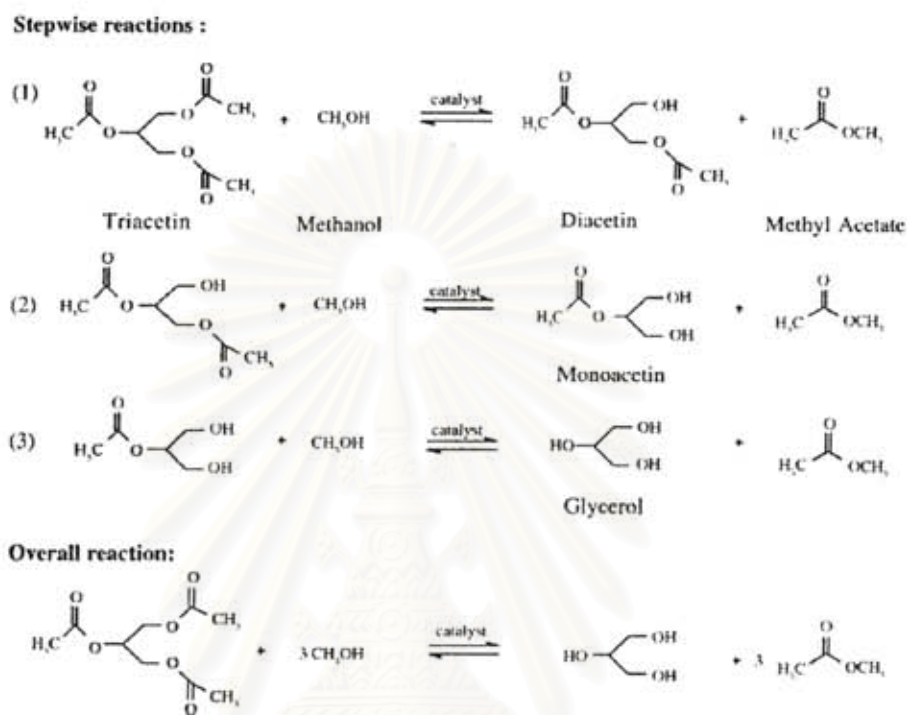


Figure. 3.8 : shows the reactions for the transesterification of triacetin with methanol[7].

3.4.2 The Reaction of biodiesel when the catalyst is potassium hydroxide

It is common for oils and fats to contain small amounts of water and free fatty acids. Free fatty acids consist of the long carbon chains described that are disconnected from the glycerol backbone. They are sometimes called carboxylic acids. (R-COOH). If an oil or fat containing a free fatty acid such as oleic acid is used to produce biodiesel, the alkali catalyst typically used to encourage the reaction will react with this acid to form soap.

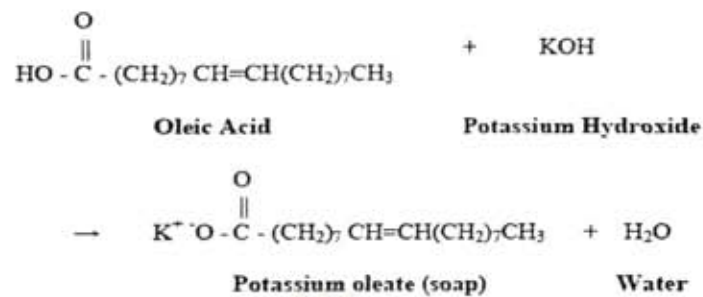


Figure 3.9 : The reaction when the catalyst is potassium hydroxide (KOH).

This reaction is undesirable because it binds the catalyst into a form that does not contribute to accelerating the reaction. Excessive soap in the products can inhibit later processing of the biodiesel, including glycerol separation and water washing. Water in the oil or fat can also be a problem. When water is present, particularly at high temperatures, it can hydrolyze the triglycerides to diglycerides and form a free fatty acid. When an alkali catalyst is present, the free fatty acid will react to form soap following the reaction given earlier. When water is present in the reaction it generally manifests itself through excessive soap production. The soaps of saturated fatty acids tend to solidify at ambient temperatures so a reaction mixture with excessive soap may gel and form a semi-solid mass that is very difficult to recover.

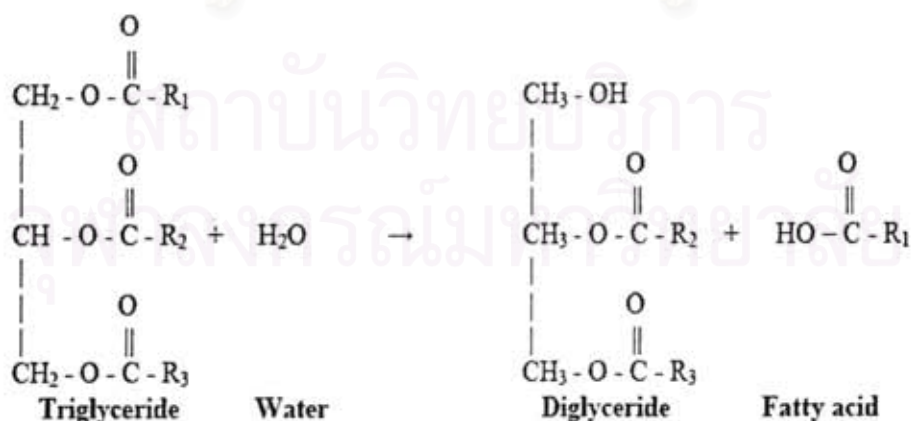


Figure 3.10 : Hydrolysis of a triglyceride to form free fatty acids.

3.4.3 Properties of common fatty acids

Table 3.1 Chemical structure of common fatty acids and their methyl esters.

Fatty acid (trivial name / rational name);	Structure ^{a)}	Common acronym	Methyl ester (trivial name / rational name)
Palmitic acid / Hexadecanoic acid;	R-(CH ₂) ₁₄ -CH ₃	C16:0	Methyl palmitate / Methyl hexadecanoate
Stearic acid / Octadecanoic acid	R-(CH ₂) ₁₆ -CH ₃	C18:0	Methyl stearate / Methyl octadecanoate
Oleic acid / 9(Z)-octadecenoic acid	R-(CH ₂) ₇ -CH=CH-(CH ₂) ₇ -CH ₃	C18:1	Methyl oleate / Methyl 9(Z)-octadecenoate
Linoleic acid / 9(Z),12(Z)-octadecadienoic acid;	R-(CH ₂) ₇ -CH=CH-CH ₂ -CH=CH-(CH ₂) ₄ -CH ₃	C18:2	Methyl linoleate / Methyl 9(Z),12(Z)-octadecadienoate
Linolenic acid / 9(Z),12(Z),15(Z)-octadecatrienoic acid;	R-(CH ₂) ₇ -(CH=CH-CH ₂) ₃ -CH ₃	C18:3	Methyl linolenate / Methyl 9(Z),12(Z),15(Z)-octadecadienoate

a) R = COOH (CO₂H) or COOCH₃ (CO₂CH₃); (CH₂)₇ = CH₂-CH₂-CH₂-CH₂-CH₂-CH₂-CH₂, etc.

Table 3.2 Characteristics of Common Fatty Acids and Their Methyl Esters.

Fatty acid Methyl ester	Formula	Molecular weight	Melting point (°C)
Palmitic acid Methyl palmitate	C ₁₆ H ₃₂ O ₂ C ₁₇ H ₃₄ O ₂	256.428 270.457	63-64 30.5
Stearic acid Methyl stearate	C ₁₈ H ₃₆ O ₂ C ₁₉ H ₃₈ O ₂	284.481 298.511	70 39
Oleic acid Methyl oleate	C ₁₈ H ₃₄ O ₂ C ₁₉ H ₃₆ O ₂	282.465 296.495	16 -20
Linoleic acid Methyl linoleate	C ₁₈ H ₃₂ O ₂ C ₁₉ H ₃₄ O ₂	280.450 294.479	-5 -35
Linolenic acid Methyl linolenate	C ₁₈ H ₃₀ O ₂ C ₁₉ H ₃₂ O ₂	278.434 292.463	-11 -52 / -57

It is extremely important to realize that vegetable oils are mixtures of triglycerides from various fatty acids. The composition of vegetable oils varies with the plant source. Often the terms fatty acid profile or fatty acid composition are used to describe the specific nature of fatty acids occurring in fats and oils.



สถาบันวิทยบริการ
จุฬาลงกรณ์มหาวิทยาลัย

CHAPTER IV

EXPERIMENTAL

The experimental system and procedures in the synthesis of zirconia and tungsten zirconia are presented in this chapter. The chemicals, preparation of nanocrystalline ZrO₂, preparation of tungstated zirconia catalyst, reaction studies and equipment are shown in sections 4.1, 4.2, 4.3, 4.4, 4.5 and 4.6 respectively.

4.1 Sample preparations

4.1.1 Chemicals

The lists of chemicals used in this research are shown in the Table 4.1.

Table 4.1: Chemicals used for sample preparations

Chemical	Grade	Supplier
Zirconium <i>n</i> -propoxide	20.5 %	Aldrich
Triacetin	99.999%	Aldrich
Tungsten(VI) Chloride	99%	Aldrich
1,4-butanediol	analytical	Aldrich
Methanol	99.8%	Fisher
2- isopropanal	99%	Fisher
Sulfuric acid	51%	J.T.Baker

4.2 Preparation of nanocrystalline ZrO₂

Nanocrystalline ZrO₂ was prepared using the solvothermal method in the same manner as reported by Kongwudthiti et al. [15]. Zirconium *n*-butoxide (97 %, Aldrich) was used as the starting material. Approximately 25 g of zirconium *n*-butoxide was suspended in 100 ml of 1,4-butanediol (Aldrich), in a test tube, which was then placed in a 300 ml autoclave. The 25 ml of same solvent was filled in the gap between the test tube and the autoclave wall. The autoclave was purged completely by nitrogen after that it was heated up to the desired temperature at 300°C with the rate of 2.5°C /min. The temperature was held constant at 300°C for 2 h and then cooled down to room temperature. After the autoclave was cooled to room temperature, the resulting product was repeatedly washed with methanol by vigorous mixing and centrifuging. The obtained powders were then dried in oven at 100°C for 1 day

A part of the product was calcined in a tube furnace in different atmospheres (H₂, N₂, O₂, Air) by heating to 500°C at a rate of 10°C min and holding at that temperature for 2 h.

4.3 Preparation of tungstated zirconia catalyst

The tungstated zirconia catalysts were prepared by incipient wetness impregnation of calcined solvothermal-made ZrO₂ support with a desired amount of an aqueous solution of tungsten (VI) chloride (99 wt%, Aldrich). The tungsten loading of the catalysts was ranged of 15 wt%. The final concentrations of catalysts were determined by atomic absorption spectroscopy (Varian Spectra A800). The catalysts were dried at 110°C for 24 h and calcined in air at 500°C for 2 h.

4.4 Reaction studies

The liquid phase transesterification reaction was carried out on well-mix batch reactor used with 3-neck round bottom flask 50-ml. Hot plate and stirrer was used for heat generation and using cooling tower to control the system to be stable (closed system). First on, filled the solution of triacetin and methanol at ratio 1: 6 in reactor. The reactor was heated to 60°C and the solid catalyst (2 wt% of triacetin) was added shortly after the reactor temperature reached the desired temperature. Sample aliquots (1 ml) were withdrawn periodically from the reactor, quenched to room temperature, and centrifuged in order to separate out the solid catalyst and prevent further reaction. Reaction sample concentrations were determined using an SHIMADZU gas chromatograph GC – 14B which N₂ was used as carrier gas. The steady-state rate was reached after 7 h.

4.5 Equipment

4.5.1 Autoclave Reactor

- Made from stainless steel
- Volume of 1000 cm³ and 10 cm inside diameter
- The thermocouple is attached to the reagent in the autoclave and maximum temperature of 350°C
- Pressure gauge in the range of 0-140 bar
- Test tube was used to contain the reagent and glycol
- Autoclave volume of 1000 cm³ and an iron jacket was used to reduce the volume of autoclave to be 300 cm³
- Thermocouple is attached to the reagent in the autoclave
- Amount of starting material = 7 g
- Amount of organic solvent in the test tube = 100 cm³ and amount of organic solvent in the gap between test tube and autoclave wall = 30 cm³

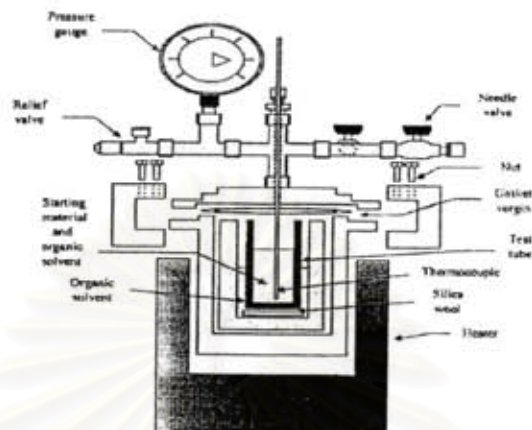


Figure 4.1 : Autoclave reactor

The diagram of the reaction equipment for synthesis of zirconia is shown in Figure 4.2

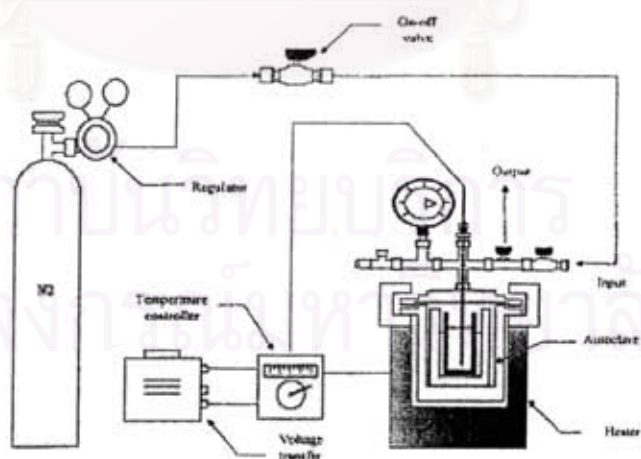


Figure 4.2 : Diagram of the reaction equipment for the synthesis of zirconia

4.5.2 Gas Chromatography (GC)

The sample 1 μl was injected to GC by using column RTX-5 Crossbond 5% diphenyl – 95% dimethyl polysiloxane 30m, 0.25mmID, 0.25 μm df maximum program temperature 350°C and used H₂, Air, He as gas carriers.

Table 4.2: Operating conditions for gas chromatography

Gas Chromatograph	SHIMADZU GC-14B
Detector	FID
Column	RTX-5
Carrier gas	He (99.999%)
Carrier gas flow (ml/min)	30 cc/min
Column temperature	
- initial temp (°C)	50
- initial time (min)	3
- final temp (°C)	210
- final time (min)	9
Injector temperature (°C)	255
Detector temperature (°C)	280
Current (Ma)	-
Analysed	Triglyceride

The effluent gas was sampled to measure the concentration of ethylene using GC-14B gas chromatograph (Shimadzu), equipped with a flame ionization detector. The operating conditions for the instrument were listed in Table 4.2. The composition was measured every 20 minutes until steady state was achieved (as indicated by constant peak areas in the gas chromatograms).

4.6 Characterization

4.6.1 Powder X-ray diffraction (XRD)

Powder X-ray diffraction (XRD) will be performed by using a SIEMENS XRD D5000 connect with a computer with Diffract ZT version 3.3 program for fully control of the XRD analyzer. The measurements were carried out by using Ni-filtered CuK_α radiation. Scans will be performed over the range from 10° to 80° with step 0.02° . To determine the average crystallite size, peak broadening analysis will be applied to anatase (101) peak using Scherrer's equation.

4.6.2 Transmission electron microscopy and selected area electron diffraction (TEM) and (SAED)

TEM and SAED characterizing the morphology, crystallite size, and diffraction patterns of the primary particles of the resulting TiO_2 samples were obtained using the JEOL JEM-2010 transmission electron microscope operated at 200 kV with an optical point to point resolution of 0.23 nm. The sample was dispersed in ethanol prior to measurement.

4.6.3 Brunauer-Emmett-Teller surface area (BET)

Total surface area (S_{BET}) of zirconia are predicted by a multipoint BET method. Before analysis, must conduct the degasation at 200°C and 10^{-3} Torr for 3 h. Adsorption measurements were carried out using UHP N_2 at -196°C in a Micromeritics ASAP 2020 device.

4.6.4 Titration technique involved an ion-exchange

The titration technique involved an ion-exchange step[7] using for prediction of acid site concentration. By using 0.2 g. dissolved in NaCl solution, 3.43 M 10 ml. Stirring took place for 30 h at 28 °C which caused the interchange ion between H⁺ of catalyst and Na⁺ of solution. Then the solid phase was filtered out. Solution was next titrated with NaOH 0.05 N. which the endpoint for this titration was measured by pH meter (pH ~ 7) and pH paper.

4.6.5 Electron spin resonance spectroscopy (ESR)

The defected surface zirconia (Zr³⁺ and F-center) are investigated by The electron spin resonance spectrometer (ESR) at STREC. It was conducted on ESR spectrometer of JEOL, model JES-RE2X on ES-IPRIT program with the X band Microwave unit and frequency : 8.8-9.6 GHz. The cavity is cylindrical and it was operating in TE₀₁₁ mode.

4.6.6 IR Raman spectroscopy

The Raman spectra of the samples were collected by projecting a continuous wave YAG laser of Nd (810 nm) through the samples at room temperature. A scanning range of 100-1000 cm⁻¹ with a resolution of 2 cm⁻¹ was applied.

สถาบันวิทยบริการ
จุฬาลงกรณ์มหาวิทยาลัย

CHAPTER V

RESULTS AND DISSION

In this chapter, the results and discussion are divided into three sections. Section 5.1 explains the characteristics of zirconia calcined at different atmospheres. Characteristics of tungsten zirconia (WZ) catalysts are discussed in section 5.2. In section 5.3, the relative catalyst activities are studied.

5.1 Characteristics of zirconia calcined at different atmospheres

The color of the zirconia changed from white to brown when zirconias were calcined under H₂ and N₂ atmosphere, which was a qualitative indication of the formation of F-center surface defect as shown in Figure 5.2 This result was consistent with the author [12] reported previously that the recognition of the color variation in solid particle from white to brown clearly revealed the existence of F-center modification within zirconia structure in terms of ESR analysis.

The XRD patterns of the as-synthesized and treated ZrO₂ powder are shown Figure 5.1 The specific reflection of tetragonal phase diffraction peaks are presented at 30.17°, 35.31°, and 49.79° and monoclinic phase peaks at 2 θ = 22.0°, 28.2° and 33.1°. Glycothermal reaction of ZNP and treated powder under different atmospheres gave the nanocrystalline tetragonal ZrO₂, which contained the small amounts of monoclinic phases.

This suggests that the calcination atmosphere (H₂, N₂, O₂, Air) does not strongly affect the phase change. The phase change is dependent on the calcined temperature [1]. For calcination temperature above 800 °C under air, zirconia phase changes from tetragonal to monoclinic phase (2 θ = 28.17° and 31.47°) [7]. It is expected that tetragonal phase is active for transesterification reaction [6-8].



ต้นฉบับไม่มีหน้านี้
NO THIS PAGE IN ORIGINAL

สถาบันวิทยบริการ
จุฬาลงกรณ์มหาวิทยาลัย

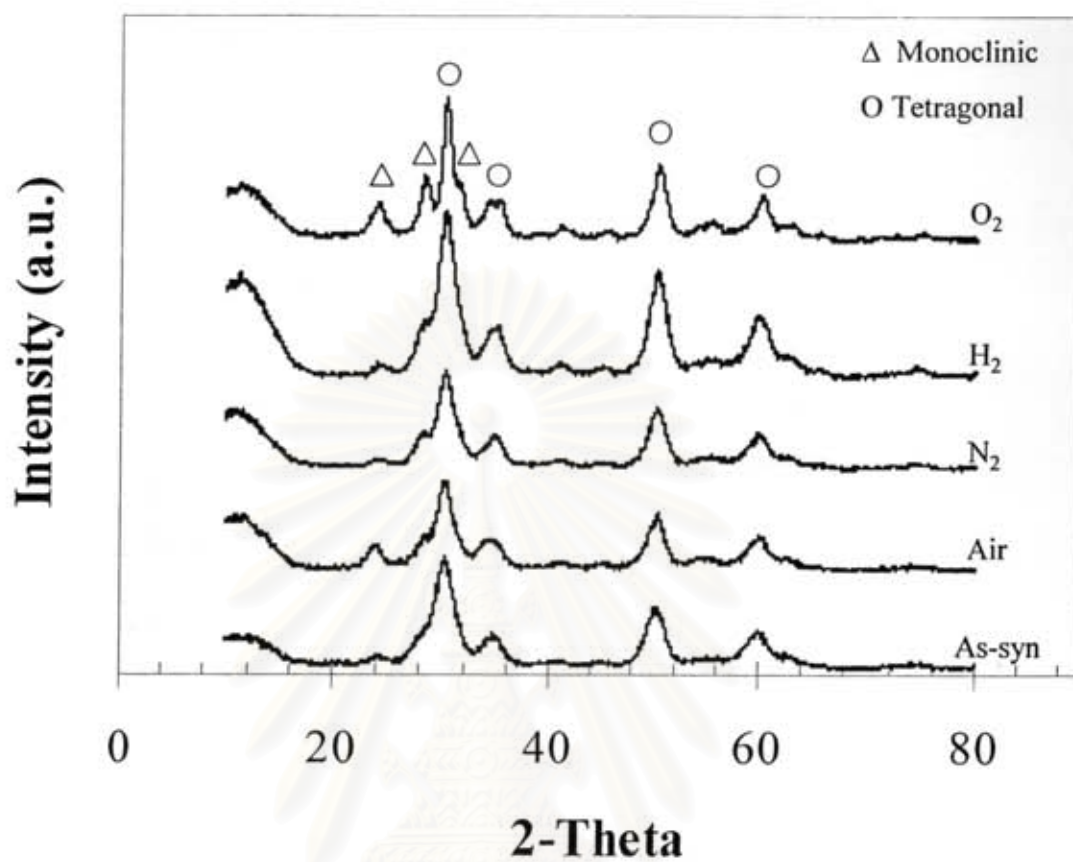


Figure. 5.1 X-ray diffraction pattern of nano zirconia prepared by solvothermal method and calcinations at difference atmosphere.

สถาบันวิทยบริการ
จุฬาลงกรณ์มหาวิทยาลัย

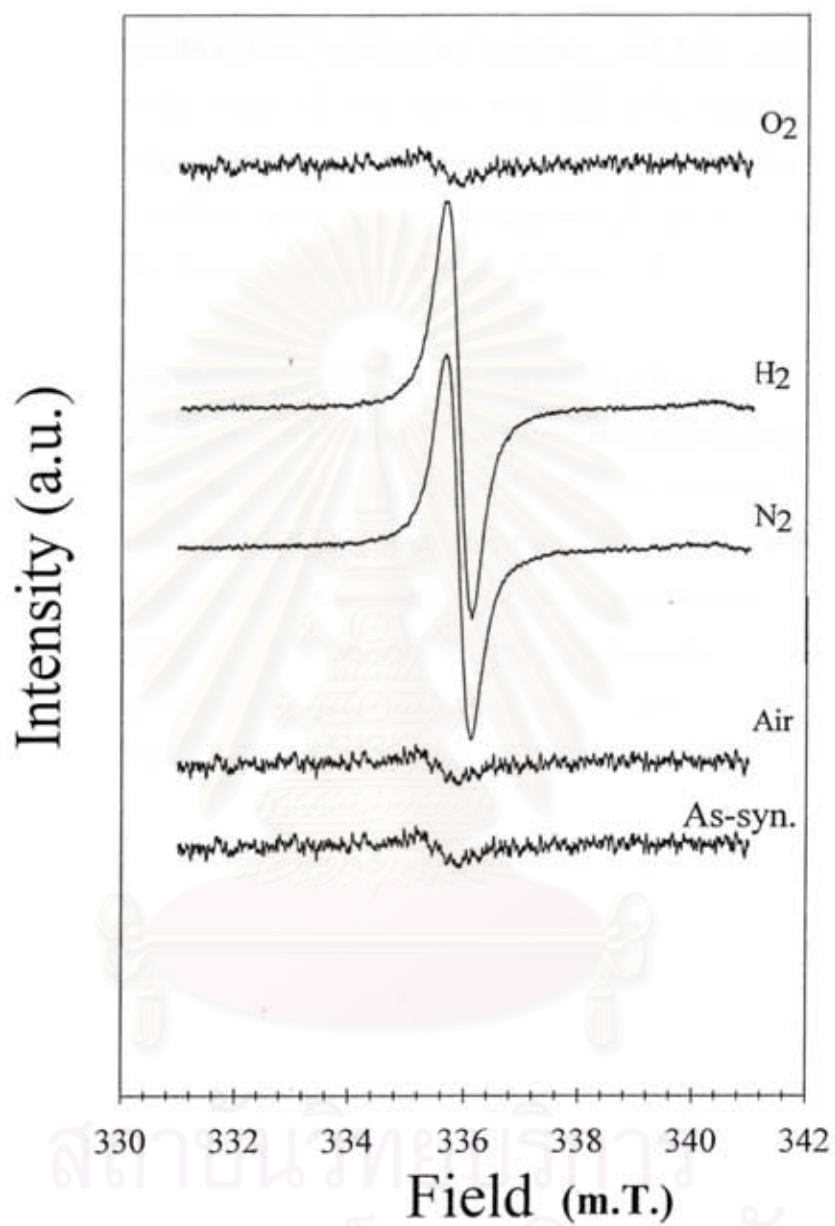
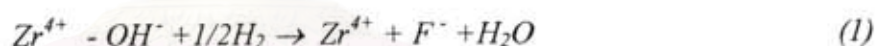


Figure 5.2 ESR spectra of sample nano ZrO₂ calcinations at different atmosphere : O₂, H₂, N₂, Air and As-syn

The physical properties of as-synthesized and treated ZrO₂ powder are summarized in Table 1. Crystallite size of tetragonal ZrO₂ and monoclinic phase contents were calculated by Scherrer equation and the equation developed by Anthon et al. [37], respectively. The crystallite sizes, monoclinic contents and BET surface area of as-synthesized ZrO₂ powder were 3.5 nm, 25% and 120 m²/g respectively. While the crystallite size, monoclinic contents and BET surface area of treated sample were ranged between 4 to 6 nm, 21 to 29% and 76 to 95 m²/g respectively. Decreasing on BET surface area of calcined samples was due to the sintering of ZrO₂ crystals.

Figure 5.2 shows ESR spectra of all ZrO₂ samples at different calcination atmospheres. The results show low ESR signal for thus-obtained and treated ZrO₂ samples under air and O₂ atmosphere as shown in Figure 5.2(O₂, Air, As-syn). While, the ESR signal for samples calcined under H₂, N₂ atmosphere was clearly found at g = 2.003, which could be assigned to F-center defects (single charged oxygen vacancy) as presented in Figure 5.2(H₂) and 5.2(N₂). This result was consistent with some researches [10-13], which reported that the calcination under reducing atmosphere would lead to the formation F-center signal as follow reaction;



The higher signal strength was caused by the more reducing atmosphere [30].

Table 5.1

Surface area, XRD phases for ZrO₂ samples calcinations at difference atmosphere

Ambient atmosphere in calcinations	BETs (m ² /g)	Crystal size(nm.)	XRD phases		Intensity of ESR signal	
			% t-ZrO ₂	% m-ZrO ₂	F-center	Zr ³⁺
H ₂	90.5	3.8	71.0	29.0	22000	-
N ₂	90.1	3.6	77.5	22.5	15510	-
O ₂	76.4	6.9	77.3	22.7	-	-
Air	94.9	4.1	78.3	21.2	-	-
As-syn.	120.2	3.5	74.8	25.2	-	-

5.2 Characteristics of tungsten zirconia (WZ) catalysts

XRD pattern of all tungsten zirconia (WZ) catalysts prepared by incipient wetness impregnation of WCl_6 on various treated ZrO_2 supports and following by calcination under air flow at $500^\circ C$, are shown in Figure 5.3. The XRD patterns shown the specific reflection of tetragonal phase diffraction peaks are presented at 30.17° , 35.31° , and 49.79° and monoclinic phase peaks at $2\theta = 22.0^\circ$, 28.2° and 33.1° . The XRD patterns for all WZ catalysts did not show any characteristic peaks of WO_3 or any other W compounds suggesting that WO_x must be in the non-crystalline form with high degree of dispersion. Moreover, the observations exhibited the presence of monoclinic and tetragonal phase of zirconia without any impregnation as shown in Figure 5.2. On the other hand, the impregnation of tungsten over zirconia with the treatment under different atmosphere gave no influence on the zirconia phase transformation.

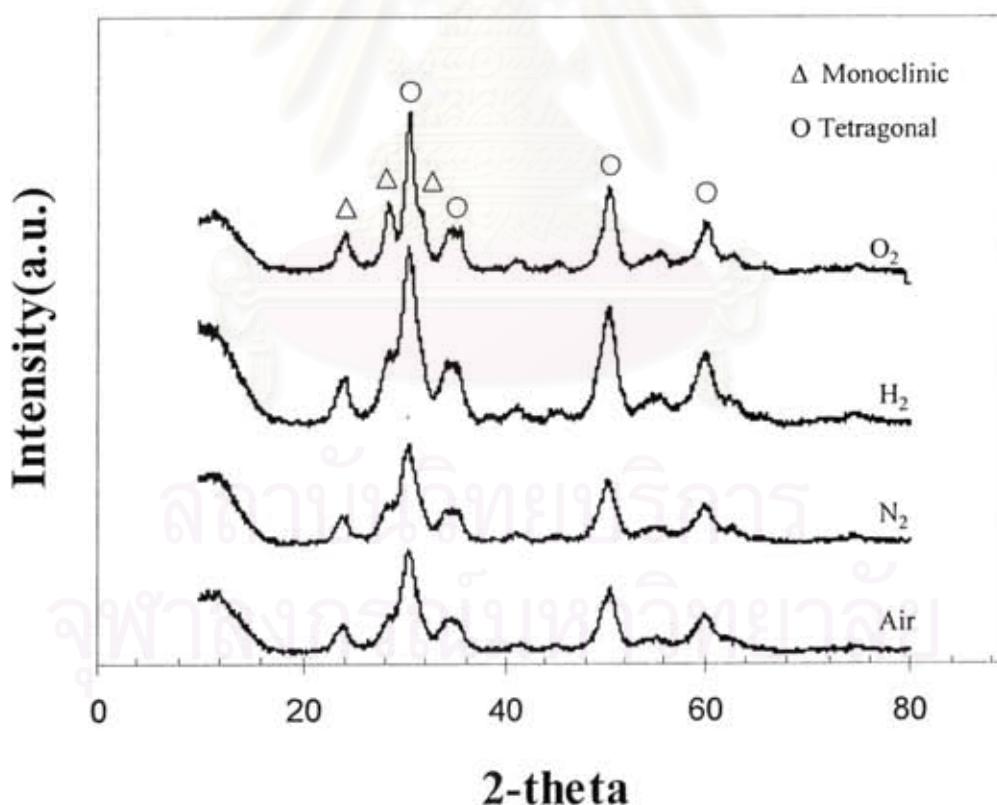


Figure 5.3 XRD patterns of WZ prepared by impregnation tungsten on zirconia (calcinations at difference atmosphere) and WZ calcinations at air atmosphere.

To determine the presence of WO_x species, Raman spectroscopy is a very sensitive technique for detecting the presence of very small WO_3 crystallites. The Raman spectra taken at ambient temperature for oxidized WZ samples prepared by impregnation on the calcined ZrO_2 supports under various atmospheres are shown in Figure 5.5 and that for pure ZrO_2 supports are shown in Figure 5.4, all samples exhibited the same characteristic absorption bands for tetragonal ZrO_2 at around 313.48, 475 and 641.16 cm^{-1} while the characteristic bands of monoclinic phase had around 383 to 399 cm^{-1} [54]. This should be due to the small amounts of monoclinic contents comparing with tetragonal one. It is also interesting that the absorption bands for tetragonal ZrO_2 became broad and disappear after impregnated with tungsten. This would be due to the coverage of WO_3 layer on ZrO_2 supports.

The Raman spectra taken at ambient atmosphere for oxidized WZ samples prepared by impregnation with different calcinations atmosphere of ZrO_2 supports are given in Figure 5.5 All samples display in the lower-frequency region the band at ca. 647 cm^{-1} as the characteristic of tetragonal zirconia. In addition, a band at ca. 620 cm^{-1} of monoclinic zirconia [54] was not seen in all samples. These features related to the zirconia support were in agreement with the XRD data as discussed above. The bands corresponding to surface tungsten species were observed at higher Raman shifts. The only tungsten bands observed at Figure 5.5 (H_2) were those at 802.92 cm^{-1} assigned to W–O–W stretching modes and the ranges of 960 to 955 cm^{-1} were attributed to W=O vibrations in hydrated interconnecting polyoxotungstate clusters [54]. These WO_x species generally have associated with the formation of strong Brønsted acid sites under a reducing environment [55]. Thus, the Raman results confirmed those previously observed by XRD.

จุฬาลงกรณ์มหาวิทยาลัย

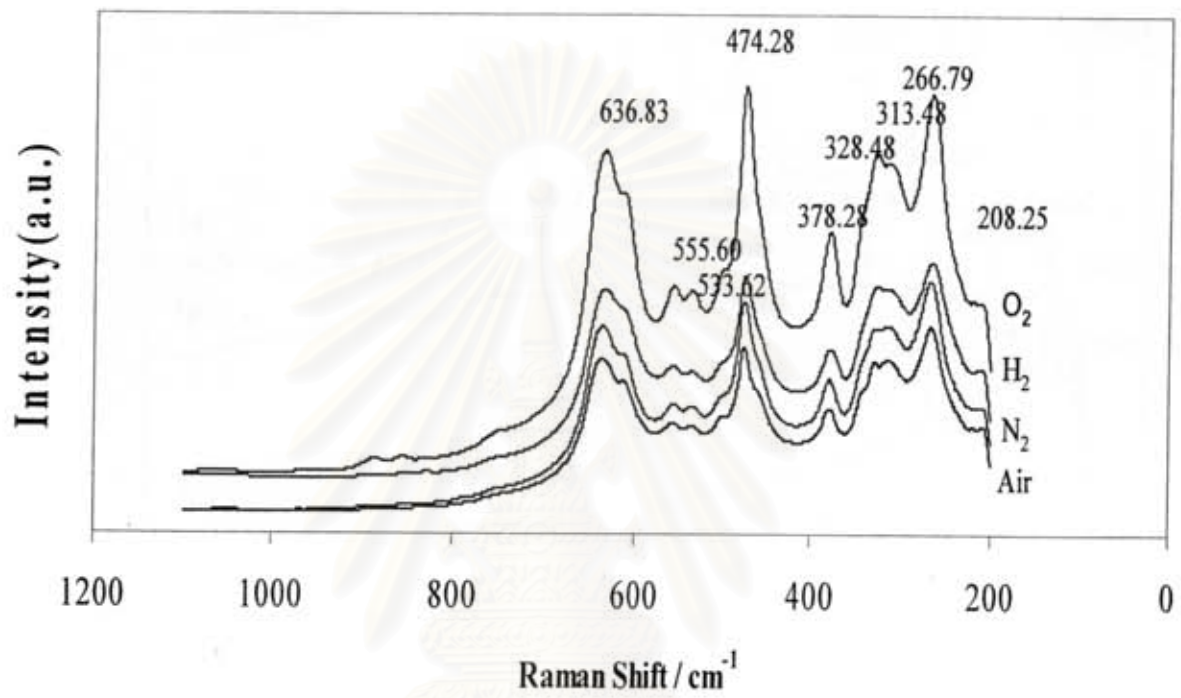


Figure 5.4 Raman spectra of nano Zirconia prepared by solvothermal method and calcinations at difference atmosphere.

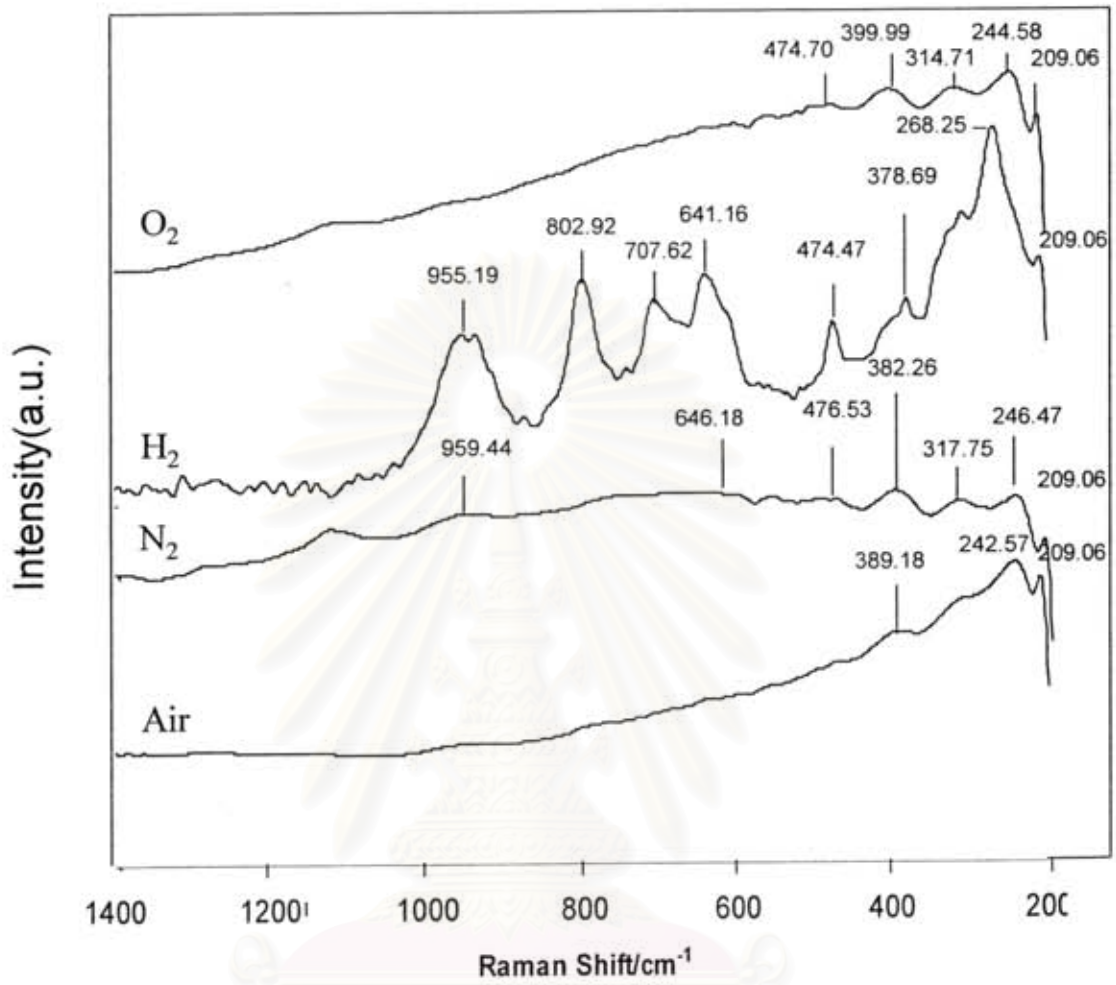
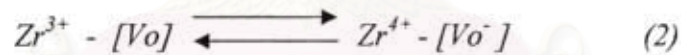


Figure 5.5 Raman spectra of tungstated zirconia prepared by impregnation tungsten on zirconia (calcinations at difference atmosphere) and tungstated zirconia calcinations at air atmosphere.

Figure 5.6 shows ESR spectra of all WZ catalyst samples. All samples exhibited the characteristic signals for Zr^{3+} as illustrated in ESR signal at $g = 1.975$ and $g = 1.957$ [11,12,29,30] while the signals for F-center for H_2 and N_2 treated ZrO_2 supports were disappeared. Early researches suggested that the Zr^{3+} detected by ESR can be described as the oxygen coordinatively unsaturated zirconium sites on the ZrO_2 surface. The amounts of Zr^{3+} (intensity of ESR signal) of all samples were determined and reported in Table 2. The amounts of Zr^{3+} of WO_x/ZrO_2 catalysts were improved as the calcination atmosphere of ZrO_2 supports was changed. It improved by following order: $H_2 > N_2 > Air > O_2$. It would be noticed that the Zr^{3+} contents in WZ catalysts increased as the F-center defects of starting support increased. According to the results, the defected surface of starting zirconia support was the F-center for WO_3^- group. In addition, the high F-center signal on zirconia surface can reverse to a high Zr^{3+} signal, this phenomenon is evident when it is impregnated by tungsten chloride and followed by the calcination in air at $500^\circ C$ for 2 h. Frolova et al. [34] suggested that the electronic density redistribution between Zr^{3+} and the closest oxygen vacancy is reversible under heating in a red/ox medium as the equation below. Oxidation of the reduced samples results in disappearance of the F-center EPR signal and the reappearance of Zr^{3+} signal.



when $[Vo^-]$ is F-center [29].

Table 2 summarized the physiochemical properties of all WZ catalyst samples. Crystallite size, BET surface area and monoclinic contents were not much changed after impregnation process. The tungsten surface density of the catalysts was calculated from the WO_3 loading content and BET surface area of the catalysts and also reported in Table 2. The tungsten surface density of all catalysts was ranged between 4.3 to 5.6 W nm^{-2} , which was in good agreement with monolayer surface coverage value (4.8 W nm^{-2}) [47]. The obtained-values also indicated that all the catalysts shown similar tungsten surface density except for the WO_x supported on O_2 -treated ZrO_2 . The acidity of ZrO_2 samples were determined using chemical titration techniques. The results indicated that the acidity of catalyst increaseds as the ZrO_2 support is treated with more reducible calcination

atmosphere ($H_2 > N_2 > Air > O_2$). Moreover, it was interesting that the catalyst acidity increased in the same order of Zr^{3+} contents determined by ESR technique.

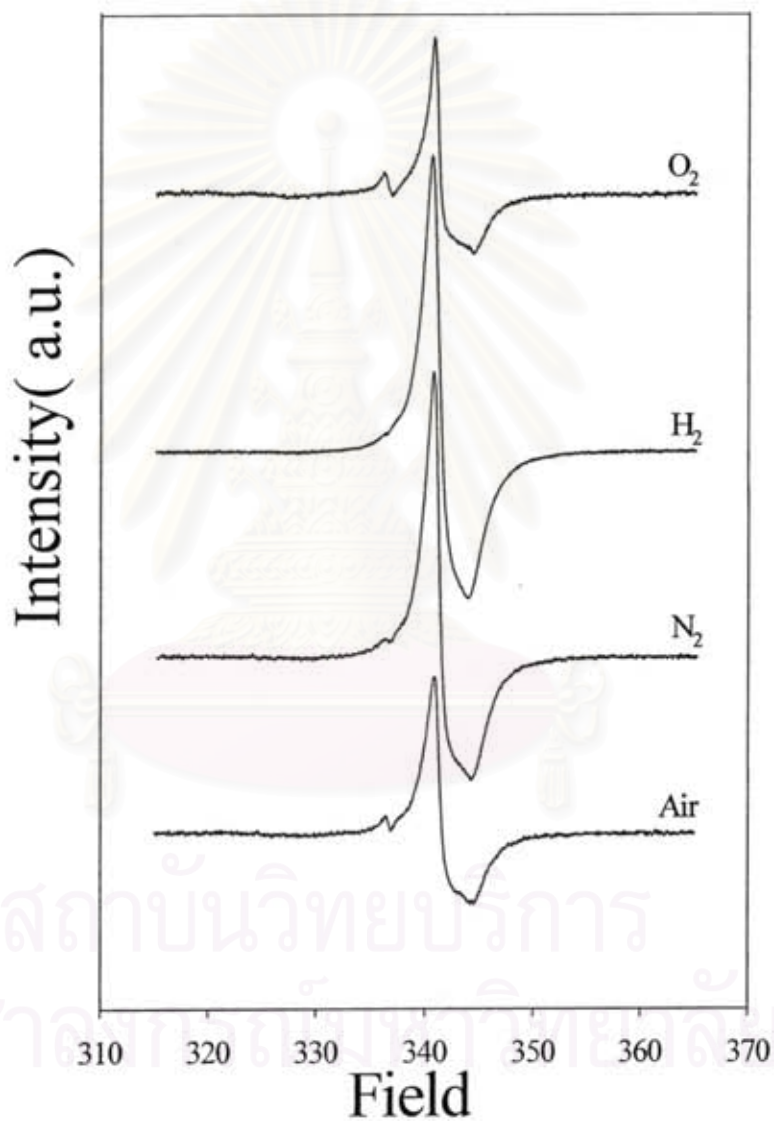


Figure 5.6 ESR spectra of tungstated zirconia prepared by impregnation tungsten on zirconia (calcinations at difference atmosphere) and tungstated zirconia calcinations at air atmosphere.

Table 5.2

Surface acidity for WZ sample calcination at difference atmosphere.

Ambient atmosphere at 500°C	Surface acidity of ZrO ₂			XRD phases		Intensity of	ESR signal
	BETs (m ² /g)	Exchange/ titration (umol/g)	Crystals size (nm.)	% t-ZrO ₂	%m-ZrO ₂	F-center	Zr ³⁺
H ₂	90.2	200	3.8	71.6	28.4	-	2362
N ₂	90.5	150	3.6	73.2	26.8	-	2105
O ₂	69.8	100	6.7	75.2	24.8	-	1260
Air	85.5	125	3.9	78.4	21.6	-	1315

TEM images, HREM, SAED and EDX results of all ZrO₂ powders calcined at 500 °C with in W/ZrO₂ catalysts samples are shown in Figure 5.7 to 5.10 The W impregnated on air and O₂-treated ZrO₂ consisted of particles with primarily spherical shape with average size around 3 to 15 nm and irregular shape large over layers. From EDX analysis, the spherical shape particles and irregular shape over layer could be assigned to ZrO₂ particles and tungsten oxide, respectively. The particle sizes calculated by TEM image were in good agreement with crystallite size calculated from XRD indicating that the tetragonal ZrO₂ was single crystal. On the other hand, tungsten impregnated on N₂ and H₂-treated ZrO₂ only consisted of irregular bulk solids which was trapped the small particles inside. From EDX analysis, all bulk solid comprised of tungsten and zirconium atoms, which indicated that W atoms were mixed with the Zr atoms within the crystallite. This result agreed with several works, which were proposed that tungsten species were entrapped inside the ZrO₂ bulk forming a solid solution [53]. The results suggested that there was more dispersion of WO_x species on ZrO₂ supports treated by N₂ and H₂ gas. All HR-TEM images of WZ catalysts clearly display crystalline ZrO₂ lattice fringes. The additional presence of an amorphous WO_x overlayers were also suggested by this sequence of images. The amorphous overlayer of the surface WO_x species appeared most prominently at the edges of the support particles.

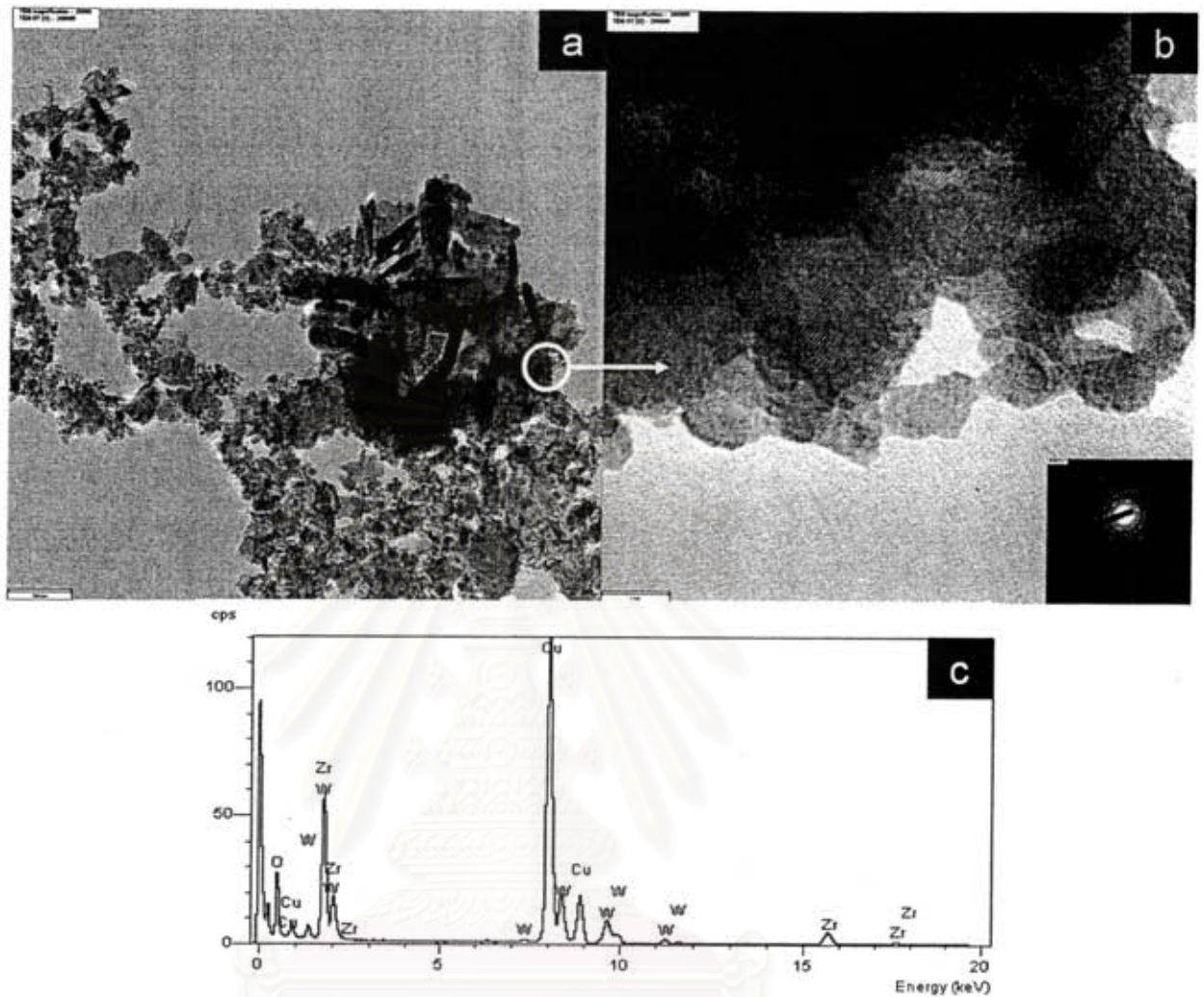


Figure 5.7 TEM micrographs of W impregnation on ZrO₂ calcination with O₂

Figure 5.7 (a) shown TEM micrographs of W impregnation on ZrO₂ calcination with O₂. The color showed different metal location, i.e, gray color referred to zirconia and black color represented the presence of tungsten. EDX measurements showed fair dispersion of tungsten on zirconia support. Tungsten agglomerated together as an superimpose structure from many layer, namely polymeric tungsten while zirconia distributed like small island without agglomeration. In addition, with higher magnification (Figure 5.7 (b)) the picture showed obviously the agglomeration of tungsten over the dispersion of zirconia. And the successive investigation by EDX confirmed the presence of tungsten as black color and the existence of zirconia as gray color.

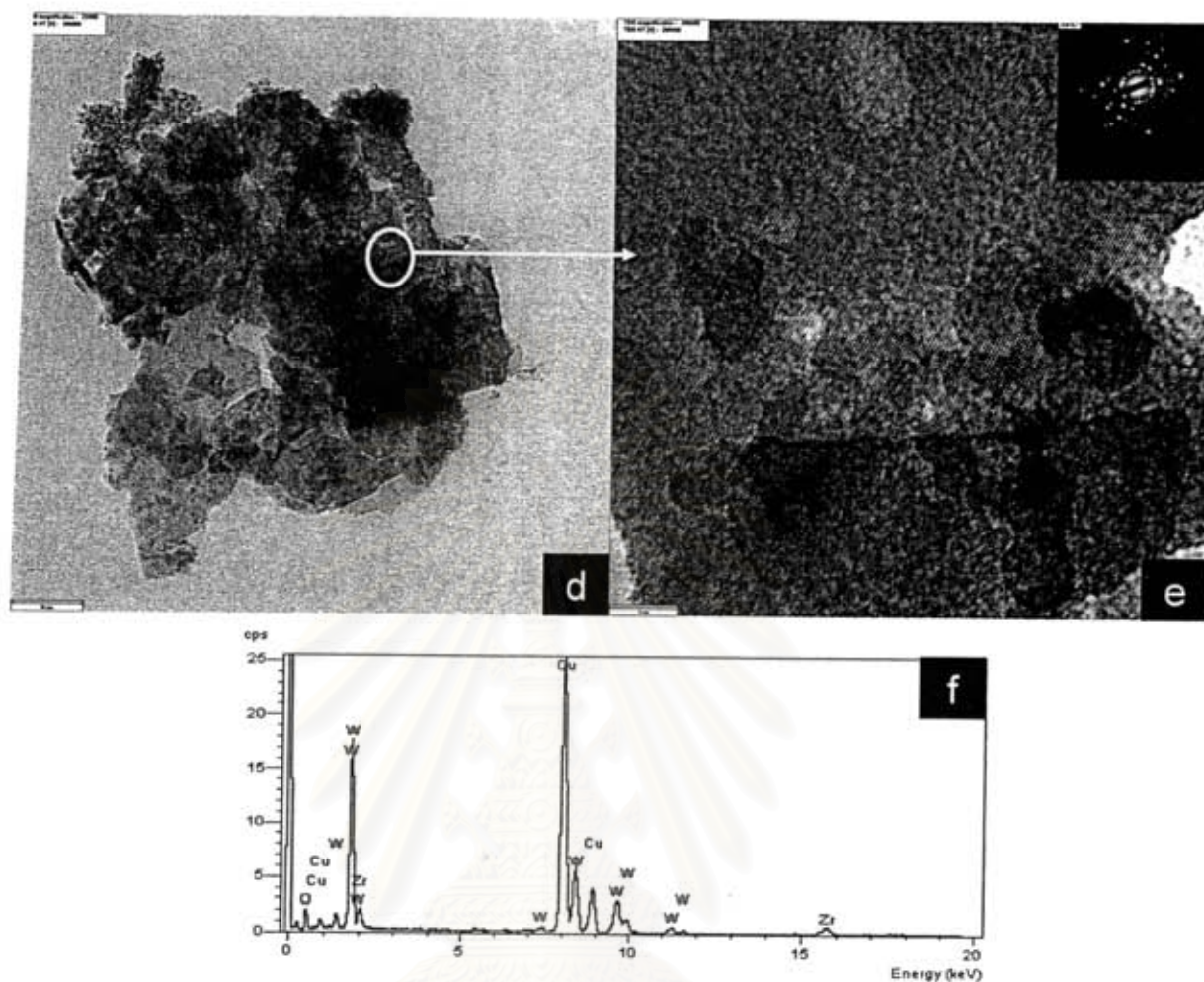


Figure 5.8 TEM micrographs of W impregnation on ZrO_2 calcination with H_2

Figure 5.8 (a) shown TEM micrographs of W impregnation on ZrO_2 calcination with H_2 . The color showed different metal location, i.e, gray color referred to zirconia and black color represented the presence of tungsten. EDX measurements showed good dispersion of tungsten on zirconia support. Tungsten agglomerated together as an superimpose structure from slime layer, namely monolayer tungsten while zirconia distributed like a film with tungsten cover on it. In addition, with higher magnification (Figure 5.8 (b)) the picture showed obviously the agglomeration of tungsten over the dispersion of zirconia. And the successive investigation by EDX confirmed the presence of tungsten as black color and the existence of zirconia as gray color.

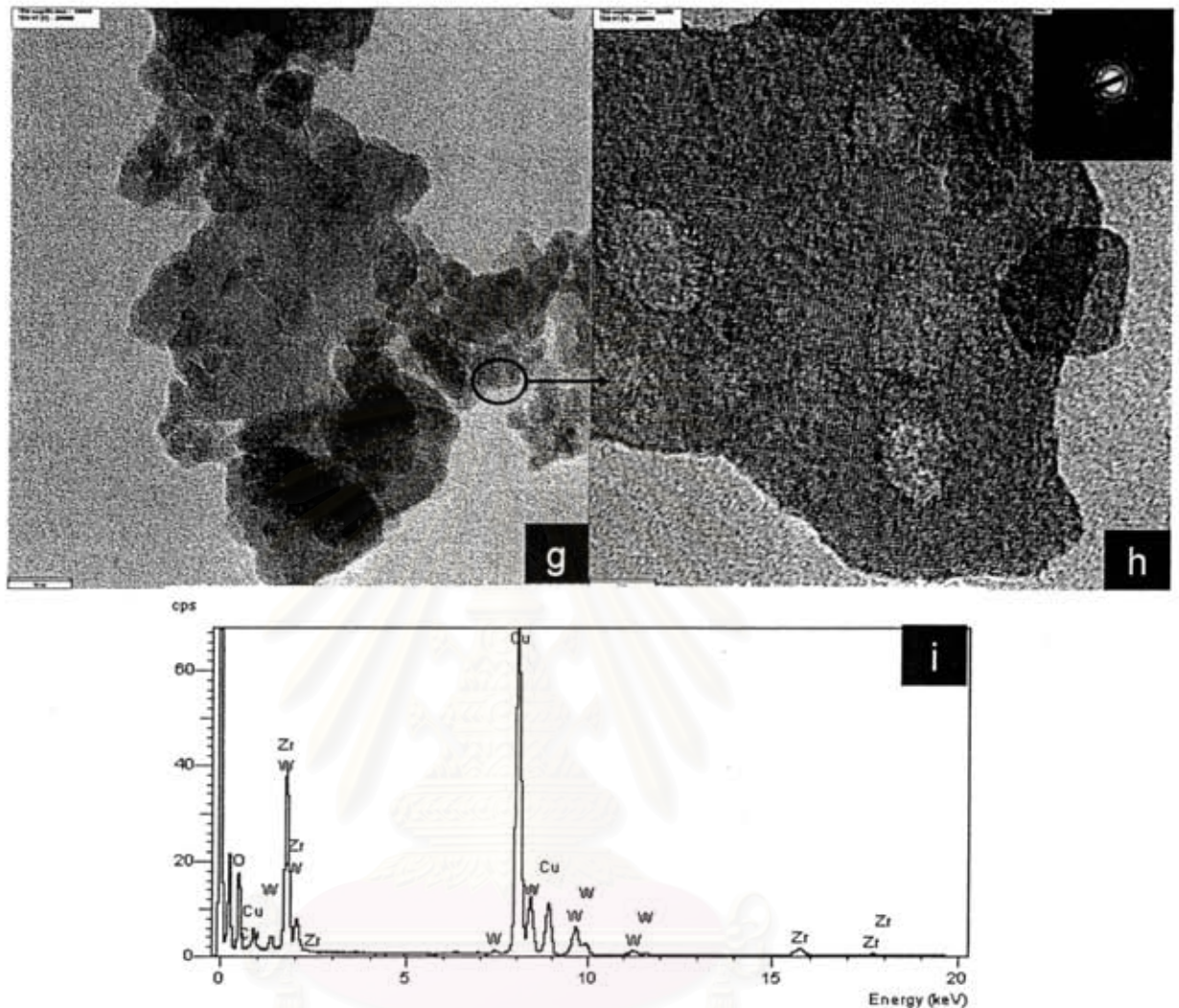


Figure 5.9 TEM micrographs of W impregnation on ZrO_2 calcination with N_2

Figure 5.9 (a) shown TEM micrographs of W impregnation on ZrO_2 calcination with H_2 . The color showed different metal location, i.e, gray color referred to zirconia and black color represented the presence of tungsten. EDX measurements showed good dispersion of tungsten on zirconia support. Tungsten agglomerated together as an superimpose structure from slime layer, namely monolayer tungsten while zirconia distributed like a film with tungsten cover on it. In addition, with higher magnification (Figure 5.9 (b)) the picture showed obviously the agglomeration of tungsten over the dispersion of zirconia. And the successive investigation by EDX confirmed the presence of tungsten as black color and the existence of zirconia as gray color.

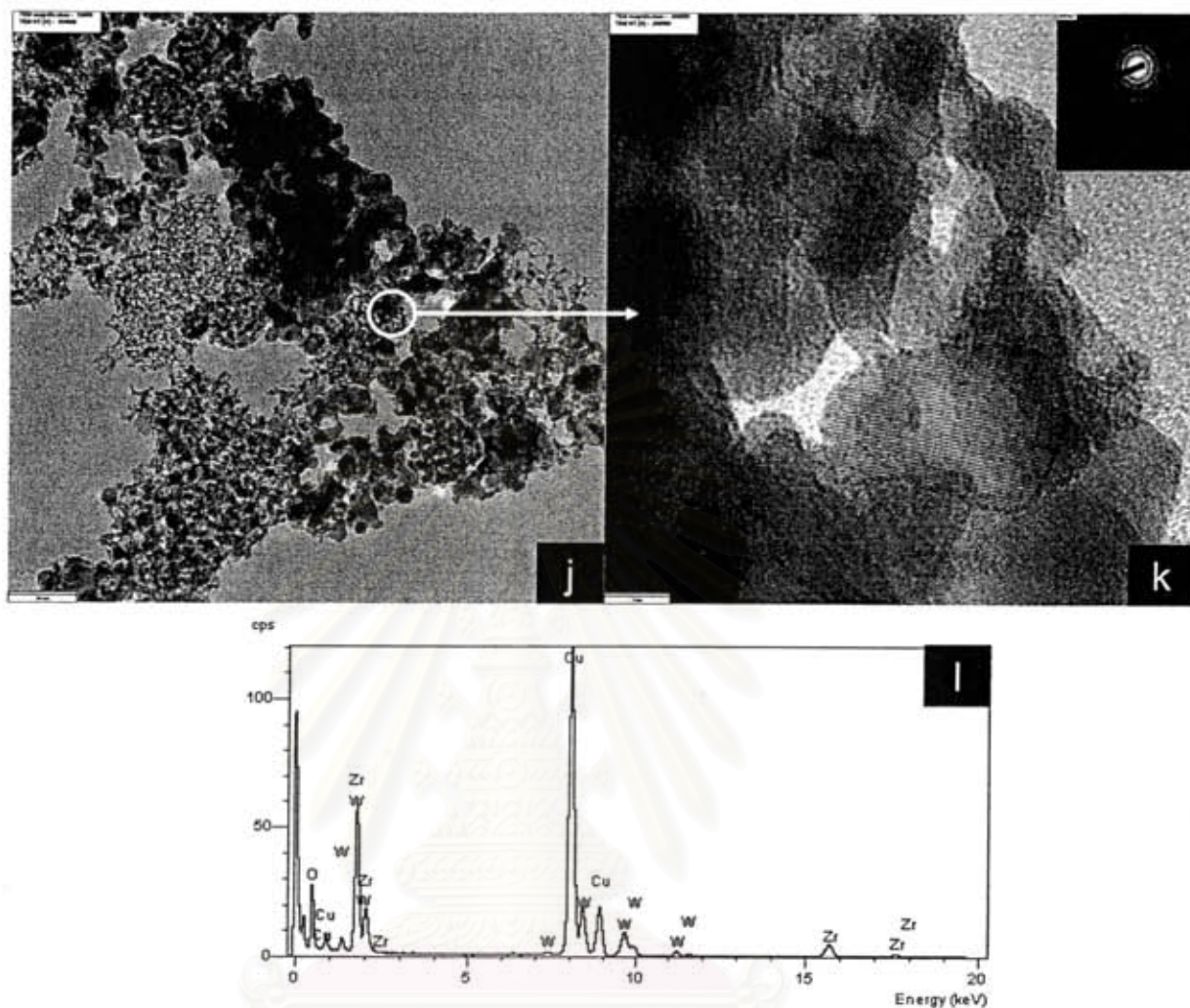


Figure 5.10 TEM micrographs of W impregnation on ZrO_2 calcination with Air

Figure 5.10 (a) shown TEM micrographs of W impregnation on ZrO_2 calcination with Air. The color showed different metal location, i.e., gray color referred to zirconia and black color represented the presence of tungsten. EDX measurements showed fair dispersion of tungsten on zirconia support. Tungsten agglomerated together as an superimpose structure from many layer, namely polymeric tungsten while zirconia distributed like small island without agglomeration. In addition, with higher magnification (Figure 5.10 (b)) the picture showed obviously the agglomeration of tungsten over the dispersion of zirconia. And the successive investigation by EDX confirmed the presence of tungsten as black color and the existence of zirconia as gray color.

5.3. Relative catalyst activity

The liquid phase transesterification of triacetin and methanol at 60 °C were used as the model reaction for comparing the catalytic activity of all WZ catalysts. The catalytic activity of all WZ catalysts is displayed in Figure 5.7 The order of catalytic activity can be arranged as $H_2SO_4 > WZ \text{ cal. } H_2 (53\%) > WZ \text{ cal. } N_2 (40\%) > WZ \text{ cal. } O_2 (17\%) \approx WZ \text{ cal. Air } (16\%) \approx WZ \text{ (commercial)}$, respectively. The results were in a good agreement with the acidity contents of catalyst. H_2SO_4 exhibited the most active (nearly 99% triacetin conversion) because of its strongest acidity and its liquid phase which was the same phase as reactants (triacetin and methanol). On the other hand, WZ catalyst was a solid phase. The acidic site on the catalyst surface and internal mass transfer for micropores limited the triacetin conversion [1, 6, 7].

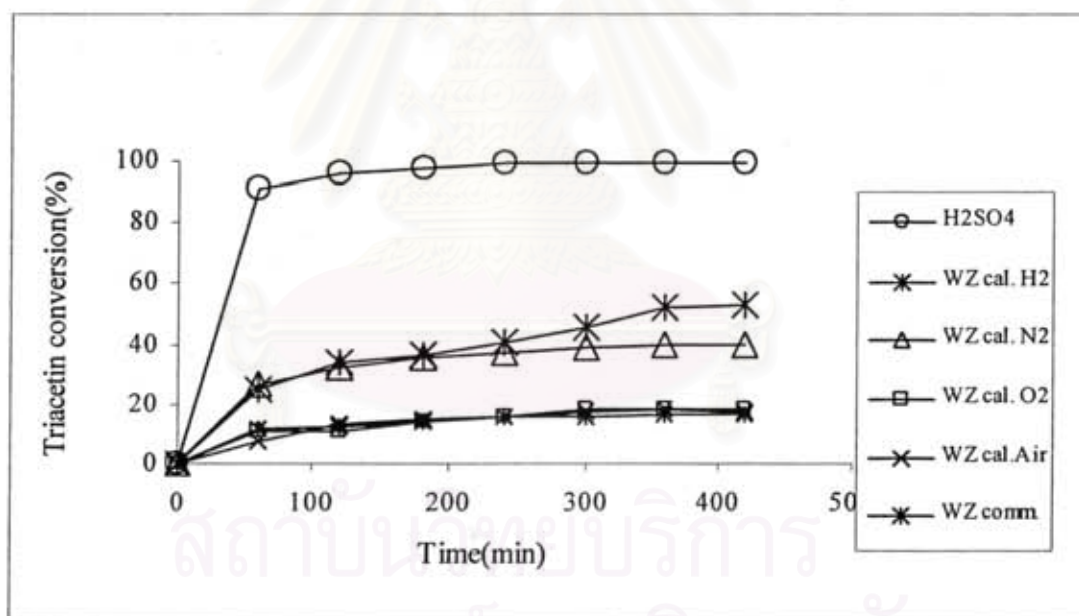


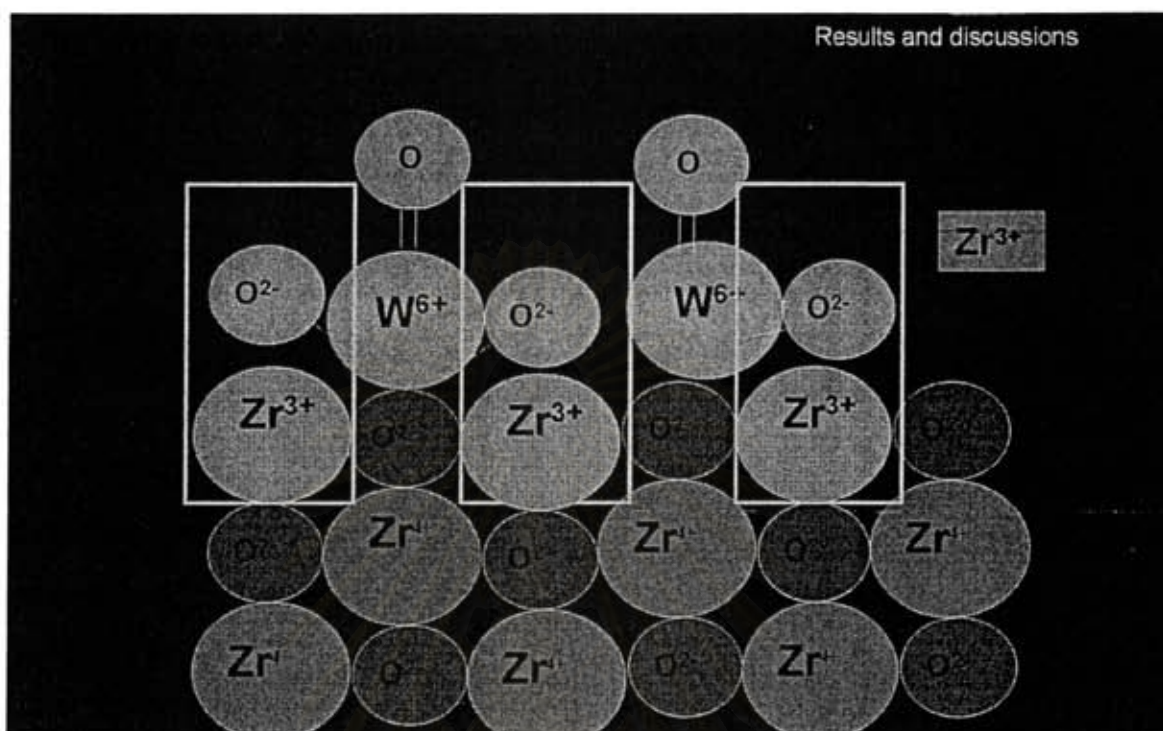
Figure 5.11 Relative activities of acid catalysts for transesterification of triacetin with methanol using a 6:1(methanol:triacetin)and 60°C (solid acids = 2 wt%)

CHAPTER VI

CONCLUSIONS AND RECOMMENDATION

6.1 Conclusions

1. Nanocrystalline supported-ZrO₂ calcined under different atmosphere, i.e. O₂, H₂, N₂ and air, at 500°C were investigated in terms of BET measurement and XRD analysis. The calcinations appeared to decrease the specific surface area while there were no influence on ZrO₂ phase taking place.
2. ZrO₂ calcined under different atmosphere, i.e. H₂, N₂, O₂ and air, at 500°C were used as support for tungsten zirconia (WZ) catalysts. The observations showed altering in defect structure from F-center to Zr³⁺ which verified by the disappearance of ESR spectra at $g = 2.003$ but instead $g = 1.975$ and $g = 1.957$ taking place. The number of Zr³⁺, related to ESR intensity, were in the following order H₂ > N₂ > O₂ > Air.
3. Catalytic performances of the W catalysts supported on these treated-catalysts were studied in the liquid phase transesterification reaction of triacetin and methanol. The catalytic activities were improved in the order: WZ cal. H₂ (53%) > WZ cal. N₂ (40%) > WZ cal. O₂ (17%) = WZ cal. Air (16%). This result was in good agreement with the increased order of acidity determined by titration and Zr³⁺ determined by ESR. Increasing of acidity was probably due to the increase of dispersion of WO_x species on ZrO₂ supports.
4. The overall results lead us to the conclusion that the impregnation of tungsten on the supported zirconia with different calcine atmosphere caused an F-center defect formation of zirconia and then gave Zr³⁺ formation as proposed in the following model.



6.2 Recommendations for Future Work

The obtained features from this WZ catalysts on transesterification was that the effect of F-center defect strongly affect the higher Zr^{3+} and higher acidity which yielded in higher activity of the reaction. It was recommended to improve the catalysts on transesterification reaction that:

Another acidic metal such as alumina should be loaded instead of tungsten. The effect of different acidic metal on Zr^{3+} and the activity of the reaction should be investigated.

REFERENCES

- [1] E. Lotero, K. Suwannakarn, D.A. Bruce, J.G. Goodwin Jr. J. Catal. **247** (2007):43-50.
- [2] M. Canakci, J. Van Gerpen, T. ASAE **46** (2003) 945.
- [3] M. Canakci, J. Van Gerpen, T. ASAE **42** (1999) 1203.
- [4] M. Canakci, J. Van Gerpen, T. ASAE **44** (2001) 1429.
- [5] M.J. Goff, N.S. Bauer, S. Lopes, W.R. Sutterlin, G.J. Suppes. J. Am. Oil Chem. Soc. **81**(2004):415.
- [6] E. Lotero, Y. Liu, D.E. Lopez, K. Suwannakarn, D.A. Bruce, J.G. Goodwin Jr. Ind. Eng. Chem. Res. **44** (2005):353.
- [7] D.E. López, J.G. Goodwin Jr., D.A. Bruce, E. Lotero. Appl. Catal. A Gen. **295** (2005):97.
- [8] D.E. López, J.G. Goodwin Jr., D.A. Bruce. J. Catal. **245** (2007):379.
- [9] S. Furuta, H. Matsushashi, K. Arata. Catal. Commun. **5** (2004):721.
- [10] S. Ramu, N. Lingaiah, B.L.A. P. Devi, P.S. S. Prasad. Appl. Catal. A Gen. **276** (2004):63-168.
- [11] Q. Zhao, X. Wang, T. Cai. Appl. Surf. Sci. **225** (2004):7-13.
- [12] H. Liu, L. Feng, X. Zhang, Q. Xue. J. Phys. Chem. **99**(1995):332-334.
- [13] K. Suriye, P. Prasertdam, B. Jongsomjit. Appl. Surf. Sci. **253** (2007):3849-3855.
- [14] U. Diebold. Surf. Sci. Rep. **48** (2003):53.
- [15] Y. Nakaoka, Y. Nosaka. J. Photochem. Photobiol. A **110** (1997):299.
- [16] T.L. Thompson, O. Diwald, J.T. Yates Jr. J. Phys. Chem. B **107**(2003):11700.
- [17] F.R. Chen, G. Coudurier, J.F. Joly, J.C. Védrine. J. Catal. **143**(1993):616-626.
- [18] M. Hino, K. Arata. J. Chem. Soc. Chem. Commun. (1987):1259.
- [19] V.C.F. Holm, G.C. Bailey, US patent 3,032,599, 1962.
- [20] T. Yamaguchi. Appl. Catal. **6**(1989):493.
- [21] G. Larsen, E. Lotero, R.D. Parra, L.M. Petkovic, H.S. Silva, S. Rahavan. Appl. Catal. A **130**(1995):213.
- [22] E. Iglesia, S.L. Soled, G.M. Kramer. J. Catal. **144**(1993):238.
- [23] M. Hino, K. Arata, in: Proc. 9 th Intl. Congr. Catal., 1988, p. 1727.
- [24] K. Tanabe, M. Misono, Y. Ono, H. Hattori, in: New solid Acids and Bases, Elsevier Science, Amsterdam, 1989.
- [25] A. Baiker, J. Kijenski. Catal. Today **5**(1989):1.

- [26] E. Iglesia, D.G. Barton, S.L. Soled, S. Miseo, J. Baumgartner, W.E. Gates, G.A. Fuentes, G.D. Meitzner. Stud. Surf. Sci. Catal. 101(1996):533.
- [27] J.G. Santiesteban, J.C. Vartuli, S. Han, R.D. Bastian, C.D. Chang. J. Catal. 168 (1997):431.
- [28] M. Hino, K. Arata, Chem. Lett.(1989) 971.
- [29] F.T.T. Ng, N. Horvat. Appl. Catal. A L23(1995):L195.
- [30] G. Larsen, E. Lotero, R.D. Parra, in: Proc. 11th Intl. Congr. Catal. Baltimore, 1996, p. 543.
- [31] R. Srinivasan, R.J. De Angelis, G. Ice, and B.H. Davis, J. Am. Ceram. Soc. 73 (1990):3528.
- [32] E. Tani, M. Yoshimura, S. Somiya, Formation of Ultrafine tetragonal ZrO₂ powder under hydrothermal conditions. J. Am. Ceram. Soc., 66(1983):11.
- [33] M.I. Osendi, J.S. Moya, C.J. Serna, and J. Soria, Metastability of tetragonal zirconia powders. J. Am. Ceram. Soc. 68(1985):135.
- [34] J. Livage, K. Doi, and c. Mazieres. J. Am. Ceram. Soc. 51(1968):349.
- [35] A.R. West, Solid State Chemistry and its Application, John Wiley & Sons, Brisbane, 1997
- [36] F. Di Gregorio and V. Keller. J. Catal 225(2004):45–55.
- [37] D.G. Barton, M. Shtein, R.D. Wilson, S.L. Soled, E. Iglesia. J. Phys. Chem. B 103(1999):630.
- [38] E. Iglesia, S.L. Soled, Kramer. J. Catal. 144(1993):238.
- [39] M. Pe'rez, H. Armendariz, J.A. Toledo, A. Va'zquez, J. Navarrete, A. Montoya, A. Ga'rcia. J. Mol. Catal. A 149(1999): 69.
- [40] E. Lo'pez-Salinas, J.G. Herna'ndez-Corte'z, M.A. Corte's, J. Navarrete, M.E. Llanos, A. Va'zquez, H. Armenda'riz, T. Lo'pez. J. Appl. Catal. A 175(1998):43.
- [41] E. Iglesia, D.G. Barton, S.L. Soled, S. Miseo, J.E. Baumgartner, W.E. Gates, G.A. Fuentes, G.D. Meitzner. Surf. Sci. Catal. 101(1996):533.
- [42] D.G. Barton, S.L. Soled, G.D. Meitzner, G.A. Fuentes, E. Iglesia, J. Catal. 181(1999):57.
- [43] M. Scheithauer, R. Grasselli, K. Knozinger, Langmuir 1998, 14,3019.
- [44] H. Armenda'riz, M.A. Corte's-Ja'come, I. Herna'ndez, J. Navarrete, A. Va'zquez, J. Mater. Chem. 13(2003):143.
- [45] R.A. Boyse, E.I. Ko. J. Catal. 171(1997):191.
- [46] D. Gazzoli, M. Valigi, R. Dragone, A. Marucci, G. Mattei.

- J. Phys.Chem.B101(1997)431.
- [47] J.G. Santiesteban, J.C. Vartuli, S. Han, R.D. Bastian, C.D. Chang, J.Catal.168(1997):431.
- [48] S. Loridant, C. Feche, N. Essayem, F. Figueras. J.Phys.Chem.B 109(2005):5631.
- [49] M. Hino, K. Arata, Proc.9th Int.Congr.Catal. 1988, 1727.
- [50] X. Bokhimi, A. Morales, A. Garca, T.D. Xiao, H. Chen, P.R. Strutt. J.Solid State Chem.142(1999):409.
- [51] O. Thomas, C. Guillaume, H. Marwan. J.Phys.Chem.B109(2005):3345-3354.
- [53] M. Agustín, P. Gonzalo, A. Maria A., C. Patricia, J.F. Sánchez-Royo. Journal of Catalysis 248 (2007):288–302.
- [54] W. Hui, L. Guangshe, X. Yanfeng, L. Liping. J. of Solid State Chemistry180 (2007):2790–2797.
- [55] S. Kuba, P. Lukinskas, R.K. Grasselli, B.C. Gates, H. Knözinger. J. Catal. 216 (2003):353.
- [56] M. Sankar, C. Madhavan Nair, K.V.G.K. Murty, P. Manikandan. Applied Catalysis A: General 312(2006):108–114.
- [57] M. Hiromi, O. Masakazu, S Hiromi and Michiko, React.Kinet.Catal.Lat.Vol. 65, No. 2, 253-258(1998).
- [58] G. Dell'Agli, A. Colantuono, G. Mascolo. Solid State Ionics 123(1999):87-94.
- [59] M. A. Corte's-Ja'come,* J. A. Toledo, and C. Angeles-Chavez. J. Phys. Chem. B 109(2005):22730-22739.
- [60] K. Taejin, B. Andrew, J.K. Christopher, E.W. Israel. Journal of Catalysis 246 (2007) 370–381.
- [61] L. Yan, G. Yejun, L. Can, L. Juan, J.G. Geok, C.L. Eng, K. Fethi. Journal of Catalysis 244 (2006) 17–23.
- [62] S. Colonna, G. Pompeo, M. Girasole, D. Gazzoli, I. Pettiti, M. Valigi. Surface Science 601(2007):1389–1393.
- [63] K.M. Parida, P.K. Pattnayak, P. Mohapatra. Journal of Molecular Catalysis A: Chemical 260(2006):35–42.
- [64] L. Haiyan, M. Zhuo, C. Ying, S. Wendong, Colloids and Surfaces A: Physicochem. Eng. Aspects 287 (2006) 10–15.
- [65] A. Marrea, J. Cortees, A.C. Carlos, B. Xim, J.A.Toledo. Journal of Solid State Chemistry 179(2006):2663–2673.
- [66] B. Ankur, T.M. Nevin, M. Biju Devassy, S.P. Mirajkar, S.B. Halligudi,

- Journal of Molecular Catalysis A: Chemical 247(2006):58–64
- [67] S. Colonna, G. Pompeo, M. Girasole, D. Gazzoli, I. Pettiti, M. Valigi. Surface Science 601(2007):1389–1393.
- [68] D. Ayhan, Energy Conversion and Management 48 (2007):937–941.
- [69] A.C. Davi Ferreira, R. Mario Meneghetti, M.P. Simoni Meneghetti, R. Carlo Wolf. Applied Catalysis A: General 317(2007):58–61.
- [70] D.E. López, J.G. Goodwin Jr., D. A. Bruce. Journal of Catalysis 245(2007):381–391.
- [71] V. Gemma, M. Mercedes, A. Jose, Bioresource Technology 98 (2007):1724–1733.
- [72] S. Carmen, M. Vinatoru, Y. Maeda, Ultrasonics Sonochemistry 14(2007):380–386.
- [73] A.C. Davi Ferreira, M.R. Meneghetti, M.P. Simoni Meneghetti, C.R. Wolf, Applied Catalysis A: General 317(2007):58–61.
- [74] O. Thomas, C. Guillaume, and H. Marwan. J. Phys. Chem. B 109(2005):3345-3354.
- [75] M. Claudio, G. Elio, O. Luciana, and V. Marco. J. Phys. Chem. 94(1990):3111-3 116.
- [76] D.R. Sergio, F. Giovanni, V. Mario, G. Delia. Applied Catalysis A: General 231 (2002):173–184.
- [77] B. Thallada, R. Kondakindi, P.K. Chinthala, R.V.S. Mamidanna Murthy, V.R. Komandur Chary. Applied Catalysis A: General 211(2001):189–201.
- [78] I.V. Bobricheva, I.A. Stavitsky, V.K. Yermolaev, N.S. Kotsarenko, V.P. Shmachkova and D.I. Kochubey. Catalysis Letters 56(1998):23–27.
- [79] S. Loridant, C. Feche, N. Essayem, and F. Figueras. J. Phys. Chem. B 109 (2005):5631-5637.
- [80] K. Watcharapong, J. Bunjerd, P. Piyasan, G. Shigeo, A. Suttichai. Journal of Molecular Catalysis A: Chemical 280(2008):35–42.
- [81] M. I. Ivanovskaya and E. V. Frolova, Russian Journal of General Chemistry, 2007, Vol. 77, No. 4, pp. 524 -531.



APPENDICES

สถาบันวิทยบริการ
จุฬาลงกรณ์มหาวิทยาลัย

APPENDIX A

CALCULATION FOR CATALYST PREPARATION

Preparation of ZrO_2 nanocrystal via solvothermal method are shown as follows:

- Reagent:
- Zirconium *n*-butoxide,
Molecular weight = 327.56
 - 1,4-butanediol
Molecular weight = 90

Calculation for the preparation of Tungsten(VI) Chloride loading catalyst (15% W/ ZrO_2)

- Reagent:
- Tungsten hexachloride (WCl_6)
Molecular weight = 396.56
Density = 3.52 g/ml at 25 °C
 - Tungsten (W)
Molecular weight = 183.56
 - Zirconia (ZrO_2)
Molecular weight = 85

Based on 2 g. of catalyst used, the composition of the catalyst will be as follow:

$$ZrO_2 = 2 \text{ g.}$$

Have to used W

$$\begin{aligned} W &= (2 \cdot 15) / 85 \\ &= 0.353 \text{ g.} \end{aligned}$$

W prepare from WCl_6

$$WCl_6 \text{ required} = \frac{\text{MW of } WCl_6 \times W \text{ required}}{\text{MW of W}}$$

$$\begin{aligned} WCl_6 &= (396.56 \times 0.353) / (183.56) \\ &= 0.763 \text{ g} \end{aligned}$$



สถาบันวิทยบริการ
จุฬาลงกรณ์มหาวิทยาลัย

APPENDIX B

CALCULATION FOR PERCENT OF TETRAGONAL AND MONOCLINIC PHASE

The fraction of crystal phase of zirconia was estimated from X-ray diffraction (XRD) profile. The amounts of tetragonal and monoclinic phase present in the zirconia were estimated by comparing the areas of characteristic peaks of the monoclinic phase ($2\theta = 28$ and 31 for (111) and (111) reflexes, respectively) and the tetragonal phase ($2\theta = 30$ for the (111) reflex). The fraction composition of each phase was calculated from the Gaussian areas $h \times w$.

% monoclinic phase

$$= \frac{\sum (h \times w)_{\text{monoclinic phase}}}{\sum (h \times w)_{\text{monoclinic and tetragonal phase}}} \quad (\text{B.1})$$

% tetragonal phase

$$= \frac{\sum (h \times w)_{\text{tetragonal phase}}}{\sum (h \times w)_{\text{monoclinic and tetragonal phase}}} \quad (\text{B.2})$$

where h = the height of X-ray diffraction pattern at the characteristic peaks

w = the half-height width of X-ray diffraction pattern at the characteristic peaks.

สถาบันวิทยบริการ
จุฬาลงกรณ์มหาวิทยาลัย

Example: Calculation of the fraction of crystal phase of zirconia

Table B.1 Calculation of the fraction of crystal phase of tungsten support on zirconia catalysts.

WZ cat.calcine at different atm.	<i>Area of zirconia</i>			
	<i>monoclinic</i>	<i>tetragonal</i>	<i>%monoclinic</i>	<i>%tetragonal</i>
O ₂	401.25	1454.22	24.8	75.2
H ₂	429.69	1173.43	28.4	71.6
N ₂	837.56	2107.49	26.8	73.2
Air	410.95	1243.06	21.6	78.4

Table B.2 Calculation of the fraction of crystal phase of tungsten support on zirconia catalysts.

Zirconia calcine at different atm.	<i>Area of zirconia</i>			
	<i>monoclinic</i>	<i>tetragonal</i>	<i>%monoclinic</i>	<i>%tetragonal</i>
O ₂	546.84	1864.69	22.7	77.3
H ₂	944.1	2312.68	29.0	71.0
N ₂	1527.93	5261.77	22.5	71.0
Air	216.27	1357.41	21.7	78.3
As-syn	585.36	1740.70	25.2	74.8

APPENDIX C

CALCULATION OF CRYSTALLITE SIZE

Calculation of crystallite size by Debye-Scherrer equation

The crystallite size was calculated from the half-height width of the diffraction peak of XRD pattern using the Debye-Scherrer equation.

From Scherrer equation:

$$D = \frac{K\lambda}{\beta \cos \theta} \quad (C.1)$$

Where D = Crystallite size, Å

K = Crystallite-shape factor (=0.9)

λ = X-ray wavelength (=1.5418 Å for $\text{CuK}\alpha$)

θ = Observed peak angle, degree

β = X-ray diffraction broadening, radian.

The X-ray diffraction broadening (β) is the pure width of power diffraction free from all broadening due to the experimental equipment. α - Alumina is used as a standard sample to observe the instrumental broadening since its crystallite size is larger than 2000 Å. The X-ray diffraction broadening (β) can be obtained by using Warren's formula.

From Warren's formula:

$$\beta = \sqrt{B_M^2 - B_S^2} \quad (C.2)$$

Where B_M = the measured peak width in radians at half peak height

B_S = the corresponding width of the standard material.

Example: Calculation of the crystallite size of zirconia

The half-height width of 111_m diffraction peak = 0.25° (from Figure A.1)

$$= \left(\frac{2\pi}{360} \right) \cdot (0.25)$$

$$= 0.0044 \text{ radian}$$

The corresponding half-height width of peak of α -alumina (from the B_S value at the 2θ of 28.36° in Figure A.2) = 0.0039 radian

$$\text{The pure width, } \beta = \sqrt{B_M^2 - B_S^2}$$

$$= \sqrt{0.0044^2 - 0.0039^2}$$

$$= 0.0021 \text{ radian}$$

$$\beta = 0.0021 \text{ radian}$$

$$2\theta = 28.36^\circ$$

$$\theta = 14.18^\circ$$

$$\lambda = 1.5418 \text{ \AA}$$

$$\text{The crystallite size} = \frac{0.9 \times 1.5418}{0.0021 \times \cos 14.18^\circ}$$

$$= 67 \text{ \AA}$$

$$= 6.7 \text{ nm}$$

สถาบันวิทยบริการ
จุฬาลงกรณ์มหาวิทยาลัย

APPENDIX D

CALCULATION OF TRIACETIN CONVERSION

The catalytic performance for transesterification reaction was evaluated in terms of triacetin conversion.

Triacetin conversion is defined as moles of triacetin converted with respect to moles of triacetin in feed:

$$\text{Triacetin conversion(\%)} = \frac{\text{moles of Triacetin converted to product}}{\text{moles of Triacetin in feed}} \times 100 \quad (\text{D.1})$$

Where mole of triacetin can be determined from triacetin peak area of the product

สถาบันวิทยบริการ
จุฬาลงกรณ์มหาวิทยาลัย

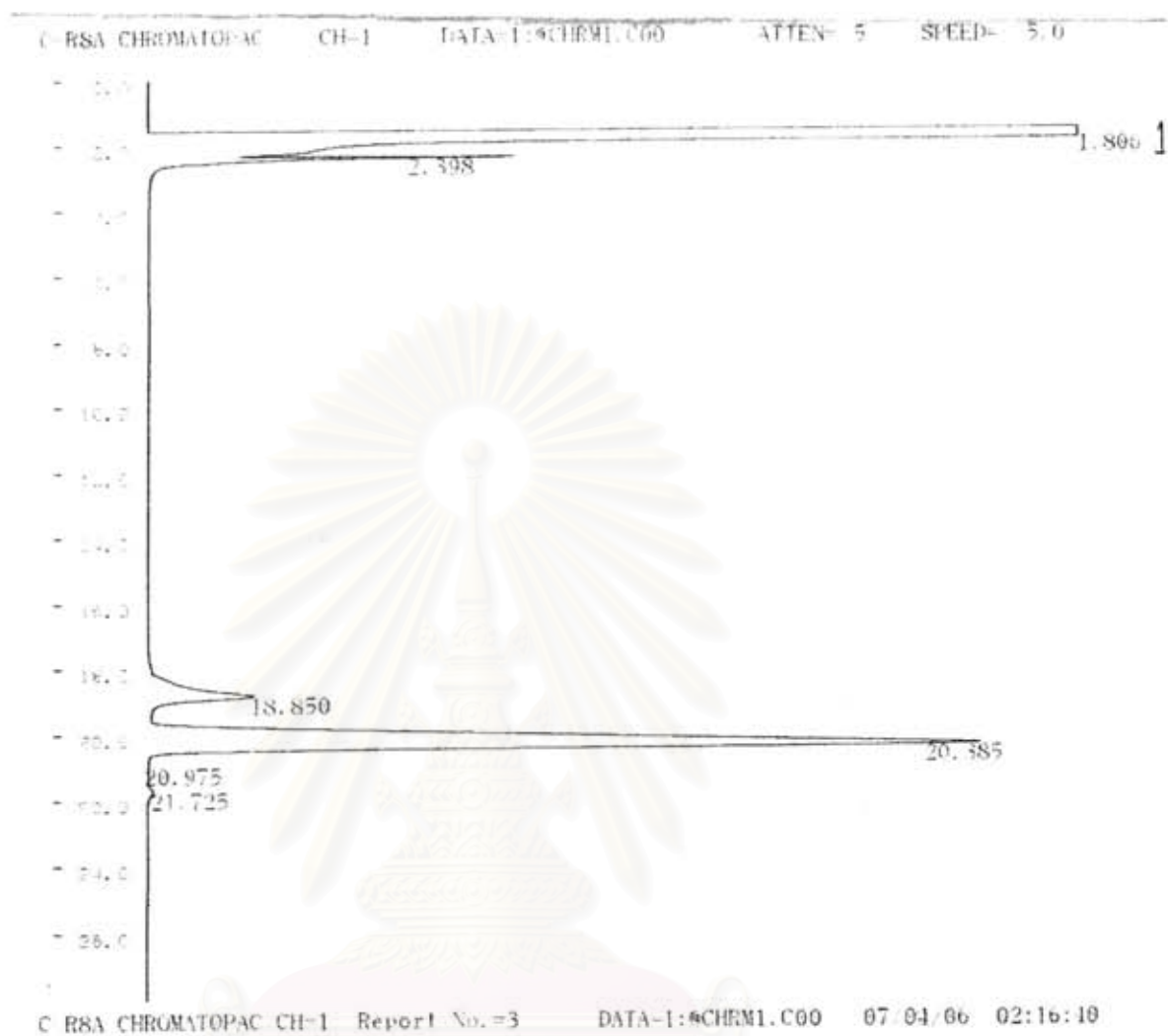


Figure D1 Gas chromatopac report of relative activities of acid catalysts for transesterification of triacetin with methanol using a 6:1(methanol:triacetin) and 60°C (solid acids = 2 wt%) when the steady-state rate was reached after 7 h.

จุฬาลงกรณ์มหาวิทยาลัย

APPENDIX E

CONDITION OF GAS CHROMATOGRAPHY

The condition of GC. were used in this reached.

Table E1: Operating conditions for gas chromatography

Gas Chromagraph	SHIMADZU GC-14B
Detector	FID
Column	RTX-5
Carrier gas	He (99.999%)
Carrier gas flow (ml/min)	30 cc/min
Column temperature	
- initial temp (°C)	50
- initial time (min)	3
- final temp (°C)	210
- final time (min)	9
Injector temperature (°C)	255
Detector temperature (°C)	280
Current (Ma)	-
Analysed	Triglyceride

สถาบันวิทยบริการ
จุฬาลงกรณ์มหาวิทยาลัย

INJ 255 °C
DET 280 °C
COLUMN: INITIAL TEMP. 50 °C
INITIAL TIME 3 min

FINAL TEMP. 210 °C
FINAL TIME 9 min
PROGRAM RATE 10 °C/min

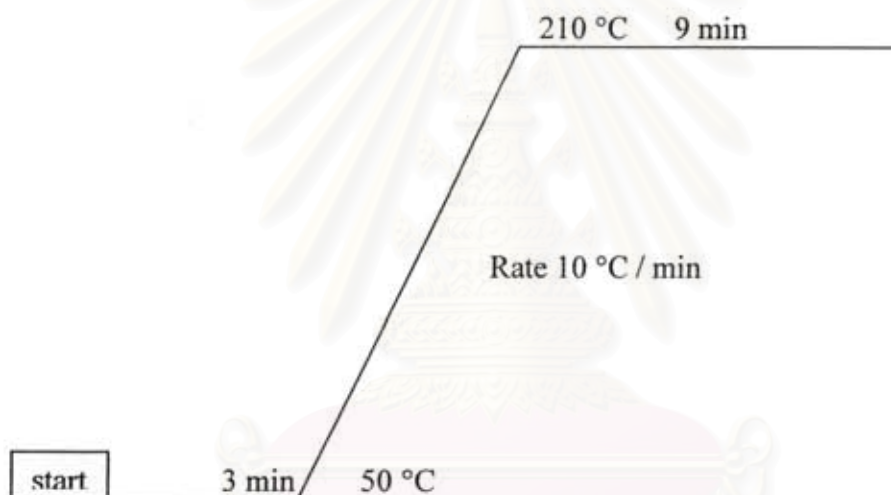


Figure E1 Operating condition of GC for this research.

สถาบันวิทยบริการ
จุฬาลงกรณ์มหาวิทยาลัย

APPENDIX F

TRANSMISSION ELECTRON MICROSCOPY AND SELECTED AREA ELECTRON DIFFRACTION (TEM) AND (SAED)

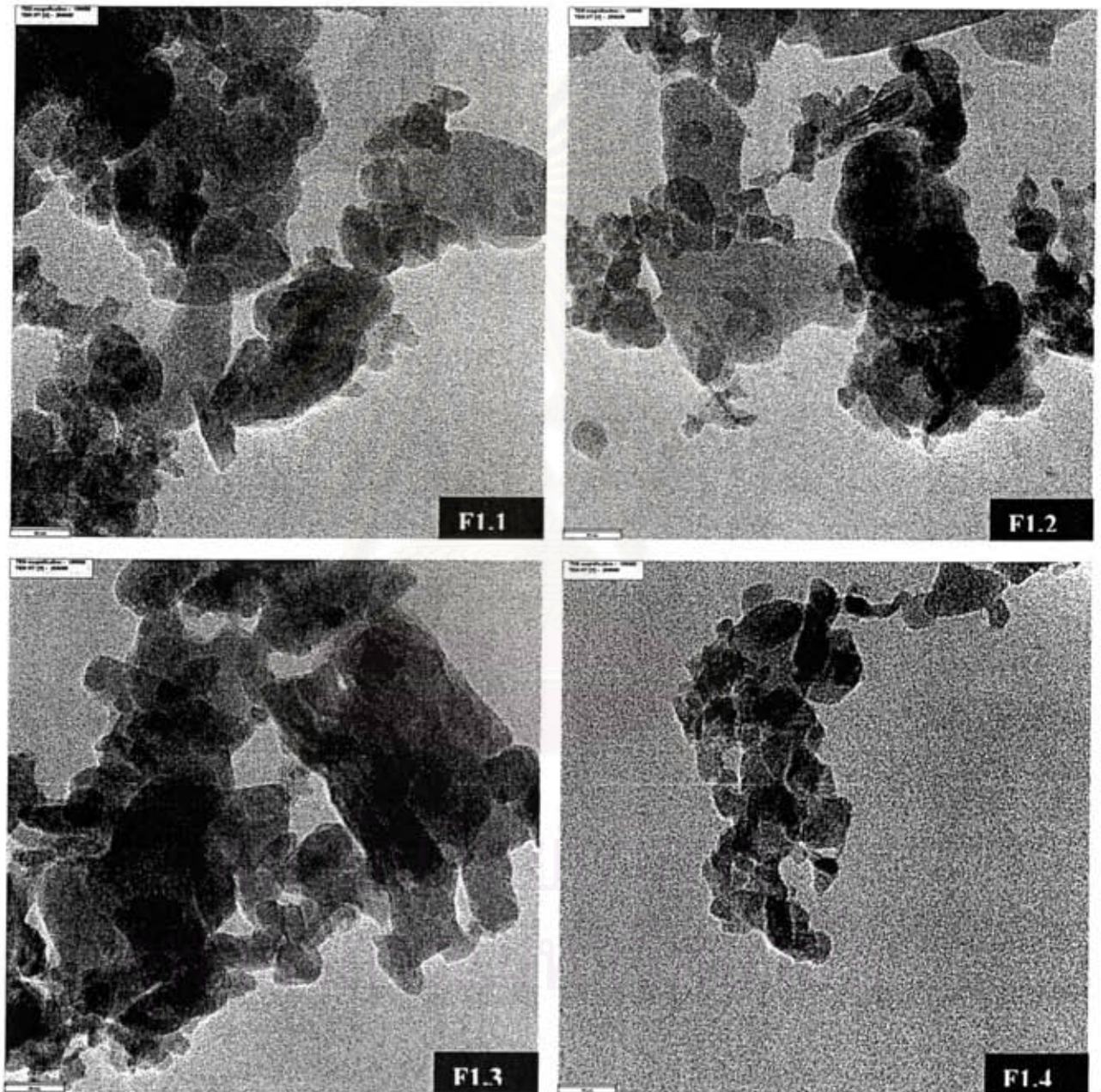


Figure F.1 TEM micrographs of W impregnation on ZrO₂ calcination with Air

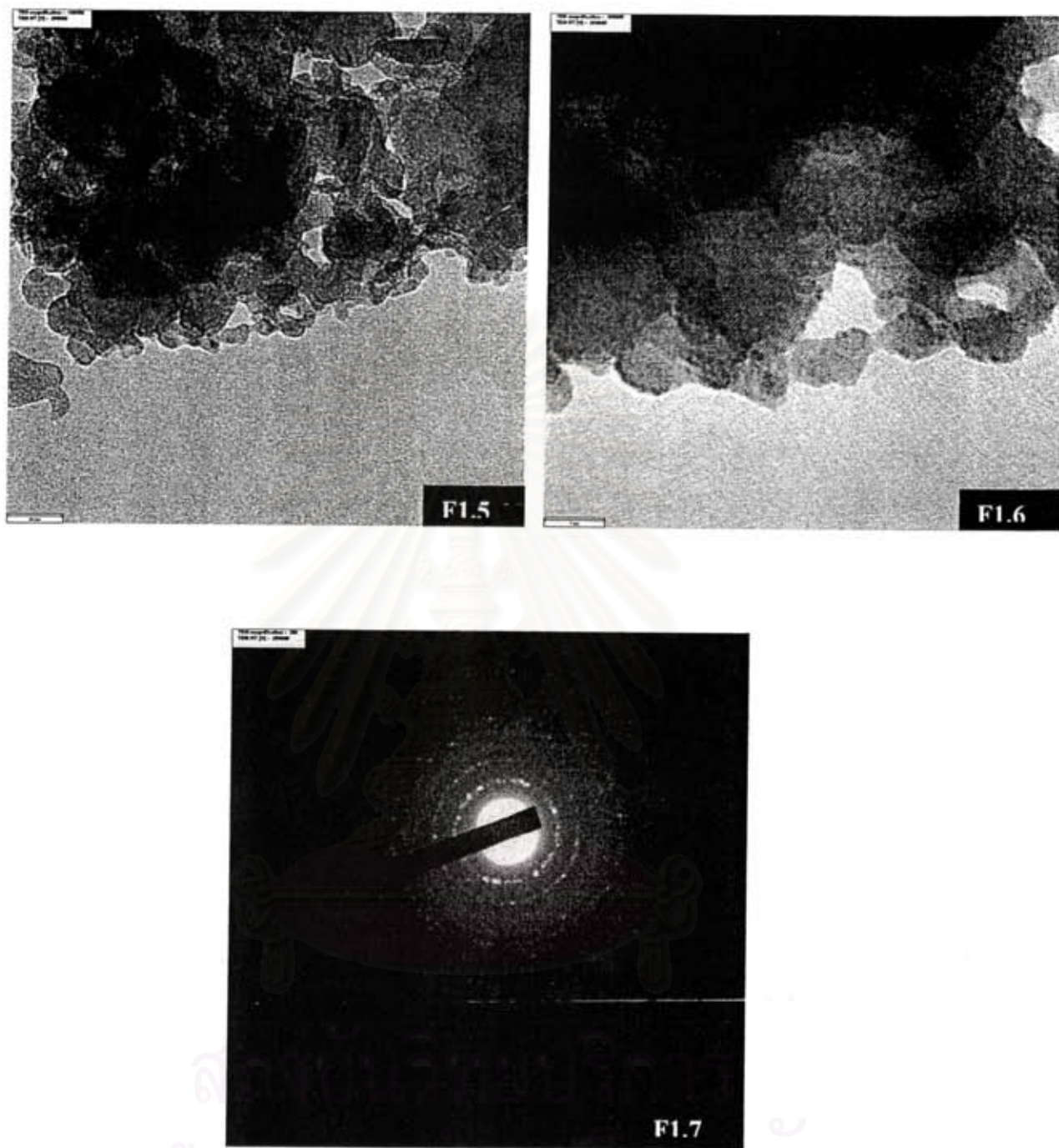
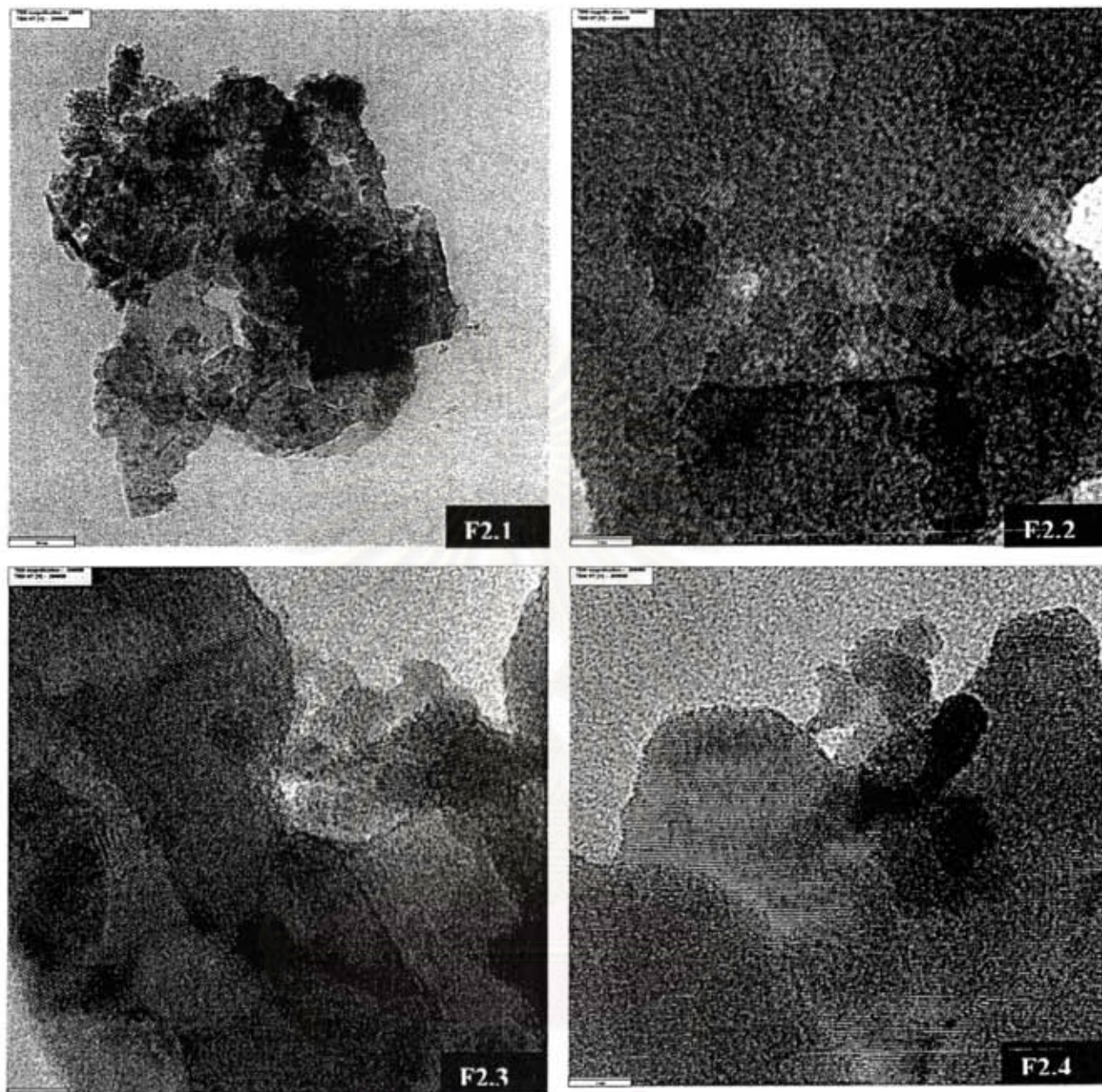


Figure F.1 TEM micrographs of W impregnation on ZrO_2 calcination with Air



สถาบันวิทยบริการ
จุฬาลงกรณ์มหาวิทยาลัย

Figure F.2 TEM micrographs of W impregnation on ZrO₂ calcination with H₂

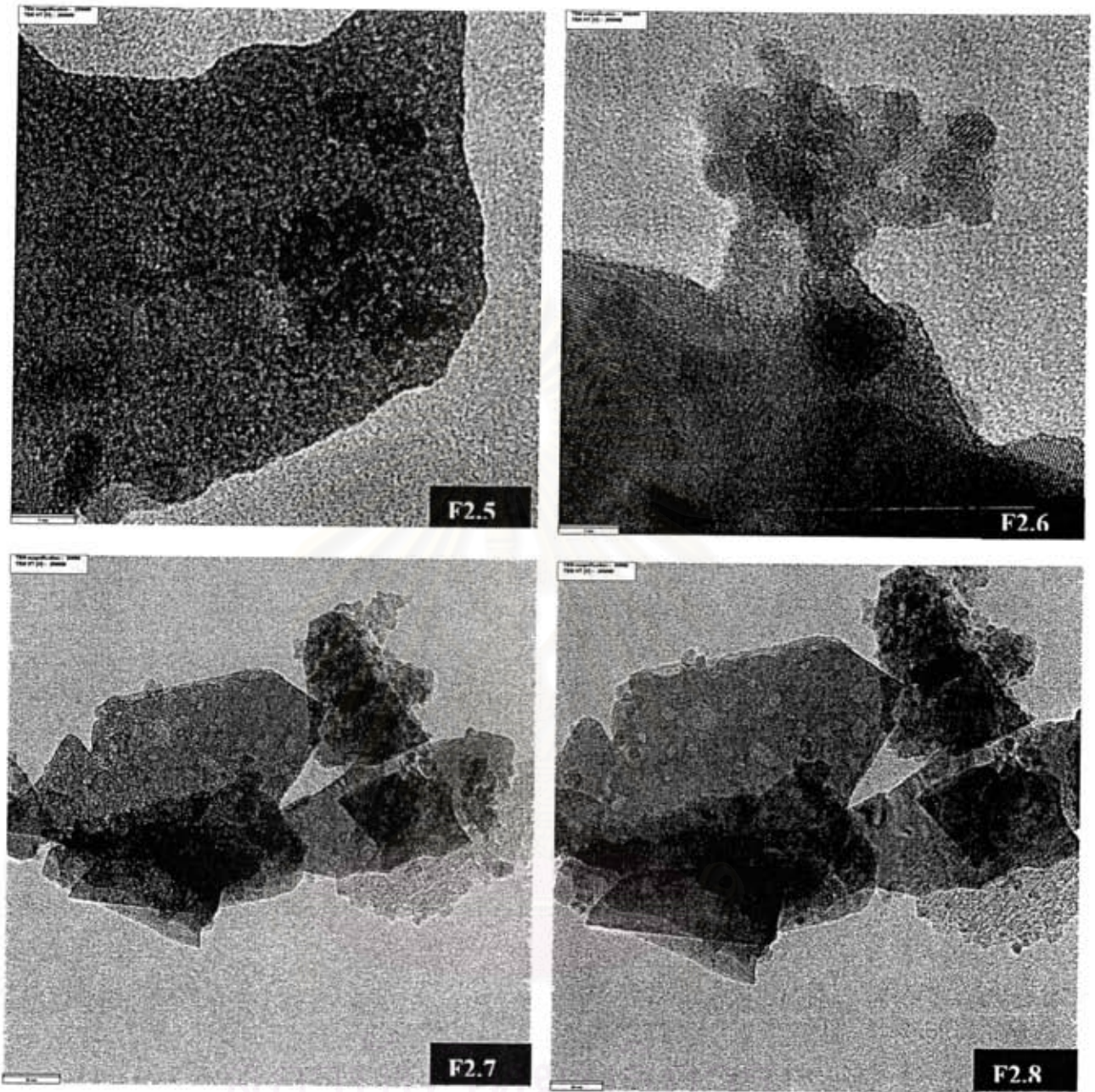


Figure F.2 TEM micrographs of W impregnation on ZrO₂ calcination with H₂

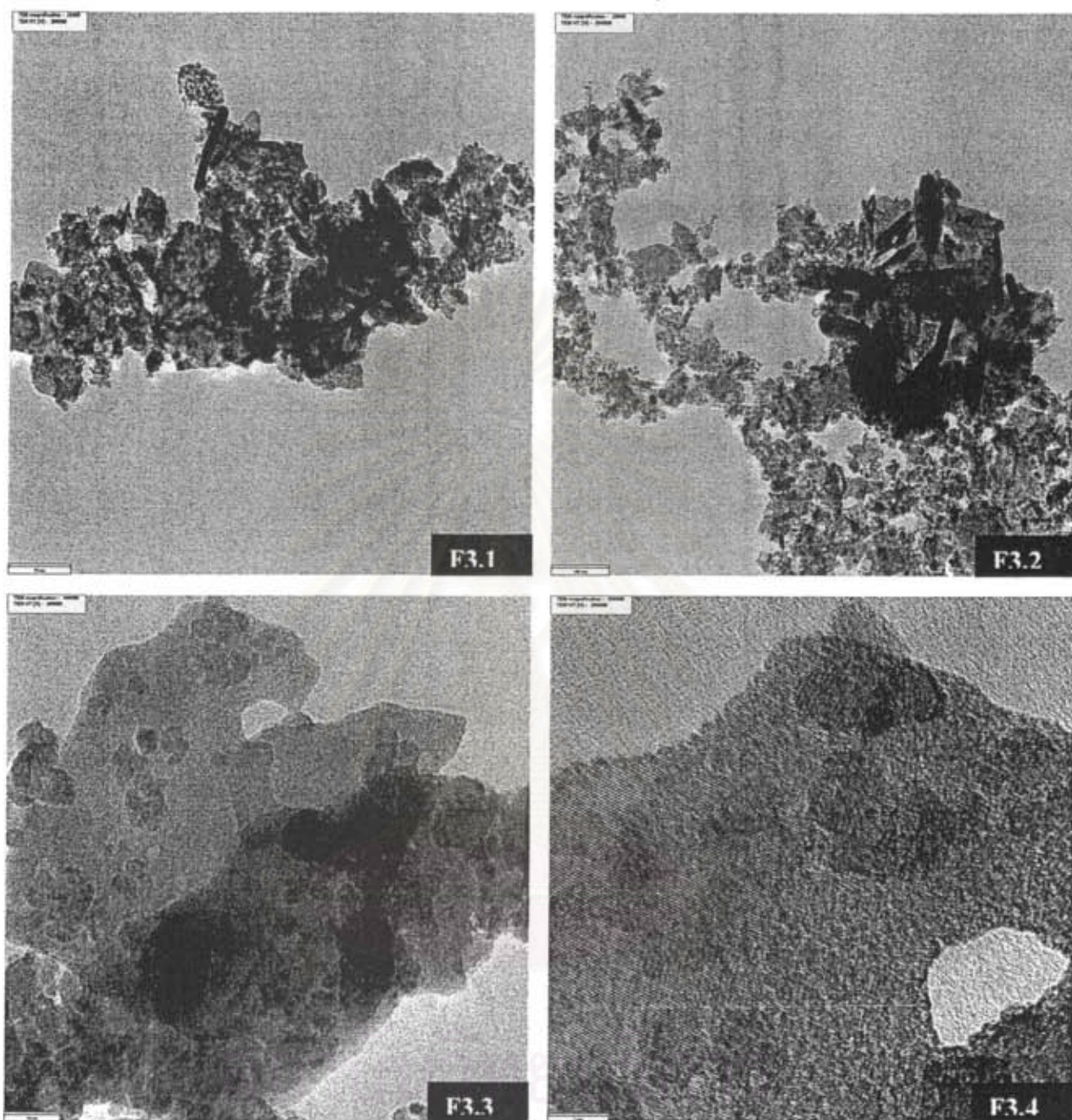


Figure F.3 TEM micrographs of W impregnation on ZrO₂ calcination with N₂

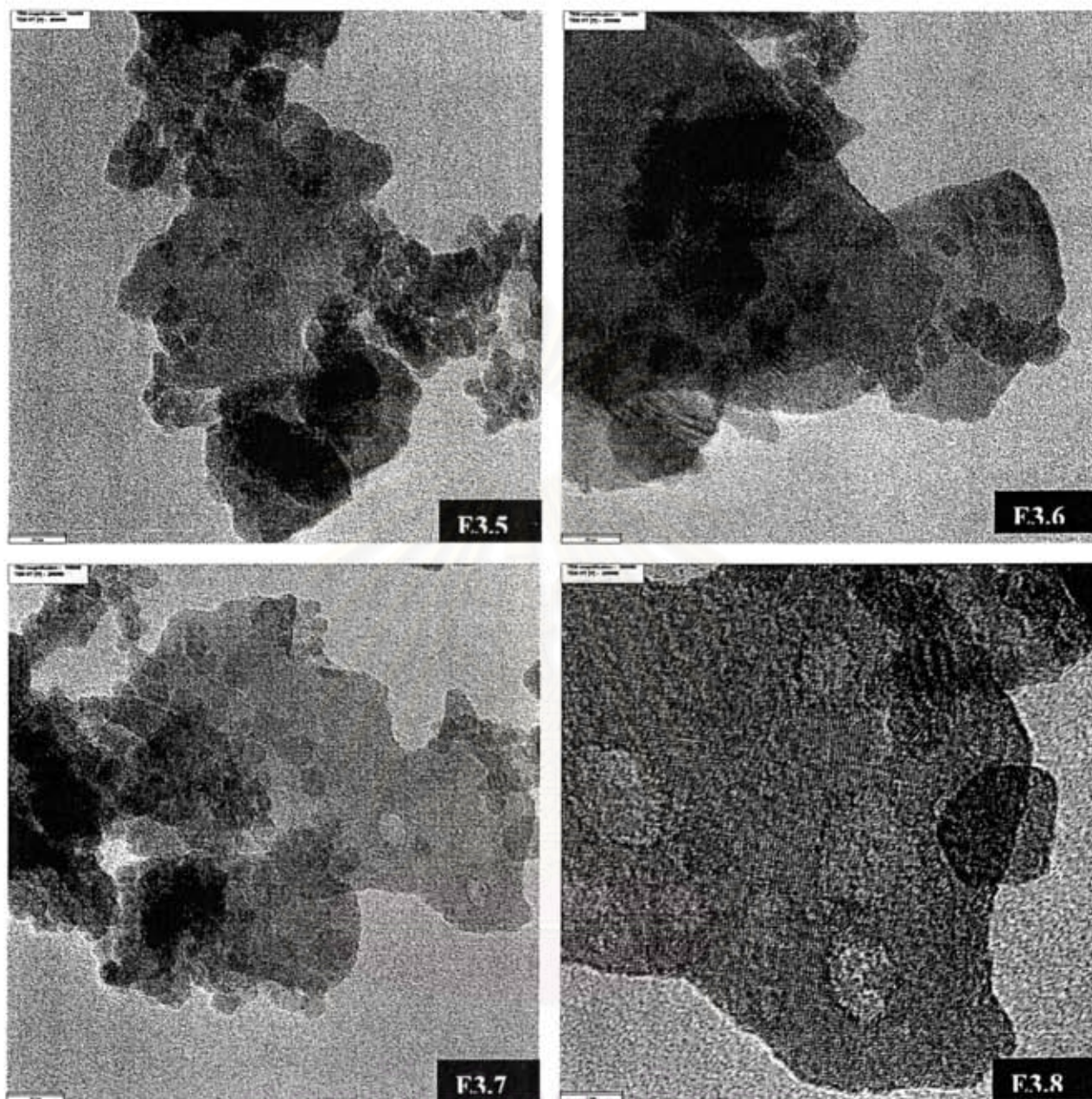
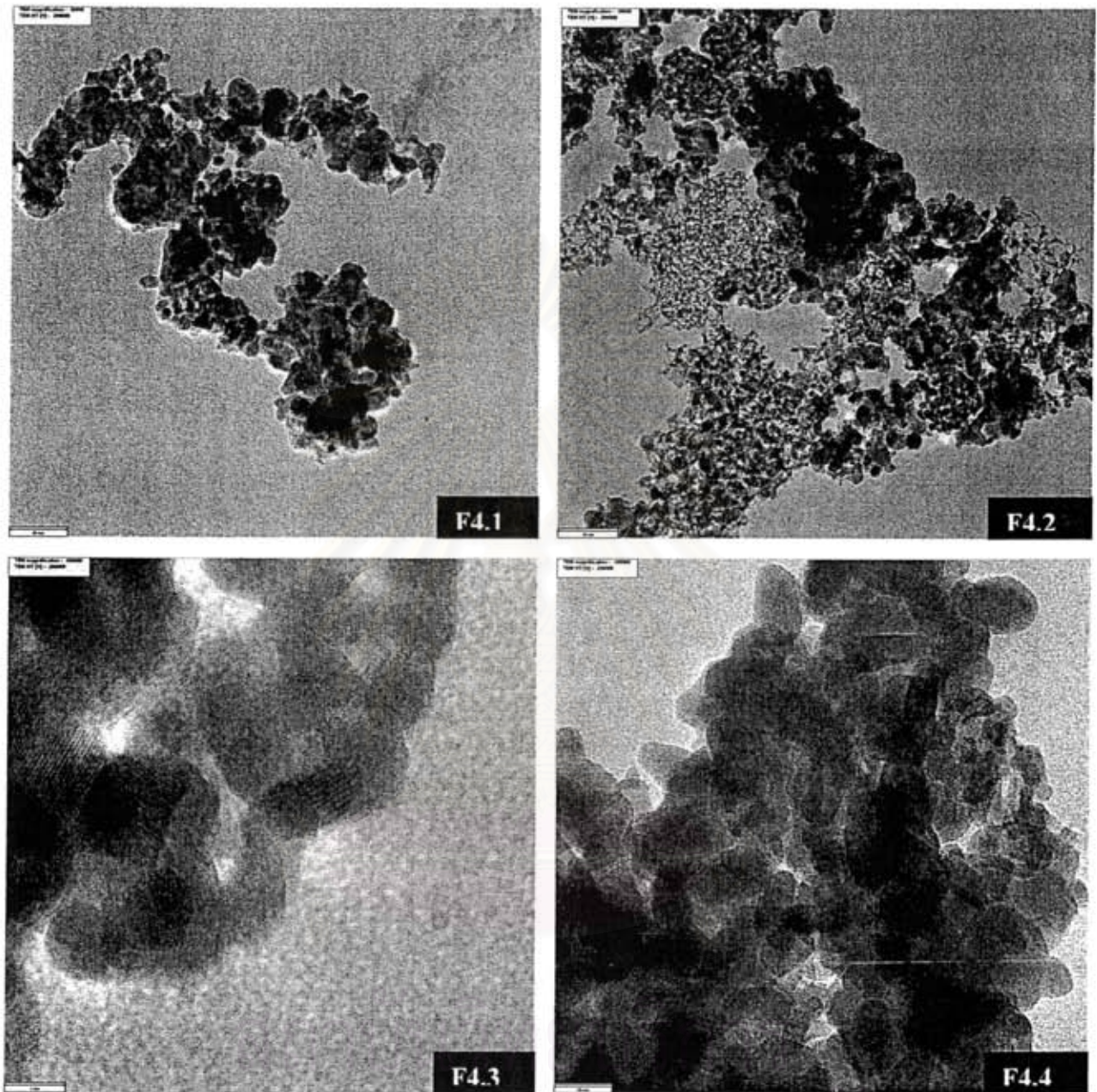


Figure F.3 TEM micrographs of W impregnation on ZrO₂ calcination with N₂



จุฬาลงกรณ์มหาวิทยาลัย

Figure F.4 TEM micrographs of W impregnation on ZrO₂ calcination with O₂

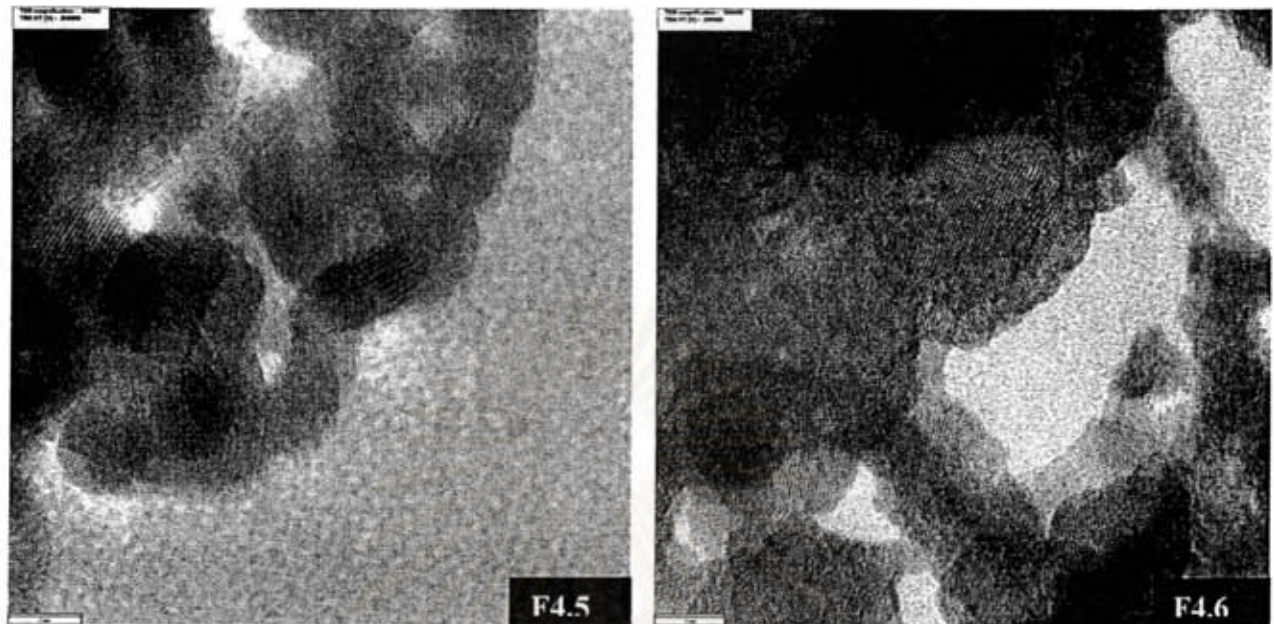


Figure F.4 TEM micrographs of W impregnation on ZrO_2 calcination with O_2

สถาบันวิทยบริการ
จุฬาลงกรณ์มหาวิทยาลัย

APPENDIX G

ESR SPECTRA OF ALL CATALYSTS SAMPLES AT DIFFERENT CALCINATION ATMOSPHERES

Nanocrystalline Zirconia supports were prepared by using the solvothermal method. The obtained ZrO_2 powders were treated at $400\text{ }^\circ\text{C}$ in different atmospheres (CO_2 , O_2 , NH_3 , He, Ar, Air, N_2 and H_2)

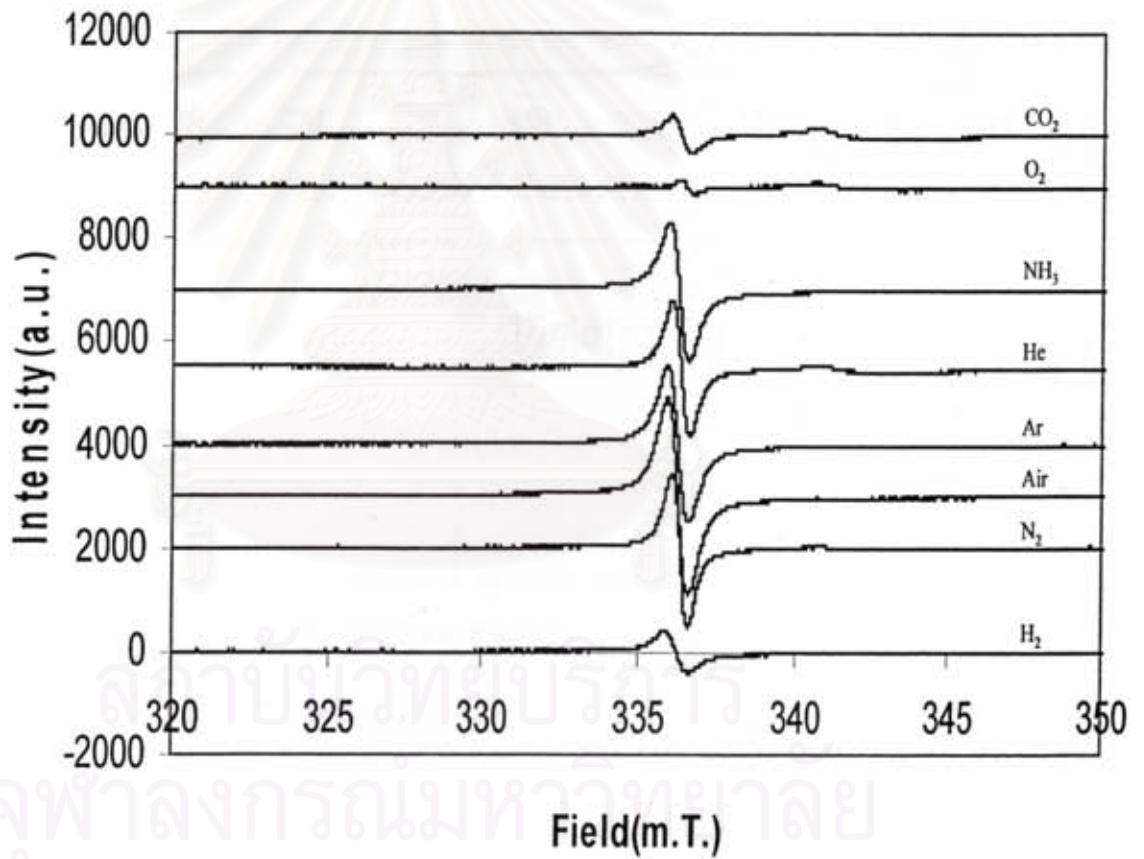


Figure G1 ESR spectra of sample nano ZrO_2 calcinations at different atmosphere : CO_2 , O_2 , NH_3 , He, Ar, Air, N_2 , H_2

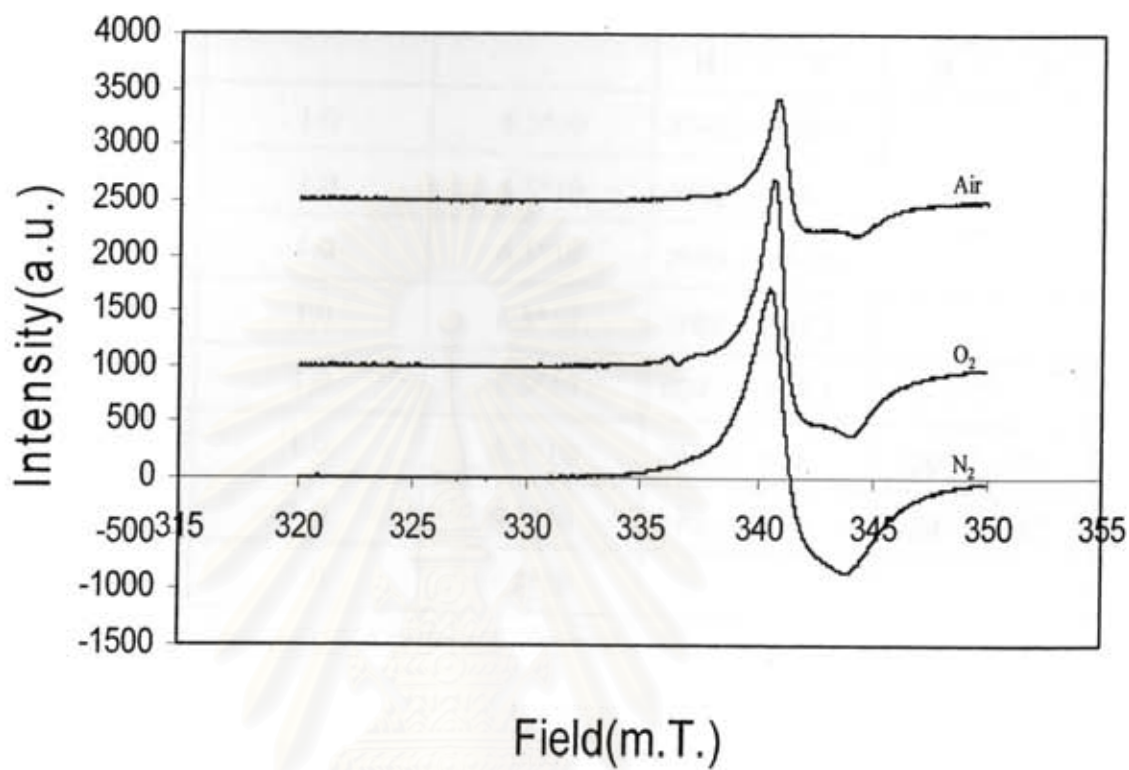


Figure G2 ESR spectra of tungstated zirconia prepared by impregnation tungsten on zirconia (calcinations at difference atmosphere) and tungstated zirconia calcinations at air atmosphere: Air, O₂, N₂

สถาบันวิทยบริการ
จุฬาลงกรณ์มหาวิทยาลัย

Table G1. Show the power, amplitude of ESR spectra for WZ sample when calcinations 400 °C at difference atmosphere.

Name	Power	Amplitude	F-center peake		Zr ³⁺	
			H	W	H	W
ZrO2 cal. NH ₃	1.0	6.3*10	83421	18941	-	-
ZrO2 cal. Ar	1.0	6.3*10	3806	660	-	-
ZrO2 cal. N ₂	1.0	6.3*10	2959	488.9	-	-
ZrO2 cal. He	1.0	6.3*10	2608	562.2	-	-
ZrO2 cal. H ₂	1.0	6.3*10	809	721.1	-	-
ZrO2 cal. CO ₂	1.0	6.3*10	746	611	220	294
ZrO2 cal. O ₂	1.0	6.3*10	276	354	150	287
ZrO2 cal. Air	1.0	6.3*10	-	-	-	-

สถาบันวิทยบริการ
จุฬาลงกรณ์มหาวิทยาลัย

APPENDIX H

RAMAN SPECTRA OF ALL CATALYSTS SAMPLES AT DIFFERENT CALCINATION ATMOSPHERES

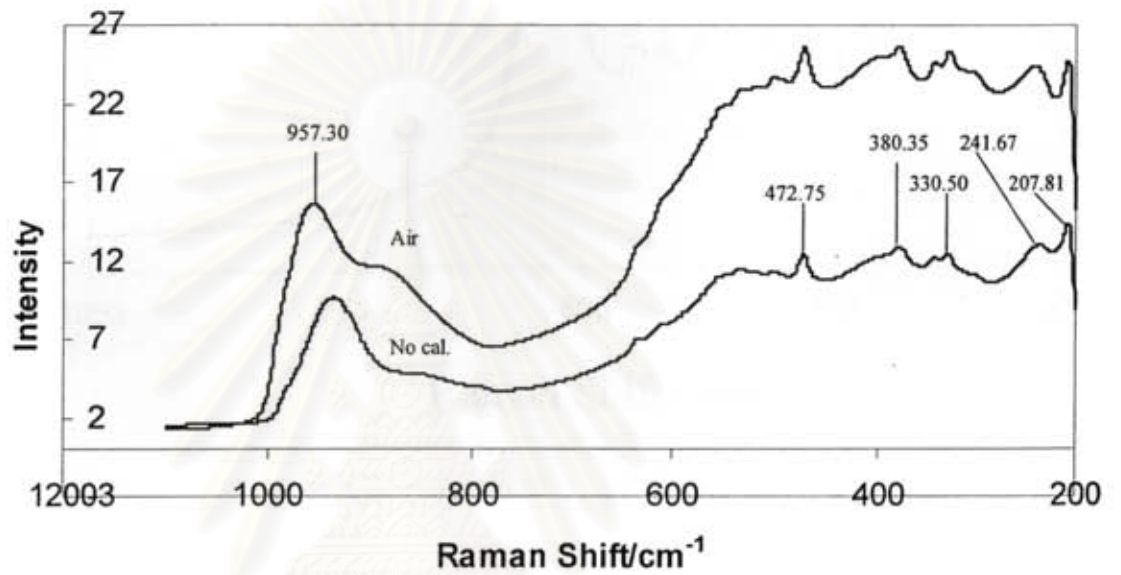


Figure H1 Raman spectra of WZ commercial prepared by sol-gel method and calcinations at atmosphere (Air) and no calcinated (no cal.)

จุฬาลงกรณ์มหาวิทยาลัย

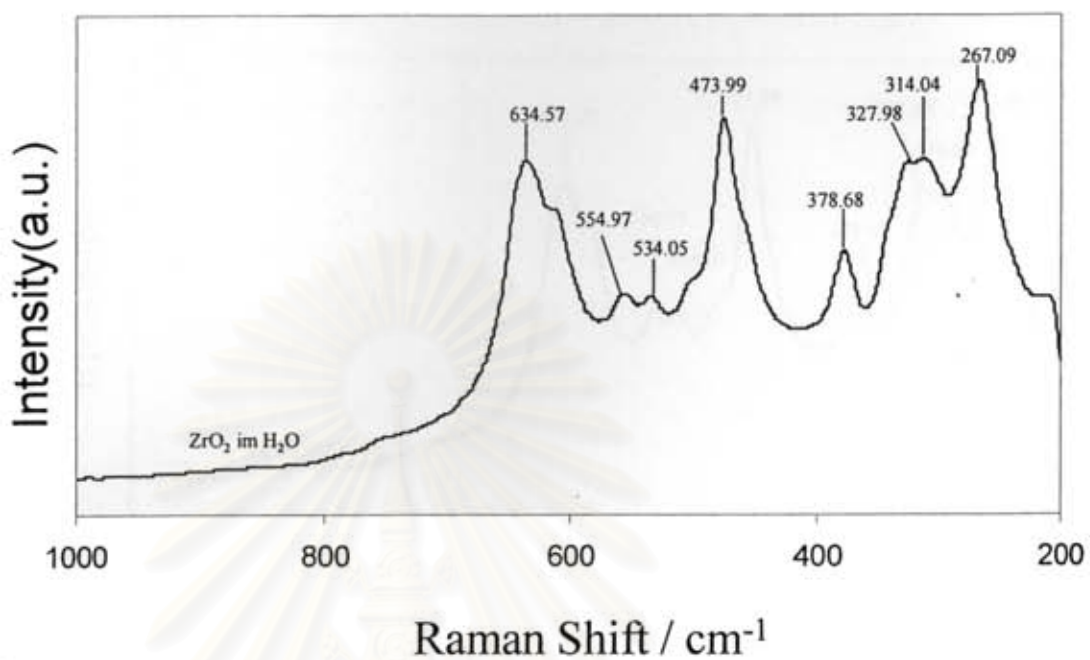


Figure H2 Raman spectra of ZrO_2 prepared by solvothermal method and impregnation with H_2O and calcinations at atmosphere.

สถาบันวิทยบริการ
จุฬาลงกรณ์มหาวิทยาลัย

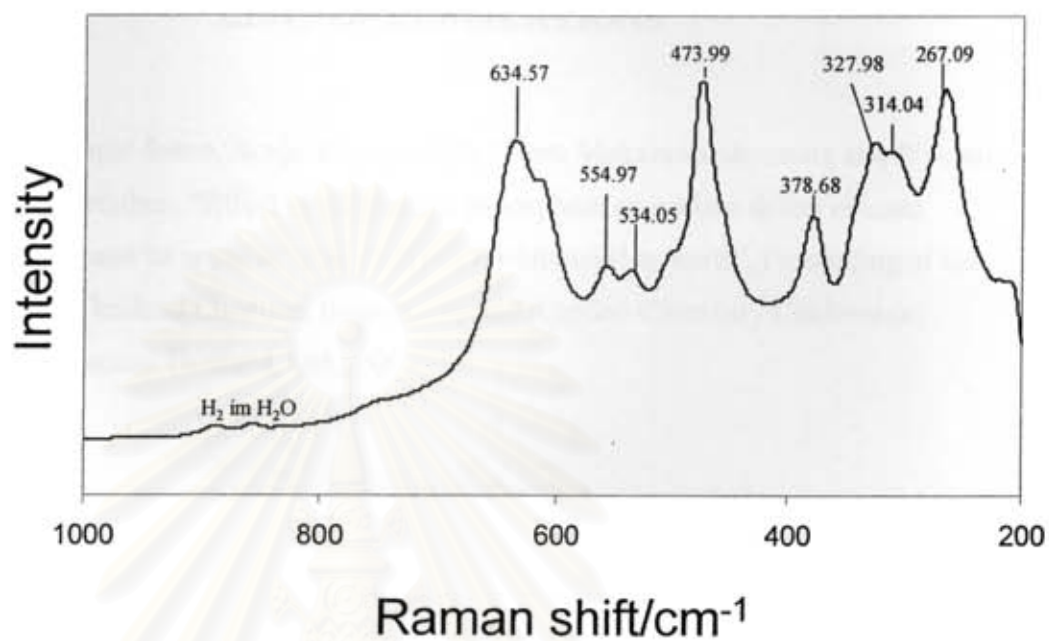


Figure H3 Raman spectra of ZrO_2 prepared by solvothermal method and calcination at H_2 atmosphere and impregnation with H_2O and calcinations at atmosphere.

สถาบันวิทยบริการ
จุฬาลงกรณ์มหาวิทยาลัย

APPENDIX I

LISTS OF PUBLICATIONS

- **Proceeding**

1. Nichapat Senso, Bunjerd Jongsomjit, Okorn Mekasuwandumrong and Piyasan Ptaserthdam, "Effect of calcination atmosphere on surface defect of nano ZrO_2 and its application as catalysts for biodiesel synthesis", Proceeding of the 17th Thailand Chemical Engineering and Applied Chemistry Conference, Chiangmai Thailand, Oct., 2007.



สถาบันวิทยบริการ
จุฬาลงกรณ์มหาวิทยาลัย

ผลของบรรยากาศในการแคลไซน์ต่อความบกพร่องที่ชั้นผิวของเซอร์โคเนียขนาดนาโน และการประยุกต์ใช้เป็นตัวเร่งปฏิกิริยาสำหรับการสังเคราะห์ไบโอดีเซล

นิชาภัทร เจ็นโส¹, โอร เมฆาสุวรรณดำรง, บรรเจิด จงสมจิต

และ ปิยะสาร ประเสริฐธรรม^{1*}

1) ศูนย์เชี่ยวชาญเฉพาะทางด้านคาตาไลซิสและวิศวกรรมปฏิกิริยาที่ใช้ตัวเร่งปฏิกิริยา
ภาควิชาวิศวกรรมเคมี คณะวิศวกรรมศาสตร์ จุฬาลงกรณ์มหาวิทยาลัย เขตพญาไท กรุงเทพฯ 10330

1. บทนำ

เป็นที่รู้กันดีอยู่แล้วว่าในปัจจุบันนี้ ราคาพลังงานเชื้อเพลิงที่มา จากแหล่งกำเนิดธรรมชาติเช่นน้ำมันปิโตรเลียมมีราคาสูงขึ้นแบบไม่หยุดยั้ง งานวิจัยในปัจจุบันจึงมุ่งเน้นไปที่การพัฒนาและคิดค้นแหล่ง พลังงานใหม่ๆ และเป็นเชื้อเพลิงที่มีราคาต่ำ เป็นมิตรต่อสิ่งแวดล้อม มี คุณสมบัติสูง [1]

ไบโอดีเซลจึงเป็นแหล่งพลังงานเชื้อเพลิงที่ได้รับความนิยมสูง เป็นอย่างมากเพราะว่ามันสามารถที่จะเตรียมได้จากวัตถุดิบธรรมชาติ หลากหลายชนิดเช่นน้ำมันพืช และ ไขมันจากสัตว์ และสามารถเปลี่ยน รูปให้เป็นน้ำมันดีเซลได้อย่างรวดเร็ว ไบโอดีเซลจะเป็นพลังงาน เชื้อเพลิงที่ดีมาก ถ้าสามารถลดต้นทุนการผลิตได้ เช่นการนำน้ำมันพืช และน้ำมันสัตว์ที่ใช้แล้วมาใช้ในการผลิตไบโอดีเซล[1] แต่ปัญหาที่ สำคัญคือน้ำมันที่ใช้แล้วจะมี กรดไขมันอิสระอยู่มาก จึงต้องมีการ กำจัดกรดไขมันอิสระ ออกก่อนในขั้นตอนของการผลิตไบโอดีเซล โดย ใช้ปฏิกิริยาเอสเทอร์ฟิเคชัน โดยทั่วไปจะใช้ตัวเร่งปฏิกิริยาที่เป็น สารละลายกรดเข้มข้นเช่น กรดซัลฟิวริก [2-6]และในขั้นที่สองจึงมา ผ่านกระบวนการทรานเอสเทอร์ฟิเคชัน เพื่อผลิตไบโอดีเซล

อย่างไรก็ตาม การใช้สารละลายกรดเข้มข้นเป็นคะตะลิสต์ จะมีการกัดกร่อนที่สูงและต้นทุนราคาแพง(เพราะไม่สามารถนำกลับมา ใช้ใหม่ได้) จึงมีการศึกษาการนำคะตะลิสต์ที่มีสถานะของแข็งที่มี สภาพเป็นกรดหรือเบส จำพวก คะตะลิสต์สถานะของแข็งที่มีสภาพความ เป็นกรดสูง, ซัลเฟตเซอร์โคเนียร์(SZ) และ ทังสเตนเซอร์โคเนียร์(WZ) มาใช้ในการผลิตไบโอดีเซล เพราะคะตะลิสต์เหล่านี้ สามารถเกิด ปฏิกิริยาเอสเทอร์ฟิเคชันและทรานเอสเทอร์ฟิเคชันได้ในคราวเดียวกัน ซึ่งปฏิกิริยาทั้งสองนี้เป็นปฏิกิริยาหลักในการผลิตไบโอดีเซล [7]โครงสร้างและความบกพร่องของ โครงสร้างของตัวรองรับคะตะ ลิสต์ (ZrO_2) ก็เป็นอีกปัจจัยที่มีอิทธิพลเป็นอย่างมากสำหรับคุณสมบัติ ของความเป็นผลึก(เช่นขนาดนาโน, Zr^{3+}) อย่างไรก็ตามการศึกษานา นข้อมูลของความบกพร่องทางโครงสร้าง เป็นเรื่องยากและเป็นอีกเรื่อง หนึ่งที่น่าสนใจกว่าคือวัตถุประสงค์ของงานวิจัยนี้จึงเพื่อทำการศึกษาคูณสมบัติ ความบกพร่องทางพื้นผิวของเซอร์โคเนียขนาดนาโน โดยทำ การเปลี่ยนบรรยากาศในการแคลไซน์(H_2 , O_2 , N_2 , Air)และนำไป ประยุกต์ใช้เป็นตัวเร่งปฏิกิริยา(ทังสเตนบนเซอร์โคเนียร์คะตะลิสต์) สำหรับ ปฏิกิริยาทรานเอสเทอร์ฟิเคชัน สำหรับผลิตไบโอดีเซล

2. อุปกรณ์และวิธีการทดลอง

2.1. สารเคมี

เซอร์โคเนีย เอ็นโทรพอกไซด์, 1-4 บิวเทนไดออกไซด์, ไครอะซิ ดิน, ทังสเตนคลอไรด์, 2 ไอโซโพรพานอล, กรดซัลฟิวริก และเมทานอล

2.2. การเตรียมตัวเร่งปฏิกิริยาทั้งสถานะบนเซอร์โคเนีย

สังเคราะห์เซอร์โคเนียร์ด้วยวิธี solvothermal โดยละลาย เซอร์โคเนีย เอ็นโทรพอกไซด์ 25 กรัม ในสารละลาย 1-4 บิวเทนได ออกไซด์ 100 มิลลิลิตร ใส่ใน autoclave ที่มีตัวละลาย 30 มิลลิลิตร ให้ความ ร้อนที่ 300 องศาเซลเซียสเป็นเวลา 2 ชั่วโมง อัตราการให้ความร้อน 2.5 องศาเซลเซียสต่ออนาที แล้วล้างโดยการหมุนเวียงด้วยเมทานอล จากนั้น อบที่อุณหภูมิ 110 องศาเซลเซียสเป็นเวลา 1 วัน ทำการสร้างความ บกพร่องบนพื้นผิวเซอร์โคเนียร์โดยนำไปเผาที่อุณหภูมิ 500 องศา เซลเซียสเป็นเวลา 2 ชั่วโมง ในบรรยากาศต่าง(ไอโคโรเจน, ไนโคโรเจน, ออกซิเจน, อากาศ) อัตราการให้ความร้อน 6 องศาเซลเซียสต่ออนาที นำ เซอร์โคเนียที่ผ่านการเผาในบรรยากาศต่างๆมาโหลดทังสเตนคลอไรด์ 15 เปอร์เซ็นต์เซอร์โคเนียร์ ด้วยวิธี incipient wetness technique นำคะ ตะลิสต์ที่ได้ไปเผาในอากาศที่อุณหภูมิ 500 องศาเซลเซียสเป็นเวลา 3 ชั่วโมง

2.3. การวิเคราะห์ลักษณะของตัวเร่งปฏิกิริยา

ศึกษาลักษณะ โครงสร้างของตัวเร่งปฏิกิริยาด้วยการ กระเจิงรังสีเอกซ์ หาพื้นที่ผิวจากการดูดซับทางกายภาพด้วยไนโคโรเจน โดยวิธี BET และหาความเป็นกรดโดยวิธีไครเดรท ศึกษาการเกิดความ บกพร่องบนพื้นผิวของเซอร์โคเนียร์ด้วยเทคนิค ESR

2.4. การทดสอบตัวเร่งปฏิกิริยา

ปฏิกิริยาเกิดในเครื่องปฏิกรณ์แบบถังกวนที่มีการควบคุมการ กวนให้คงที่ ที่ความดันบรรยากาศผสมสารตั้งต้น ไครอะซิดินใน เมทานอล อัตราส่วน 6:1 ใช้ตัวเร่งปฏิกิริยา 2 เปอร์เซ็นต์ไครอะซิดิน ทำการ ทดลองที่อุณหภูมิคงที่ 60 องศาเซลเซียส ไล่ละลายและหยุดปฏิกิริยาโดย 2 ไอโซโพรพานอล ผลิตภัณฑ์ที่ได้วิเคราะห์โดย แก๊สโครมาโทกราฟี (GC/FID)

* corresponding author(s); piyasan.p@chula.ac.th

3. ผลการทดลองและวิจารณ์ผล

3.1. การตรวจสอบคุณสมบัติของตัวเร่งปฏิกิริยา

พื้นที่ผิวและขนาดผลึกของตัวเร่งปฏิกิริยาดังตารางที่ 1 แสดงให้เห็นว่าพื้นที่ผิวและขนาดผลึกของเซอร์โคเนียที่ผ่านการเผาที่ บรรยากาศต่างๆมีค่าใกล้เคียงกันซึ่งไม่เกี่ยวข้องกับการเกิดปฏิกิริยา

ตารางที่ 1 พื้นที่ผิวและขนาดผลึกของตัวเร่งปฏิกิริยาเมื่อทำการเผาใน บรรยากาศต่าง

	H ₂	N ₂	O ₂	Air
พื้นที่ผิว (ตารางเมตรต่อกรัม)	140.94	181.57	130.21	124.77
ขนาดผลึก(นาโนเมตร)	5	4	6	6

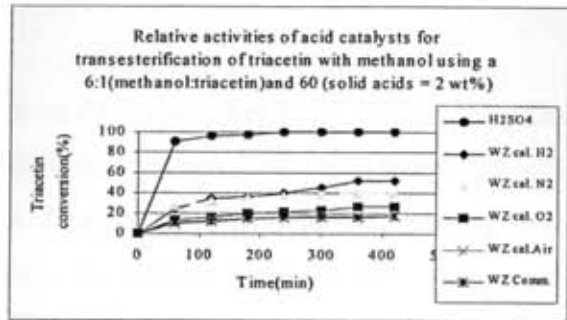


รูปที่ 1 ความสัมพันธ์ระหว่างความเข้มสัญญาณ ESR ของ ทั้งสแตนเซอร์โคเนียกับความเข้มแสง(tesla)ที่ใช้เมื่อทำการเผาที่ บรรยากาศอากาศ (เซอร์โคเนียที่ผ่านการเผาที่บรรยากาศต่างๆ: บรรยากาศ N₂, b) H₂, c) O₂, d) อากาศ, e) H₂ และทำการแคลไซน์ที่ บรรยากาศอากาศอีกครั้ง

รูปที่ 1 แสดงความสัมพันธ์ระหว่างความเข้มสัญญาณ ESR ของทั้งสแตนเซอร์โคเนียกับความเข้มแสง(tesla)เมื่อทำการเผาที่ บรรยากาศอากาศ(เซอร์โคเนียที่ผ่านการเผาที่บรรยากาศต่างๆ) จะเห็น ได้ว่าเซอร์โคเนียที่ผ่านการเผาที่บรรยากาศ H₂, N₂, O₂ และ Air เมื่อมา ทำการ โหลดด้วยทั้งสแตนคลอไรด์และนำมาเผาอีกครั้งในบรรยากาศ อากาศ จากรูปที่ 1 จะเห็นว่าเกิดสัญญาณ Zr³⁺ (g = 1.975 , g = 1.957) แทนสัญญาณ F-center ความเข้มสัญญาณ Zr³⁺ ทั้งสแตนเซอร์โคเนีย จากเซอร์โคเนียที่ผ่านการเผาที่บรรยากาศ H₂, N₂, O₂ และ Air สูงสุด และรองลงมาเรียงตามลำดับ

3.2. ความว่องไวของตัวเร่งปฏิกิริยา

รูปที่ 2 แสดงให้เห็นว่าคะตะลิสต์ที่ผ่านการเผาด้วย บรรยากาศไฮโดรเจนมีความว่องไวมากกว่าคะตะลิสต์ที่ผ่านการเผาด้วย ไนโตรเจน, ออกซิเจน, อากาศ ตามลำดับเนื่องจากเซอร์โคเนียที่ผ่านการ เผาด้วยไฮโดรเจน และไนโตรเจน มีความบกพร่องของผลึกมากที่สุด และรองลงมาตามลำดับ ส่วนเซอร์โคเนียที่ผ่านการเผาด้วยบรรยากาศ ออกซิเจนและอากาศไม่เกิดความบกพร่องทางผลึกทำให้ความว่องไวใน การเกิดปฏิกิริยาน้อย



รูปที่ 2 ความว่องไวของตัวเร่งปฏิกิริยาจากปฏิกิริยาทราน เอสเทอริฟิเคชัน ของไตรอะซิทีนกับเมทานอล 6:1 ที่อุณหภูมิ 60 C

4. สรุปผลการทดลอง

พื้นที่ผิวและขนาดผลึกของตัวเร่งปฏิกิริยาแต่ละแบบมีค่าไม่ ต่างกันมากนัก เมื่อทำการเผาเซอร์โคเนียที่บรรยากาศต่างๆพบว่าเซอร์ โคเนียมีสถานะคะตะลิสต์ เซอร์โคเนียที่ผ่านการเผาที่บรรยากาศ H₂, N₂, O₂, Air มีความเข้มสัญญาณ F-center(g = 2.003) สูงที่สุดและ รองลงมาเรียงตามลำดับ และผลทั้งสแตนเซอร์โคเนียที่ผ่านการเผาด้วย บรรยากาศอากาศมีสัญญาณ Zr³⁺ (g = 1.975, g = 1.957) ปรากฏขึ้นแทน สัญญาณ F-center เซอร์โคเนียที่มีสัญญาณ F-center มากเมื่อแปลงมาเป็น Zr³⁺ จะปรากฏความเข้มสัญญาณที่มากขึ้น และความบกพร่องทางผลึก ส่งผลถึงความเป็นกรดที่มากขึ้นของคะตะลิสต์ และส่งผลให้คะตะลิสต์ ทั้งสแตนเซอร์โคเนียมีความว่องไวเพิ่มขึ้นในปฏิกิริยาทรานเอสเท อริฟิเคชันสำหรับไบโอดีเซล WZ cal. H₂ > WZ cal. N₂ > WZ cal. O₂ > WZ cal. Air > WZ comm. เรียงตามลำดับ

5. เอกสารอ้างอิง

- [1] Dora E. Lotero, K. Suwannakarn, D.A. Bruce, J.G. Goodwin Jr., J. Catal. 247 (2007) 43-50
- [2] Canakci M. J. Van Gerpen, T. ASAE 46 (2003) 945.
- [3] Canakci M.,J. Van Gerpen, T. ASAE 42 (1999) 1203.
- [4] Canakci M.,J. Van Gerpen, T. ASAE 44 (2001) 1429.
- [5] Goff M.J., N.S. Bauer, S. Lopes, W.R. Sutterlin, G.J. Suppes, J. Am. Oil Chem. Soc. 81(2004) 415.
- [6] Dora E. Lotero, Y. Liu, D.E. Lopez, K. Suwannakarn, D.A. Bruce, J.G. Goodwin Jr., Ind. Eng. Chem. Res. 44 (2005) 5353.
- [7] Dora.E. López, J.G. Goodwin Jr., D.A. Bruce, E. Lotero, Appl. Catal. A Gen. 295 (2005) 97.

VITA

Miss Nichapat Senso was born on 24th November 1983, in Bangkok, Thailand. She finished high school from Somposkrung anuson(200 year) school, Bangkok in 2002, and received her Bachelor's Degree of Chemical Engineering from the Department of Chemical Engineering, Faculty of Engineering, King Mongkut's University of Technology, Thonburi, Thailand in March 2006. She continued her Master's study at the department of Chemical Engineering, Faculty of Engineering, Chulalongkorn University in 2006.



สถาบันวิทยบริการ
จุฬาลงกรณ์มหาวิทยาลัย